DOE DISCLAIMER

EERC DISCLAIMER

ACKNOWLEDGMENT

The authors would like to acknowledge the following employees and students for their contribution to this work: Kurt Eylands, James Ford, Kelley Fox, Doug Hajicek, Steven Hawthorne, Saiprasad Jangiti, Ray Johnson, John Kay, Srinivas Kolli, Alena Kubatova, Tim Kujawa, Ronald Kulas, Dennis Kyle, Alan Lilke, Al Olson, Edwin Olson, John Richter, Prasanna Seshadro, Ramesh Sharma, Richard Shockey, Michael Swanson, Ronald Timpe, and Karen Uhrich.

DEVELOPMENT AND TESTING OF A THERMALLY INTEGRATED SOFC–GASIFICATION SYSTEM FOR BIOMASS POWER GENERATION

ABSTRACT

The Energy & Environmental Research Center has designed a biomass power system using a solid oxide fuel cell (SOFC) thermally integrated with a downdraft gasifier. In this system, the high-temperature effluent from the SOFC enables the operation of a substoichiometric air downdraft gasifier at an elevated temperature (1000°C). At this temperature, moisture in the biomass acts as an essential carbon-gasifying medium, reducing the equivalence ratio at which the gasifier can operate with complete carbon conversion. Calculations show gross conversion efficiencies up to 45% (higher heating value) for biomass moisture levels up to 40% (wt basis). Experimental work on a bench-scale gasifier demonstrated increased tar cracking within the gasifier and increased energy density of the resultant syngas. A series of experiments on wood chips demonstrated tar output in the range of 9.9 and 234 mg/m^3. Both button cells and a 100-watt stack was tested on syngas from the gasifier. Both achieved steady-state operation with a 22% and 15% drop in performance, respectively, relative to pure hydrogen. In addition, tar tolerance testing on button cells demonstrated an upper limit of tar tolerance of approximately 1%, well above the tar output of the gasifier. These results demonstrate the feasibility and benefits of thermally integrating a gasifier and a high-temperature fuel cell in small distributed power systems.

TABLE OF CONTENTS

LIST OF FIGURES

Continued…

LIST OF FIGURES (continued)

LIST OF TABLES

DEVELOPMENT AND TESTING OF A THERMALLY INTEGRATED SOFC–GASIFICATION SYSTEM FOR BIOMASS POWER GENERATION

EXECUTIVE SUMMARY

Introduction

The U.S. Department of Energy (DOE) recently reported that biomass has surpassed hydropower as the largest renewable energy source in the United States (1). Estimates report that by 2010 biomass has the potential to grow to 10% or more of the total energy produced (2). But even with such growth, the vast majority of potential biomass resources simply go unutilized. In many cases, ideal biomass fuel sources are more economical to landfill than to convert to energy. This is due primarily to the distributed nature of biomass and its relatively low energy density. This makes transportation costs to a centralized power plant for conversion prohibitively expensive.

Fuel costs for biomass power systems can be prohibitively expensive if the fuel is transported long distances or extremely profitable if generated on-site. In a regional study of biomass resources, Schmidt and Pinapati (3) concluded that the cost of biomass fuel could vary from $20/ton to $55/ton delivered, depending on the transportation distance. However, fuel costs were negligible when generated on-site. In many cases, biomass fuel with a negative value (disposal cost) will generate additional revenue (savings) if used in a power system. In many regions in the United States, tipping fees for municipal solid waste can approach $60/ton. Tipping fees for wood wastes are generally lower, between $10/ton to $35/ton.

Landfilling a potentially clean energy source puts additional burden on the environment by increasing the land space needed for disposal and increasing overall greenhouse gas emissions from transportation and decomposition of organics. Technologies capable of converting biomass at the generation source would provide the dual environmental benefit of producing energy with zero net greenhouse gas emissions and eliminating the land space and transportation fuel needed for disposal. In many cases, revenue saved from eliminating the costs of disposing of the biomass would be comparable to the revenue obtained from the production of electricity and heat. However, even with these dual economic and environmental benefits, conventional conversion technologies are just not suited for converting solid carbonaceous fuel to electricity at plant sizes that match the distributed biomass resources, between 200 kWe and 1 MWe. Studies have shown that conventional power plants below approximately 10 MWe are economically unviable (3).

Project Goal

Through funding from the Xcel Energy Renewable Development Fund and the Energy & Environmental Research Center (EERC) Jointly Sponsored Research Program with DOE, the EERC has completed a project to design and test to proof of concept a thermally integrated biomass gasification system. The purpose of the project was to design a system to economically convert biomass to electricity at the point of biomass production. A power system able to convert

waste biomass to electricity on-site would provide dual revenue streams. Electricity and heat could be produced to reduce base utility costs or sell onto the grid. The utilization of a waste biomass would reduce disposal costs. The net gain from both revenue streams would provide a faster payback to the owner, providing a market pull for the technology.

System Concept

A systems-level approach was used where the high-quality waste heat from a solid oxide fuel cell (SOFC) stack was used to externally heat the biomass gasification reactor. The controlled heating profile of the reactor creates an ideal gasification and tar-cracking environment in the reactor. This significantly reduces the tar levels in the producer gas and produces a near-equilibrium gas composition that may be used directly in an SOFC. The reduction in capital and operating costs as a result of the cleaner raw producer gas from the biomass reactor increases the overall economics for the system in smaller size ranges.

For this system, a stratified cocurrent gasifier was chosen as the gasification technology because of its simplicity, easy scalability from 10 kW_{th} to 2 MW_{th}, and extremely low tar production. An SOFC was chosen as the electricity converter because of its increased tolerance to contaminants, ability to utilize carbon monoxide and methane as fuel, lower projected maintenance costs, high efficiency, and high-temperature anode and cathode effluent streams. The high-temperature effluent from the anode is combusted with the depleted oxygen air stream from the cathode. The high-temperature combustion product is then used to maintain gasification reactor temperature through indirect heating of the various gasification zones of the gasifier. This enables the integrated system to utilize high-moisture biomass (up to 40%) under very low equivalence ratios (ERs). The lower ER improves gas quality from approximately 5 MJ/kg (in a self-sustained, stand-alone downdraft gasifier) up to a theoretical maximum of 20 MJ/kg. This makes the system design unique in terms of its ability to utilize low-grade fuel (biomass) for producing electricity at theoretical system efficiencies approaching 40%.

Test Results

To characterize the biomass reactor, a total of 18 experiments were run under a range of gasifying conditions that included variable equivalence ratios and variable feed conditions. During these experiments, the producer gas was meticulously sampled for tar (BTX [benzene, toluene, xylene] and higher hydrocarbon), H_2S, HCl, NH_3, and particulate levels. Solid oxide fuel cells were tested to determine if operation on syngas was feasible. A series of tar-screening experiments and variable gas composition experiments were performed on button cells. Both button cells and a 100-watt stack were operated on a slipstream of syngas directly from the biomass reactor. The findings from these experiments were then used to refine the system performance predictions.

It was found that controlled heating of the biomass reactor bed created a very favorable gasification and tar-cracking condition. The raw producer gas composition was very close to the predicted equilibrium composition. The contaminant levels in the raw producer gas were very low. The measured tar levels were between 8.5 and 234 ppm, depending on the operating conditions and biomass feed. The H_2S levels were all less than 30 ppm. The NH_3 levels were all

less than 85 ppm, with the majority of tests producing NH_3 levels lower than 10 ppm. The BTX levels were less than 2 ppm. The HCl levels were not detectable in the parts per million range. The particulate levels were less than 119 ppm, with the majority of tests showing particulate matter less than 50 ppm in the raw producer gas.

For very low reactor ERs, the biomass conversion rates were prohibitively low. Good conversion rates, and subsequently good reactor power outputs, were obtained with equivalence ratios above 0.20. Self-sustained system operation was achieved on the reactor with 30% moisture pinewood. The gas composition for this condition was close to equilibrium, and the total measured tar level in the raw producer gas was 8.5 ppm.

In the SOFC experiments, immediate degradation of fuel cell performance was observed when the tar levels in the hydrogen fuel streams were increased above 1.1% and 1.9% by volume for hydrogen flow rates of 0.34 and 0.44 slpm, respectively. This equates to a level of 10,000–20,000 ppm, well above the tar levels produced by the gasifier. These results are preliminary, and additional testing should be performed, including long-term tar testing. Additional thermodynamic analysis shows that the compositions of the raw producer gas from the biomass reactor are below the carbon deposition boundary line in the fuel cell. The relationship between fuel power and gas composition was found to be dependent upon fuel cell type. Anode-supported fuel cells demonstrated much more variability in power output to gas composition than electrolyte-supported fuel cells. The testing on actual syngas demonstrated that a stable fuel cell output was achievable in the short term. Button cell operation on syngas experienced a drop in cell output of approximately 22%. Stack operation on syngas experienced a drop in output of about 15%.

Thermal integration of the system uses the excess energy on the back end of the system to increase gasifier performance on the front end, increasing efficiency and decreasing tar levels. The increased efficiency (more than double a conventional system) reduces the mass throughput by more than half for a given system size. As a result, materials and equipment for the overall system are also reduced, producing a substantial savings in capital costs. By designing the system to operate near atmospheric pressure conditions, material specifications for the gasifier and accessory components are kept to a minimum. These cost-saving measures result in a capital cost estimate of \$1,800/kW_e for power systems as low as 200 kW_e, if the fuel cell stack reaches its project cost target of \$300/kW. Electricity costs are estimated to vary between \$0.04/kWh to \$0.07/kWh, depending on the primary cost factors of the system. The low maturity level of SOFC technology increases the uncertainty level in the capital cost assessment, resulting in a wide variation in the cost of electricity (COE) estimates. Sensitivity analysis indicates that the SOFC stack costs and the cost of recovering capital are the primary cost factors affecting electricity costs. After the capital costs are recovered, the COE drops to less than 2 cents per kWh. If the operating and maintenance costs (O&M) can be kept low, the COE provides an attractive return rate over the long term. A 20-year economic assessment on the 10-kW_e system and a projected 200-kW_e system show an internal rate of return of 17.0% and 34.9%, respectively.

Lessons Learned

The intention of this project was to design a biomass power system from concept to proof-of-concept testing that could economically convert waste biomass and opportunity fuels to electricity at the point of biomass production. This has the potential to provide favorable economics by reducing disposal cost and increasing income through electricity and heat production. The favorable economics would provide a market pull for the technology, possibly increasing penetration and the use of biomass for power production beyond the push provided by government incentives.

The project discovered that thermal integration of the SOFC and gasifier provided system synergies that went beyond increased efficiency. Heating of the gasifier with the SOFC exhaust reduced tars down to single-digit ppm levels. The practical moisture range for the biomass feed was increased from 15% up to 40%. Both of these factors have been practical impediments to implementing small-scale biomass gasification technologies to date. The economic analysis discovered that efficiency was a secondary issue, behind operating costs. The greater stability of the gasifier and simplification of the system brought about by thermal integration has the potential to reduce operating and maintenance costs significantly, making small-scale gasification an economically viable technology.

This discovery is useful to the public and private sector because it provides a technical and economic path toward increasing the use of waste biomass and opportunity fuels. World demand for energy will mimic the increase in world population and subsequent increase in the overall standard of living around the world. At the same time, evidence is mounting that global warming, caused primarily by CO_2 emissions, is real, with unknown consequences to civilization. Both of these issues are mutually incompatible with most conventional energy technologies. This project provides a technical solution for both of these problems. Political willpower around the world is shifting toward requiring power companies to increase renewable technologies in their energy portfolio. By emphasizing economics in the system design, this technology may eventually provide a market pull, allowing power companies and investors to economically increase their use of renewable technologies.

Several lessons were learned from this project. Both theoretical and experimental work demonstrated the potential benefits of integrating a high-temperature fuel cell with a gasifier. The overall benefits are:

1. The maximum theoretical gasifier output is 119% of the feed input. The maximum experimentally measured output was 90% of the input.

2. Biomass with moisture levels as high as 40% produced clean gas.

3. Typical tar levels were below 100 ppm, with the maximum tar measured only at 234 ppm at the output of the gasifier.

4. Syngas energy density was slightly higher than typical air-blown gasifiers because of the lower nitrogen dilution.

5. Initial indications are that the fuel cell should be able to handle the tars output from the gasifier.

6. Fuel cell operation on syngas achieved a steady state output with a drop of about 15% in output as compared with hydrogen.

Practical limitations of current technology did provide challenges that must be overcome before a full-size system could be realized. These were:

1. At very low ER (less than 0.2), the gasification rates were impractically low, limiting the ability of the gasifier to perform up to its theoretical maximum efficiency.

2. Fuel cell stack technology must progress to the point where it can take thermal cycling and reoxidation of the anode before real-world systems can be employed utilizing fuel cells.

3. The price of fuel cells must come down several orders of magnitude before the economics become viable.

Overall, experimental work on the gasifier proved to be very successful. The results with the fuel cell were a little less conclusive; however, it did demonstrate the ability of the fuel cell to handle syngas. If the fuel cell reaches its full development potential, then there should be no real technical issues with developing a full-size system.

DEVELOPMENT AND TESTING OF A THERMALLY INTEGRATED SOFC–GASIFICATION SYSTEM FOR BIOMASS POWER GENERATION

SECTION I: THERMALLY INTEGRATED POWER PLANT CONCEPT AND DESIGN

The dominant operating characteristics of high-temperature fuel cell systems are the theoretically high conversion efficiencies possible with the fuel cell and the high-temperature effluent generated by the fuel cell. Most system designs employ a secondary converter to utilize the high energy effluent from the fuel cell. These designs obtain maximum overall system efficiencies by converting the heat in the fuel cell effluent to electricity through a gas turbine or steam engine bottoming cycle. The use of a bottoming cycle, however, increases overall system complexity and operating costs, while reducing system reliability.

For a small biomass system, reliability and operating costs are the primary factors determining economic viability. To maintain high system efficiency, the energy from the high-temperature effluent of the fuel cell is recycled into the front end of the system, as opposed to being converted in a bottoming cycle. The high-temperature effluent from the fuel cell is used to improve gasifier performance by maintaining a favorable thermal profile in the gasifier. The additional heat from the fuel cell theoretically increases the maximum energy output of the gasifier to 119% higher heating value (HHV) of the feed energy input. The additional energy of the producer gas comes from the high-energy waste effluent of the fuel cell, which is recycled into the producer gas through endothermic gasification reactions. This increases the gross system efficiency to 45% HHV, with a net efficiency as high as 38% HHV.

In addition to increasing the gasifier conversion efficiency, the favorable thermal profile of the gasifier increased tar conversion within the gasifier. By minimizing tar output from the gasifier and maintaining a high system temperature between the gasifier and fuel cell, tar-scrubbing equipment was minimized. This reduced overall capital and operating costs. Less equipment increases system reliability and decreases the labor requirements to operate the system.

System Description

The flow sheet of the 10-kW_e integrated SOFC–gasification system design and the schematic for the twin shell gasification system is shown in Figure 1. The biomass feed consists of wood chips or other wet biomass with very low ash (<1%), sulfur (~0.01%), and alkali content. Biomass is stored in a closed hopper and fed to the gasifier through an auger. Primary air is injected into the gasifier. The biomass sequentially undergoes pyrolysis, partial combustion, and then reduction within the gasification reactor to produce a low-tar, medium-energy content producer gas. The producer gas is then filtered through a particulate cyclone train after exiting the gasifier, while residue char and ash in the reactor is fed to a closed ash extraction system at the bottom of the gasifier. The producer gas enters the SOFC, where it is electrochemically converted to electricity at 38% efficiency and 80% utilization. Preheated air is provided to the SOFC cathode to provide the necessary heat removal for the SOFC. The vitiated fuel leaving the anode is oxidized in a combustor with the oxygen-depleted air (O_2 ~ 18% and N_2

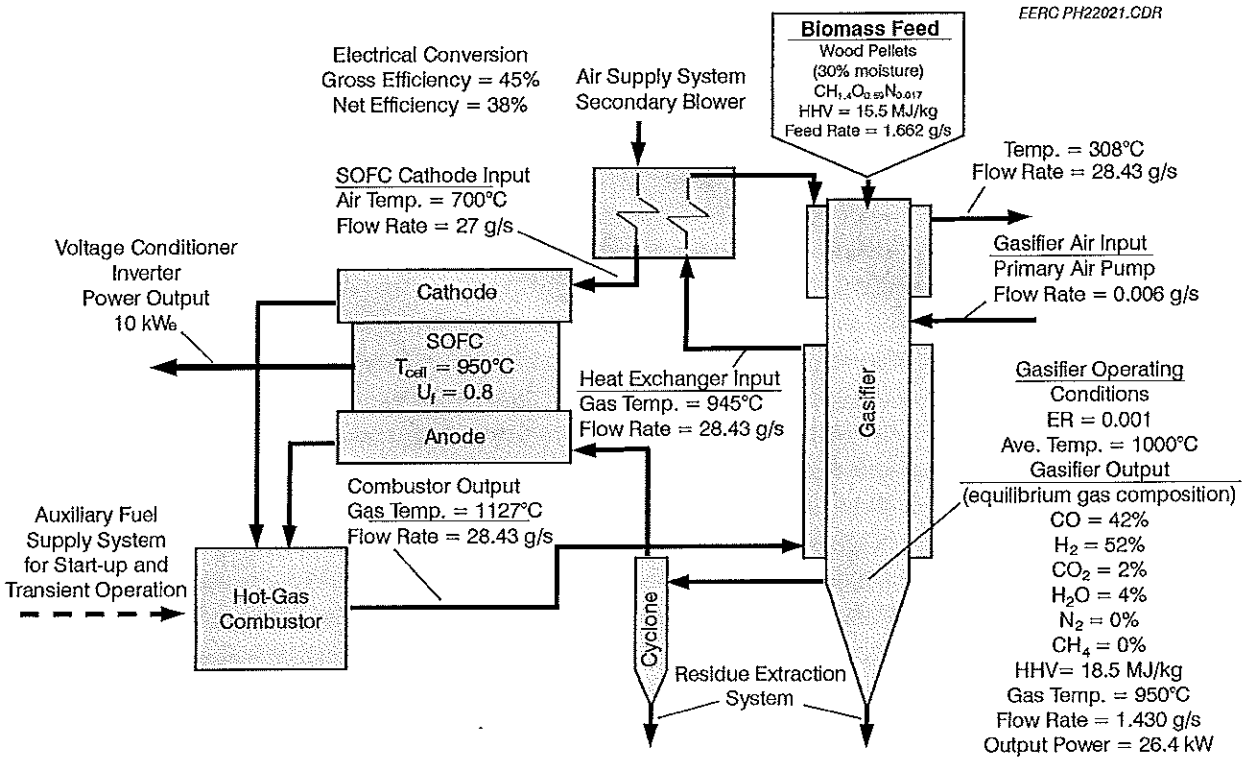

Figure 1. Flow sheet of 10-kWe thermally integrated SOFC–gasification system.

~82%) leaving the cathode of the SOFC. The temperature of the product gas leaving the combustor is 1080°–1130°C, approximately 100°–150°C higher than the SOFC outlet streams. This hot product gas from the combustor is fed to the outside annular section of the gasifier to recuperatively heat the reduction zone of the reactor. After exiting the reduction zone annular section, the product gases are fed into a heat exchanger, where the SOFC cathode air temperature is raised from room temperature to 700°C prior to entering the SOFC. The product gases are then fed into the annular section of the gasifier at the pyrolysis zone to provide pyrolysis heat and sensible heat to the incoming biomass. The product gas is subject to either waste heat extraction (via process or space heating) or is exhausted to atmosphere.

The gasification reactor is designed to minimize tar output by maintaining a uniform high-temperature operating condition and modifying the popular downdraft gasification concept, known for its low tar and particulate levels in the producer gas. Devi et al. (4) have reviewed efforts of several researchers aimed at reducing tar within the gasifier, what they have referred to as primary tar reduction methods. The proposed gasifier has features that promise low tar in the output gas stream. This reactor is a moving packed-bed gasifier that is modeled after a stratified downdraft gasifier earlier developed through cooperative efforts among various researchers (5), with modifications. The biomass fed to the gasifier first undergoes pyrolysis, then oxidation (when applicable), and then reduction within distinct zones along the vertical axis of the gasifier, as shown in Figure 2. The pyrolysis zone is where tars are initially formed. Tars formed in this stage are subsequently cracked in the high-temperature oxidation zone or reformed to CO and H_2 in the reduction zone. The exothermic reactions in the oxidation zone provide sensible heat to the

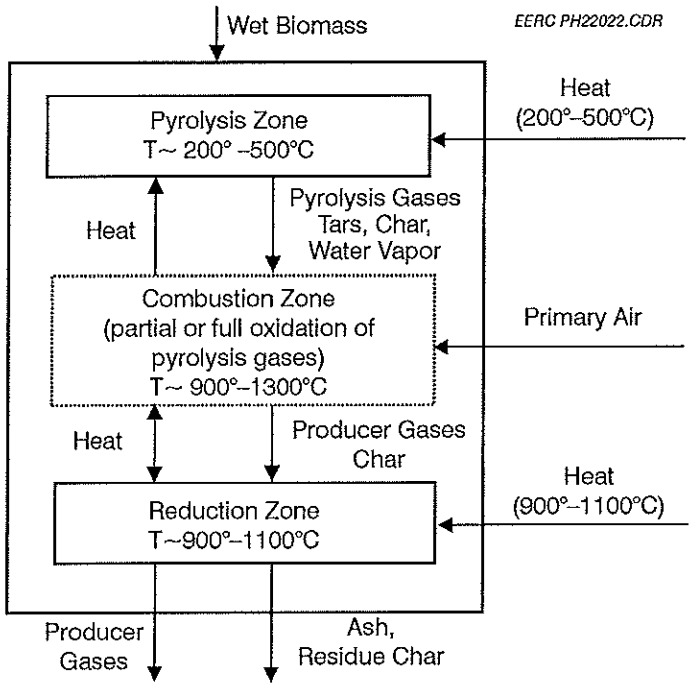

Figure 2. Gasification concept.

biomass in the pyrolysis zone, cracking of the devolatilized products (as well as tars), and the necessary heat for additional reforming in the reduction zone. The extent of reactions in the oxidation zone is dependent upon the amount of injected primary air, which is in turn dependent upon the balance of heat needed to maintain the reduction zone between 900°C and 1100°C. Hot gases from the combustor supply the other source of heat to the reactor.

In their technology review, Devi et al. report typical tar contents on the order of 15–100 mg/m^3 in systems employing fixed-bed multistage gasification, a concept similar in many ways to the proposed gasification concept (4). Miln et al. (6) report typical tar contents in air-blown, atmospheric pressure downdraft gasifiers (a variant of the dual-stage concept) to be of the order 0.01–5 g/m^3. These concentrations compare well with more energy intensive secondary tar scrubbing technologies. Aboltzoglou et al. (7) report tar contents ranging from 4.2 to 30 mg/m^3 after scrubbing with a gas-conditioning module that uses a cooling tower, venturi scrubber, and demister. The tar concentration in the proposed gasifier is expected to be in the lower range because of the large and uniform high-temperature reduction zone formed by indirect heating by the hot combustion gases.

Overall flow control will be provided through independent control of the three input motor controllers. The air supply system provides the input air to the system through a high-flow, low-pressure blower for the cathode air stream and a (relatively) high-pressure, low-flow air pump through the gasification reactor. The first air stream flows to the cathode of the fuel cell and requires a relatively high flow rate of the order of 27 g/sec, with a maximum pressure drop of only 2.84 psi. The second air stream travels through the packed bed of the gasifier, filter train,

SOFC, and downstream components shown in Figure 1 and is estimated to overcome a maximum pressure drop of approximately 10.2 psi through the system. This path requires a very low airflow rate between 1.0 and 2 g/sec. A small compressor sized to deliver high flow rates across a high-pressure drop is very inefficient. The parasitic draw for a single compressor to deliver air to the system is approximately 2.5 kW. In addition, a step-down valve would be required to equalize pressure between the two air streams before to the fuel cell. As a result, two air movers are used instead of one to reduce the overall parasitic draw and cost of the air supply system. A small blower is used to deliver 27 g/sec of air across a 2.84-psi pressure drop through the first air stream. For the second air stream, a small air pump is employed to deliver approximately 1.5 g/sec across a 10.2-psi drop. The maximum parasitic draw from both air movers is only 1.2 kW_e. Both air movers can be controlled independently to minimize the pressure differential between the SOFC cathode and anode. The third motor controller is for the biomass feed control. The biomass feed controller, in conjunction with the reactor air pump will be used to control the fuel flow rate to the SOFC. The cathode blower will control air flow rates to the SOFC. A single programmable logic controller (PLC) can act as the motor controller for all three motors.

The gas outlet of the gasification reactor is designed to minimize entrainment of large char and ash particles. The particulate filter train will use multiple cyclones arranged in series to minimize the particulate level in the gas stream. Each cyclone is designed to accommodate producer gas flow rates in the range of 1.45–3.7 g/s at 800°–1000°C, respectively. The expected pressure drop is approximately 0.17 kPa in each cyclone. The cyclone cut size, defined as the size of particle that will be collected with 50% efficiency, is 7.5 μm for char and 3 μm for ash and carbon fines, resulting in over a 75% reduction in particulate levels for particles down to 3 μm. If additional filtering is necessary, then additional cyclones or a ceramic filter will be included.

Modeling Parameters

Process temperatures, system configuration, component definition, mass, and energy balances were performed using GCTool system modeling software for all system components downstream of the gasification reactor. GCTool is a general computational toolkit developed at the Argonne National Laboratory specifically for designing, analyzing and comparing different fuel cell system configurations. The GCTool software kit contains linkable subcomponent modules for integrating a host of subsystem components into the system design. These include various types of fuel cells, combustors, heat exchangers, and reformers. All subsystem components contain a set of user-defined system constraints that allows the designer to optimize the component for various system configurations.

The input specifications to the GCTool fuel cell module are presented in Table 1. All calculations were assumed to occur at ambient pressure. Cathode air is used for primary heat removal. This requires a stoichiometric air ratio of 5–6. Calculations for the fuel cell analysis were performed with an air input of 27 g/s. The air is preheated to 700°C to prevent thermal shock in the fuel cell. The fuel gas temperature is anticipated to be 950°C, but the low fuel flow rates allow sufficient heat removal with the cathode side air. The fuel flow rate is varied between

1.3–2.9 g/s, depending on the heating value of the producer gas. The SOFC fuel utilization is conservatively anticipated to be 80%.

Since the integrated SOFC–biomass gasifier project utilizes the downdraft gasifier design as the producer gas generator, the gas composition used in the analysis of the complete cycle is based on the values obtained from the equilibrium calculations. The equilibrium calculations were made using the computer program NASA SP-273 developed by Sanford Gordon of the National Aeronautics and Space Administration (NASA) Glenn Research Center at Lewis Field. The calculations were based on the analysis for sulfur- and ash-free wood shown in Table 2.

When the final system design was completed, Fred Robeson of kraftWorks Systems, Inc. (kWS) performed an external verification of a base case system performance to ensure that modeling assumptions and parameters were consistent with industry-accepted standards. The United Technologies Corporation (UTC)/kWS State-of-the-Art Performance Program (SOAPP) was used to simulate the system for kWS. The SOAPP simulation program was originally developed by UTC for gas turbine and fuel cell design analyses and extended by kWS to model complete power plants. The SOAPP SOFC model is based on data from Siemens–Westinghouse (S–W) tubular design in the literature (8, 9). The model assumes a given current density of 2881 amps/m^2, a value based on information on tubular SOFCs from the Electric Power Research Institute (EPRI). The fuel utilization factor and loss factors (resistivities) were input from the literature and are consistent with the EPRI baseline model. The model has been validated against several DOE SOFC representations. The SOAPP reformer model was also validated against both values in the literature and on Industry Foundation Classes data.

Table 1. Fuel Cell Model Specifications

Voltage	Current	Fuel Utilization	Fuel Inlet Temp.	Air Inlet Temp.	Air Inlet Flow	Fuel Inlet Flow
0.7 V	14,286 A	0.8	950°C	700°C	27 g/s	Varies

Table 2. Biomass Fuel Properties

Biomass Moisture, wt%	Stoichiometric Air/Wood Ratio, wt basis	HHV, MJ/kg	Chemical Composition of Wood
0	6.391	22.21	$CH_{1.408}O_{0.589}N_{0.0016}$
10	5.752	19.989	$CH_{1.408}O_{0.589}N_{0.0017}$
20	5.113	17.768	$CH_{1.408}O_{0.589}N_{0.0018}$
30	4.474	15.547	$CH_{1.408}O_{0.589}N_{0.0019}$
40	3.835	13.326	$CH_{1.408}O_{0.589}N_{0.0020}$
50	3.195	11.105	$CH_{1.408}O_{0.589}N_{0.0021}$

Reactor Analysis

In a typical downdraft gasifier, products of pyrolysis and combustion are drawn over a bed of charcoal at temperatures between 800° and 1000°C. At these temperatures, chemical equilibrium is approached fast enough so that thermodynamic calculations can predict important trends and gas compositions. The temperatures, residence times, and gas–solid contacting methods employed in the gasifier strongly affect the degree of attainment of equilibrium. The present-day manufactured downdraft gasifiers (Imbert as well as Stratified types) have reached design maturity and are capable of achieving gas compositions close to equilibrium. In a well-designed autothermal biomass reactor, gasification requires 1.92–2.3 kg of air for each kg of biomass to produce a near-equilibrium gas. More air will produce a higher fraction of combustion products such as CO_2, H_2O, and N_2, which are diluents that reduce the overall system efficiency. Less air will result in unconverted char, as well as increased levels of tar in the producer gas. Unconverted carbon in the gasifier represents unutilized chemical energy, which also results in lower system efficiency. This characteristic of downdraft gasifiers limits the types of fuels available for use and the maximum achievable performance of typical downdraft gasifiers. A brief explanation of the kinetics and limitation of typical downdraft gasifiers will provide insight into the advantages of thermally integrating a downdraft gasifier with an SOFC.

The plot in Figure 3a shows the adiabatic flame temperature (AFT) of a downdraft gasifier as a function of ER, defined as the ratio of actual air-to-fuel ratio to stoichiometric air-to-fuel ratio, and biomass moisture content. The plot shown in Figure 3b depicts the effect of ER on the equilibrium char content for the wood–air reaction at various wood moisture levels. These plots also show the regime of operation for a typical gasifier (Regime I) and the low ER operating regimes (Regime II and III).

The AFT rises very slowly from 639° to 754°C with increasing ER from 0 to 0.25, beyond which it rises much faster with increasing ER. This break in the curve corresponds to the point at which char or carbon gets completely converted. The chemical energy of the producer gas is highest at this point (ER = 0.25). Beyond this ER, the chemical energy reduces to zero as the ER increases to 1 because of oxidation of CO and H_2 in the producer gas. At lower ER, a substantial fraction of unconverted carbon remains in the gasifier, even when operated at high moisture levels. Since the AFT reduces with an increase in the moisture levels, the reaction kinetics, a strong function of temperature, are adversely affected. An ER of 0.25 is the theoretical point at which a conventional air-blown gasifier is expected to produce the best results in terms of achieving a steady-state gas composition close to equilibrium. However, the low AFT at ER = 0.25 (shown in Figure 2b) reduces the reaction kinetics, making it difficult to sustain gasification reactions. Most conventional downdraft gasifiers are operated at an ER in the range of 0.30–0.37 (Regime I), a value slightly higher than the optimum value, to drive the reaction rates.

A typical downdraft gasifier operating in Regime I will oxidize sufficient fuel to provide the necessary exothermic heat profile to drive the endothermic gasification reactions, primarily the Boudouard reaction and the water–gas reactions (the reaction kinetics and mechanisms for carbon/char gasification are well documented in the literature). These reactions control the operating temperature limits of the gasification reactor. The first reaction rapidly establishes equilibrium at temperatures above 1100°C, while the second reaction becomes significant at

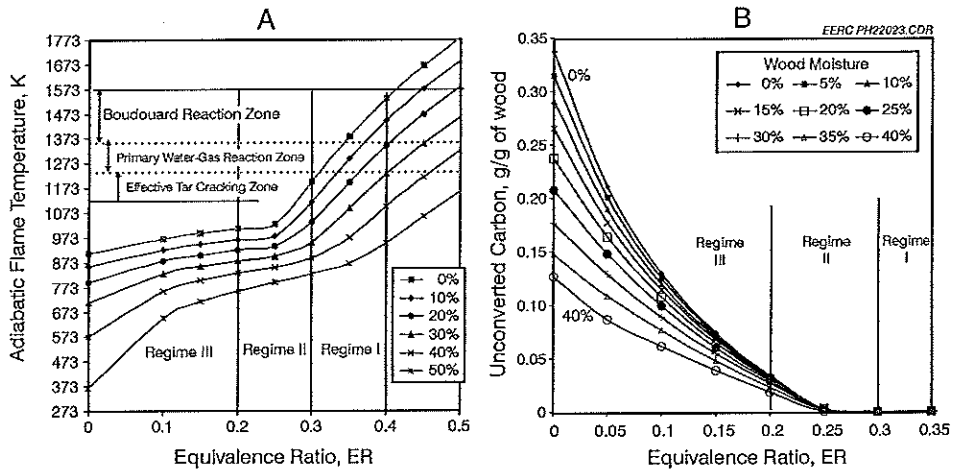

Figure 3. Effect of equivalence ratio on the a) adiabatic flame temperature and b) char conversion for wood with moisture contents ranging from 0% to 50%.

temperatures from 1000° to 1100°C. At lower operating temperatures, the reaction kinetics of both the Boudouard reaction and water–gas reactions decrease substantially. This limits both the wood moisture content and the operating ER in achieving self-sustained gasification. Figure 3 shows that, even under the most optimistic conditions (dry wood and adiabatic enclosure), the minimum ER is 0.30. For biomass with moisture content of 20%, the minimum ER to reach the lower operating temperature range increases to 0.37. However, if the gasifier temperature is maintained above 1000°C by external heating, the kinetic limitations of operating at lower ER and higher biomass moisture content can be eliminated. The thermally integrated SOFC–gasification system for biomass has the capability of maintaining a gasifier operating temperature in the range of 900°–1100°C, owing to the availability of high-temperature SOFC anode-side and cathode-side effluents for heating. This allows the gasifier to operate at extremely low ER and with very wet or "green" biomass as the feedstock.

Figure 4 shows the effect of various reactor operating temperatures and biomass moisture on the unconverted carbon at different ERs. Both ER and reactor temperature affect the unconverted carbon fraction for a given biomass moisture. In the case of dry wood (Figure 4a), no reduction of unconverted carbon occurs, regardless of the temperature, when the reactor is operated at an ER lower than 0.2. Increased biomass moisture will decrease the ER (i.e., air input) necessary for complete carbon conversion at any given temperature. At 20% moisture and a 900°C reactor bed temperature (Figure 4c), the gasifier can be operated down to ER = 0.05 with complete carbon conversion. At 30% moisture, carbon is completely converted if the gasifier is operated at a reactor bed temperature of 800°C or higher. Theoretically, the gasifier can be operated with no air input if the reactor bed temperature is maintained above 800°C for biomass moisture greater than 30%. For biomass moisture greater than 20% and a bed temperature of 900°C, the reactor should be able to operate at an ER as low as 0.05, which for all practical purposes can be considered leakage air with the biomass feed. These limits fix the lower reactor operating temperature at 800°C. The upper limit is fixed primarily by material concerns.

The gas composition for a thermally integrated gasifier and a nonintegrated gasifier (or autothermal reactor) can be modeled by calculating the equilibrium compositions at constant temperature and constant enthalpy conditions, respectively. In contrast to a thermally integrated gasifier, a nonintegrated gasifier is autothermal, and the required heat is obtained by oxidation of fuel fed to the reactor.

The integrated gasification–SOFC system is designed to maximize the available chemical energy in the producer gas by completely converting carbon to fuel gas, unlike that observed in the case of a nonintegrated system. The direct effect of this is to increase output gas calorific value by 50% as compared to a nonintegrated system. This effect is clearly depicted in Figure 5, which compares the dry gas heating value at different ERs and biomass moisture contents from 0% to 50%.

Both cases show the heating value of the producer gas increasing as the ER decreases, but substantial char is left unconverted at ERs less than 0.20 in the case of Figure 4a, sacrificing reactor efficiency for gas heating value. Figure 4d shows complete carbon conversion at 1000°C for biomass moisture greater than 30% at all ERs. For lower moisture levels, an ER in Regime II appropriate to the given moisture content will provide complete carbon conversion. For an externally heated reactor, very high energy gas can be produced at complete carbon conversion, increasing both reactor efficiency and gas quality.

The dry-gas heating value is typically used for conventional systems to quantify reactor performance since tar and moisture-free gas is used for most electrical conversion applications. Also, for accurate measurement in gas analyzers, moisture in the gas is completely eliminated. Therefore, most data are available on a dry basis. In order to have apt comparison between integrated and conventional nonintegrated systems, heating values are calculated on a dry-gas basis, although gas is not cooled in the proposed integrated system.

Figure 6 shows the effect of moisture on the reactor energy output at different ERs when the reactor is operated at 1000°C. In Figure 6, the reactor efficiency, Pe, is the ratio of output chemical energy of the producer gas (higher heating value) to the input chemical energy of the biomass feed. The addition of heat to the gasifier is not summed with the input chemical energy of the biomass.

The plot shows that the maximum theoretical reactor efficiency, when the reactor is maintained at the isothermal temperature condition of 1000°C, occurs at ER = 0.2 for a moisture level of 0.0%, ER = 0.15 for a moisture level of 10%, ER < 0.1 for a moisture level of 20%, and an ER = 0.0 for moisture level greater than 30%. The introduction of external heat for the reduction reactions increases the gasification efficiency from 95% for bone-dry wood to 119% for "green" wood. The efficiency greater than 100% is an indication of maximization of chemical energy in the product gas as a resulting effect of thermal integration with the SOFC. As a comparison, an autothermal (nonintegrated) reactor achieves a maximum cold-gas efficiency of approximately 75%–80% for bone-dry wood. In the case of the proposed gasifier, bone-dry wood provides the lowest reactor efficiency at 95%. Additional moisture increases reactor efficiency up to a biomass moisture of 50%.

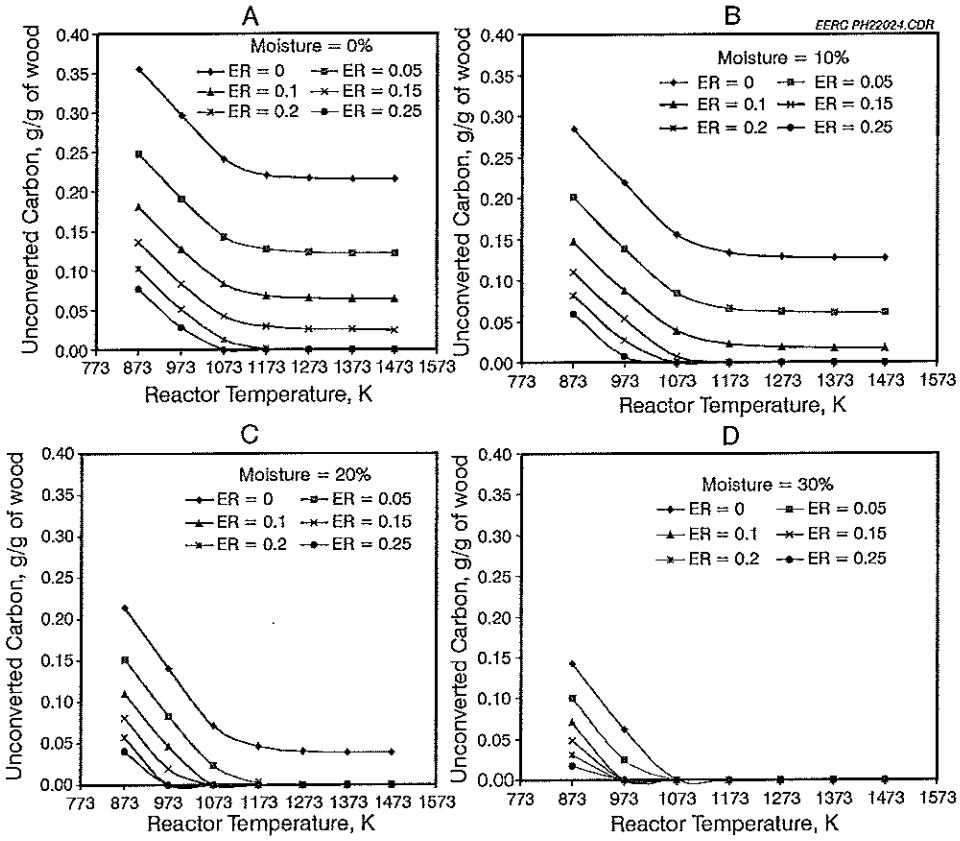

Figure 4. The variation in carbon conversion with reactor temperature as a function of ER at various biomass moistures.

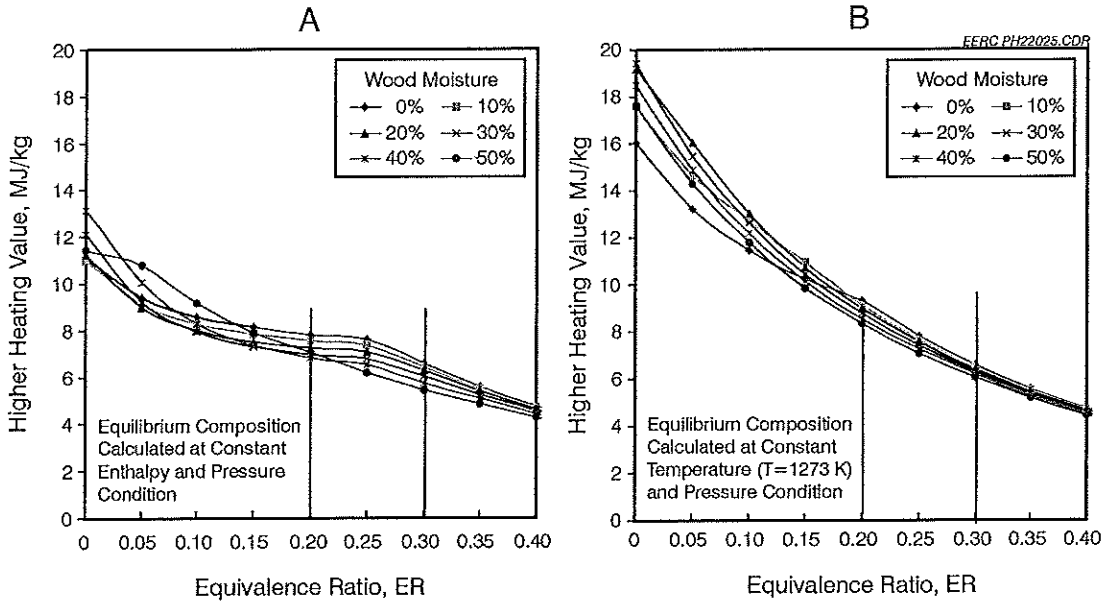

Figure 5. Higher heating value as a function of equivalence ratio for wood at a) constant enthalpy and pressure condition and b) constant temperature and pressure condition.

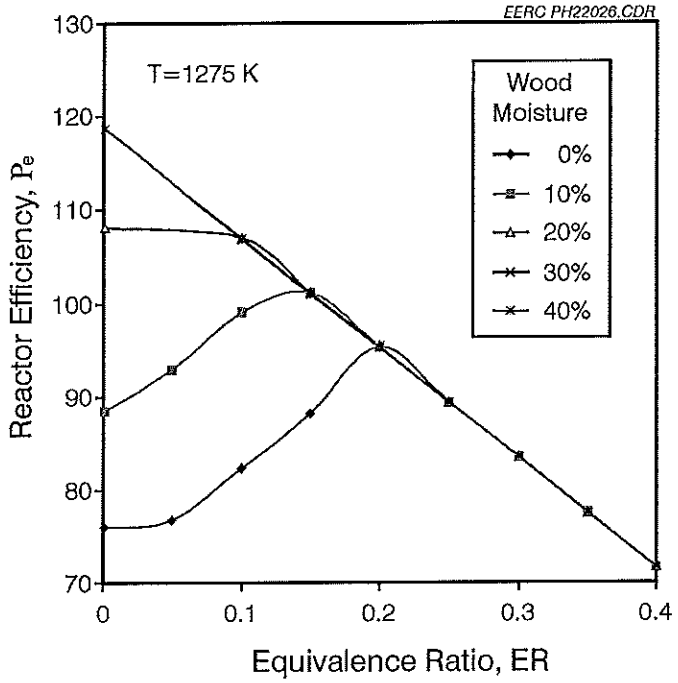

Figure 6. Reactor efficiency as a function of ER.

Reactor output energy greater than input indicates recycling of waste energy from the SOFC effluents into the producer gases through the endothermic Boudouard and water–gas reactions. The reactor reaches maximum cold-gas efficiency between 20% and 30% biomass moisture content. This is the minimum biomass moisture needed to completely reduce the char and pyrolysis gases in the absence of air. Excess biomass moisture above this point does not contribute to increasing the producer gas heating value, since there is no carbon left to convert. It is simply vaporized and exits the gasifier at the same temperature of the producer gases. While the additional moisture does not contribute to the cold-gas heating value of the producer gas, excess water vapor may have a beneficial effect in stabilizing the overall system temperature profile and further reducing tar and particulate levels in the gasifier.

To obtain a producer gas with reasonable gasification efficiencies, conventional gasifiers must limit the biomass moisture level to below 20%. This generally requires additional equipment and operational expenditures for drying the biomass before gasification. Regime I is the typical operating range of conventional downdraft gasifiers. The heating value of the producer gas in this region varies between 4–5 MJ/m^3, for moisture levels below 30%. Since moisture acts as a thermal sink for energy that would otherwise be used for the endothermic gasification reactions, biomass with moisture levels above 30% produce high CO_2 and tar contents for conventional downdraft gasifiers. For this reactor design, the external heat provided by the combustor converts the moisture into an essential gasification medium, allowing a much wider range of biomass moisture levels. The reactor is designed to operate in Regime III, resulting in wet producer gas heating values from 7–12 MJ/m^3. The sensible heat of the SOFC effluents and the heat released through the oxidation of unconverted fuel in the combustor provide sufficient energy to achieve sustained evaporation of moisture in the pyrolysis zone of

the gasifier and promote the gasification reactions and reduction of tars in the reduction zone. Adequate heat transfer to the reduction zone is expected through the reactor wall according to the initial heat-transfer estimates in the case of a packed bed. If poor heat-transfer characteristics occur in the reactor or if the combustor energy is insufficient to maintain the isothermal boundary conditions of 1000°C, additional primary air can be added (increased ER) to increase the interstitial temperatures within the char bed. This will produce a heating value penalty in the producer gas output.

Fuel Cell Analysis

Gas composition can have a significant effect on SOFC operation. The sensitivity of SOFC output characteristics to fuel gas composition was analyzed by Sasaki et al. (8) for simulated producer gases with varying H_2:CO ratios and water vapor concentration. Sasaki et al. experimentally demonstrated cell voltage variations of less than 5% for fuel gases with H_2:CO ratios from 0.43 to 2.3. He also concluded that cell performance was little affected by water vapor concentrations in the fuel gas from 1.1% to 20%.

Figure 7 shows the gas characteristics for the fuel gas entering the SOFC for biomass moisture from 0%–50%. Figure 7a shows the H_2:CO ratio, and Figure 7b shows the expected water vapor content of the fuel gas. The producer gas composition is predicted to vary from a H_2:CO ratio of 0.7 to 1.84 in Regime III, well within the boundary conditions established by Sakai et al. The water vapor concentration in the fuel gas is expected to be 21% for biomass moisture up to 50%.

Carbon deposition is another concern for SOFCs operating on varying fuel gases. The ternary plot shown in Figure 8 is adapted from Sasaki and Teraoka (9). The plot shows the carbon deposition boundary lines for fuels with varying C-H-O ratios. This boundary line is derived from the thermodynamic decomposition of various C-H-O fuels into their equilibria products at 1000° and 800°C. The boundary line is taken at the points where solid carbon formation is thermodynamically favored at a mole fraction of 10^{-6} of the carbon initially present in the fuel. As such it does not take into account carbon formation due to kinetic mechanisms that may occur with higher hydrocarbons and at high current densities. Prior research (10) has shown that carbon formation can occur below this line for higher hydrocarbons. Studies have also shown (13–15) that carbon formation above this line can be suppressed by operating the SOFC at higher current densities, essentially providing additional oxygen flow to the anode. In that case, the boundary lines in Figure 7 may represent the worst-case scenario for producer gases, occurring only during extended no-load or low-load conditions.

The SOFC gas compositions for biomass moisture levels from 0% to 40% are also plotted in Figure 8 for comparison with the carbon deposition lines. The diagram indicates that biomass with moisture levels greater than 30% should experience no carbon deposition problems. Biomass with lower moisture levels is on the boundary and may exhibit problems with carbon deposition under extended no-load or low-load operating conditions. This should not be a problem during normal operation. During extended no-load or low-load conditions, carbon deposition can be suppressed by increasing the air input to the gasification reactor. An increase

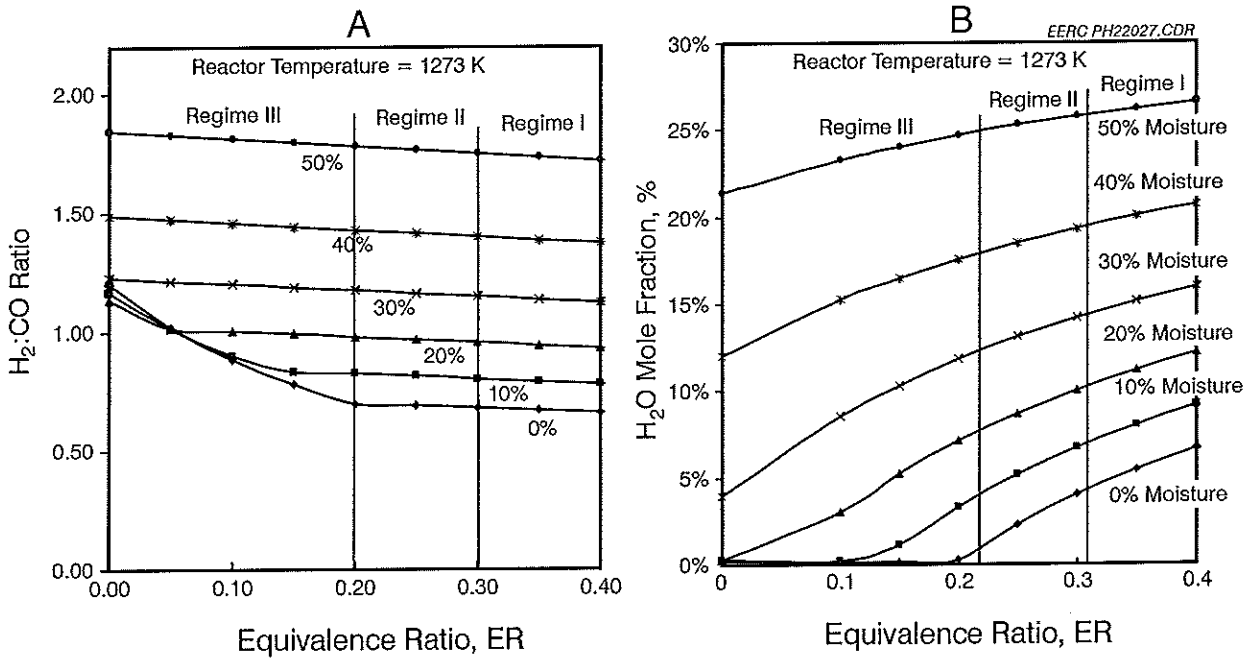

Figure 7. H_2:CO ratio and steam mole fraction in the producer gas.

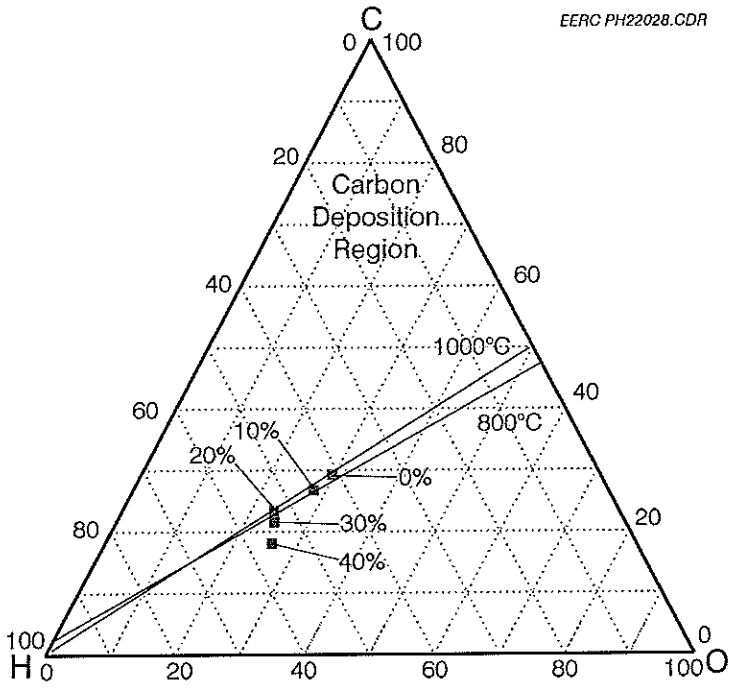

Figure 8. Carbon deposition for various biomass moisture levels.

in the ER in the gasification reactor will shift the fuel gas composition toward the oxygen-rich region in the ternary plot by increasing the H_2O fraction in the producer gas, as shown in Figure 6b.

Another area of concern for most fuel cell systems is sulfur contamination of the fuel cell catalyst. For intermediate temperature SOFCs, sulfur contamination takes the form of physical adsorption onto the nickel catalyst, blocking reactive sites for electrochemical reactions. This type of contamination has been reported to produce reversible SOFC performance degradation ofless than 5% for H_2S levels as high as 500 ppm (14). Other developers show widely varying sulfur specifications for their anode-supported SOFC. Published data show sulfur tolerance levels as low as 1 ppm to levels as high as 3,000 ppm (15). This widely reported range indicates that stack design and operating conditions may play as large a role in sulfur tolerance as material specifications. Nonetheless, the high level of uncertainty in this area dictates that the sulfur content in the fuel gas be kept to as minimum a level as economically feasible. The choice of woody biomass as the initial feedstock is dictated by this requirement. The table in Appendix B shows the proximate/ultimate analysis of typical woody biomass. The majority of woody biomass in the list contain sulfur levels from 0.00% to 0.02%, with ash levels lower than 1% by weight. While very little evidence exists in the literature that can equate this low level of sulfur in the feed to the producer gas H_2S content, in personal experience by one of the authors (Dr. Patel), producer gas H_2S content for woody biomass measured in the range from 1 to 85 ppm, depending on gasification conditions. One goal of the experimental phase in this project is to characterize the fate of sulfur during gasification for different gasification conditions.

Overall System Analysis

The ideal system performance is summarized in Table 3. The ER in Table 3 is the minimum necessary for the system to obtain complete carbon conversion and maintain the isothermal boundary condition of 1000°C for the reactor reduction zone and 400°C for the pyrolysis zone. However, this is based on sufficient heat transfer into the reactor bed and acceptably low tar and sulfur contents within the producer gas. Depending upon the experimental results, the system may be operated under less efficient conditions to ensure acceptable heat transfer into the reactor and acceptable levels of tar and sulfur. This is accomplished primarily by increasing the ER (air input) for a given biomass moisture. The higher ER increases the internal heat released in the reactor at the expense of reactor efficiency.

The maximum system temperature is expected to be in the range of 1080°–1130°C (AFT of the combustor). This temperature is low enough to be within the upper operating limits of 310SS, but high enough to initiate rapid Boudouard and water-gas reaction rates, ensuring gas compositions close to equilibrium. Figure 9 presents the gross system efficiency for biomass moisture levels up to 50% and ERs up to 0.4. The fuel cell conversion efficiency is assumed 38%. However, the high reactor efficiency of 119% increases the overall gross system efficiency to 45%. When inverter and motor power losses are factored in, the net system efficiency drops to 30% for dry wood and 38% for green wood. As the biomass moisture level increases, overall parasitic losses decrease due to the decreased air input requirements for the reactor. While the electrical conversion efficiency increases with the biomass moisture level, the system output effluent temperature decreases. The high-temperature system effluents can be used for additional

Table 3. Ideal System Performance for 10-kWe Biomass Power System

Type	Woody Biomass				
Chemical Composition	$CH_{1.4}O_{0.59}N_{0.017}$				
Ash, wt% basis	0.1%–1.0%				
Sulfur, wt% basis	0.00%–0.02%				
Moisture Content, wt% basis	0%	10%	20%	30%	40%
HHV, MJ/kg	22.2	20.0	17.8	15.5	13.3
Gasifier Conditions					
Optimum ER	0.20	0.15	0.00	0.00	0.00
Feed Rate, g/s	1.243	1.301	1.318	1.424	1.662
Airflow In, g/s	1.589	1.122	0.007	0.006	0.006
Power Input, kW_{th}	27.6	26.0	23.5	22.1	22.1
Power Output, kW_{th}	26.4	26.4	26.4	26.4	26.4
Rx Efficiency	96%	102%	113%	119%	119%
SOFC Input					
CO, % mole basis	40%	40%	44%	42%	34%
H_2, % mole basis	28%	33%	50%	52%	49%
CH_4, % mole basis	0%	0.0%	0.3%	0.0%	0.0%
CO_2, % mole basis	0%	1%	0%	2%	5%
H_2O, % mole basis	0%	1%	0%	4%	12%
N_2, % mole basis	32%	24%	0%	0%	0%
HHV, MJ/kg	9.3	10.9	20.0	18.5	15.8
Gas Temperature, °C	950	950	950	950	950
Flow Rate, g/s	2.832	2.423	1.325	1.430	1.668
Cathode Flow Rate, g/s	27.0	27.0	27.0	27.0	27.0
Cathode Air Temperature, °C	700	700	700	700	700
Combustor Output					
Gas Temperature, °C	1127	1128	1127	1127	1120
Flow Rate, g/s	29.832	29.423	28.325	28.430	28.668
Heat Exchanger					
Hot-Side Gas Temperature Input, °C	1053	1024	974	945	947
Hot-Side Gas Temperature Output, °C	504	469	400	375	386
System Output					
Gas Temperature, °C	456	416	347	308	300
Flow Rate, g/s	29.832	29.423	28.325	28.430	28.668
Efficiency Calculations					
Energy Input, kW_{th}	27.6	26.0	23.5	22.1	22.1
SOFC Input, kW_{th}	26.4	26.4	26.4	26.4	26.4
SOFC Output, kW_e	10	10	10	10	10
SOFC Efficiency	38%	38%	38%	38%	38%
Gross System Efficiency*	36%	38%	43%	45%	45%
Parasitic Losses					
8% Conversion Losses, kW_e	0.80	0.80	0.80	0.80	0.80
Air Pump, 0.57 kW max	0.18	0.13	0.00	0.00	0.00
Blower, 0.8 kW max	0.56	0.56	0.56	0.56	0.56
Feed Screw, 0.15 kW max	0.11	0.12	0.12	0.13	0.15
Discharge Screw, 0.15 kW max	0.01	0.01	0.01	0.00	0.00
Total Losses, kW_e	1.66	1.61	1.49	1.50	1.52
Net Power Output, kW_e	8.34	8.39	8.51	8.50	8.48
Net System Efficiency	**30%**	**32%**	**36%**	**38%**	**38%**

* Gross efficiency neglects parasitic losses.

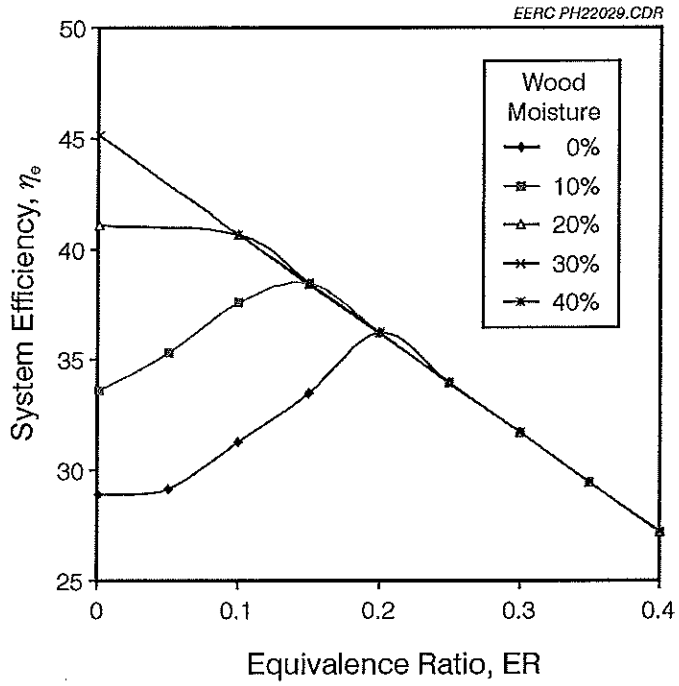

Figure 9. Gross system efficiency.

process heat or space heating needs. If the initial feedstock has an unacceptably high moisture level, the system effluents may be used in an evaporator, essentially increasing the overall biomass moisture range.

Economic Analysis

Table 4 provides a capital cost summary for the 10-kWe demonstration plant and a projected costs summary of the 200-kWe system. The costs for the 10-kWe unit include the power converter suitable for grid connectivity, the biomass feed system, the ash extraction system, and the hoppers for feed and ash removal. Equipment costs for the motors, the heat exchanger, the inverter, and the control instrumentation are quoted at retail prices. For smaller systems, material costs are often limited to minimum purchase requirements resulting in very large material waste factors. In this case, the material costs are prorated only for materials used. The labor cost is an estimate of construction time at $50/hr. Since the 10-kWe demonstration system is not anticipated to be large, no provision was included to account for foundations or other support structures. For the larger system, however, the cost summary includes a provision to purchase a trailer and feed conveying equipment. The material cost estimates for the larger system assumes a simple scale-up of the 10-kWe system design. The labor estimate for the 10-kWe unit includes a significant contingency to address unanticipated issues that may occur in fabricating a one-of-a-kind gasifier for the first time. The labor estimate for the larger system assumes a 50% decrease in the per-kWe labor costs for fabricating larger, repeat units. Power conditioning costs for a 200-kWe system are not readily available off-the-shelf. These estimates were the result of phone conversations with equipment manufacturers and solar power system

Table 4. Capital Cost Summary

10-kWe System Cost Estimates		
System Components	System Costs	Per-kWe Costs
Gasification System Materials	$11,874	$1187
Power Conditioning Equipment	$7530	$753
Labor	$7500	$750
Piping, Controls, Accessories	$3294	$329
FC Stack	$3000	$300
Trailer Mount	N/A	N/A
Total	$33,198	$3319
200-kWe System Cost Estimates		
System Components	System Costs	Per-kWe Costs
Gasification System Materials	$71,000	$355
Power Conditioning Equipment	$100,000	$500
Labor	$75,000	$375
Piping, Controls, Accessories	$17,617	$88
FC Stack	$60,000	$300
Trailer Mount	$30,000	$150
Total	$353,617	$1768

manufacturers (18, 19). Without a specific design for the larger system, the uncertainty level is high. Consequently, the capital cost summary for the 200-kWe system should be considered a ballpark figure. Actual costs can be higher or lower. As an example, the assumption of a simple scale-up to the gasifier probably inflates the overall material cost estimates. Ceramic casting material could be used in place of much of the 310SS with some minor design changes. It should also be noted that retail costs for 310SS are unstable. Direct cost quotes on 310SS, only several days apart, have shown variances of 10%–20%. Nevertheless, the 200-kWe system was included to illustrate the economic potential of this concept at more practical system size ranges.

The SOFC stack is anticipated to cost approximately $300/kWe, based on a literature review (20, 21). However, entry-level costs are expected to be significantly higher. A long term sensitivity analysis was performed for SOFC stack costs as high as $2000/kWe.

If SOFC stack costs meet projections, the dominant system costs for the 10-kWe system are the gasification system materials costs (including combustor, recuperater, and cleanup train) and power conditioning equipment costs. The total capital cost is estimated to be $3320/kWe. The high net efficiency of the design reduces mass throughput for a given power size in half compared to more conventional systems. This, in turn, reduces the overall size of the system, allowing material costs to scale very favorably on a per-kW basis as system size increases. For a 200-kWe system, material costs for the gasification system are projected to decrease from $1187/kWe to approximately $355/kWe. Total capital costs fall to approximately $1800/kWe. In the short term, however, stack costs are expected to be substantial and may outweigh other components by a significant margin for the next few years. For SOFC stack costs of $1000/kWe, the 10-kWe demonstration unit will increase to $4020/kWe. The 200-kWe system is projected to cost less than $2500/kWe.

The COE is calculated based on the fuel cost, maintenance costs, and capital recovery costs. Maintenance costs do not include additional operating labor, as the system is expected to run automatically and is initially targeted toward farms or other biomass waste producers that are currently managing a waste product. Presumably, no additional labor over current waste management procedures will be necessary to operate the system. The COE estimate also does not factor in salvage values for equipment and the fuel cell stack. In practice, a high salvage value for the fuel cell stack and other equipment may result in an additional reduction in COE. Table 5 shows the projected COE for the demonstration unit and the larger 200-kW_e system. Capital recovery costs are based on a 7% loan over a 10-year period. The biomass fuel costs are assumed to be $5/ton. The maintenance costs are calculated in 5-year intervals for stack and motor replacements and 20-year intervals for inverter and control electronics replacements and are averaged over the life of the equipment to provide the annual O&M costs.

Sensitivity Analysis

For the case given in Table 5, the COE varies from 4 to 7 cents/kWh during the capital recovery period, depending on the initial capital investment. Since the capital recovery costs are the principal cost factor in determining the COE, it should come as no surprise that both the stack costs and the financing terms have the largest impact in COE. For every $100/$kW_e$ increase in SOFC stack costs, the COE will increase by 0.4 cents/kWh ($0.004/kWh). Each percentage point increase in the interest rate will raise the COE by 0.25 cents. The COE will also increase by 0.6 cents for every $10/ton-increase in fuel costs. Conversely, the COE will decrease by a proportional amount if the fuel has a negative value. Since the system is hydrophilic in nature, moisture level in the biomass does not impact the COE for biomass moisture below 50%. After the capital costs are recovered, the COE due to fuel costs and annual O&M costs is expected to drop to less than 2 cents/kWh. The low operating costs provide an attractive rate of return over the long term.

Table 5. Cost of Energy Projections

Size, kW_e	10	200
Stack Costs, $/$kW_e$	$300	$300
Capital Cost, $	$33,200	$353,600
Rate	7%	7%
Loan Term, years	10	10
Annual Payment, $	($4727)	($50,345)
Biomass Moisture, %	30%	30%
Fuel Costs, $/ton	$5	$5
HHV, MJ/kg	15.5	15.5
Gross Elect. Eff., % HHV	45%	45%
Feed Input, kW_{th}	22.2	444.4
Annual Feed Input, tons/yr	50	994
Annual Fuel Cost, $	($248)	($4969)
Capacity, %	**100%**	**100%**
Annual O&M, $	($1240)	($19,263)
COE, $/kWh	0.071	0.043

Table 6 summarizes the parameters used in the 20-year economic evaluation. The investment performance over 20 years for the 10-kWe prototype and the 200-kWe system ($1800/kWe assumed) is provided in Table 7. These calculations assume an electricity rate of 7 cents/kWh and credit for process heat at $5/MMBtu. Maintenance costs are calculated in 5-year intervals for stack and motor replacements and 20-year intervals for inverter and control electronics replacements. A salvage value of 10% of initial capital costs is assumed after 20 years. The fuel cost in this case is assumed $0/ton.

Simple payback for the base case is within 6 years for the 10-kWe system and 3 years for the 200-kWe system. The internal rate of return over the 20-year evaluation period is 17.07% and 34.95% for both systems, respectively. These calculations do not take into account tax credits or other types of subsidies for renewable energy systems. If factored in, these would undoubtedly make the systems even more economically attractive.

Input parameters were varied from the base case assumptions given in Table 6 to determine the sensitivity of the long-term rate of return and simple payback period to variances in the base assumptions. Table 8 provides a summary of the sensitivity analysis over the 20-year evaluation period for variances in fuel costs, SOFC stack costs, electricity credits, and heating credits.

The larger system is less sensitive to variances to input parameters and has a simple payback period in a little over half the time of the 10-kWe system. In almost all cases, the internal rate of return for the 200-kWe system is double that of the 10-kWe case. Surprisingly, fuel costs have only a moderate effect on the payback period, especially for the 200-kWe system. Table 7 shows that a $30/ton difference in fuel costs provided essentially the same payback

Table 6. Assumptions for a 20-year Economic Evaluation

	10-kWe System	200-kWe System
Capital Cost	**$33,198**	**$353,617**
Electricity, kWh	74,489	1,489,788
Rate, $/kWh	$0.07	$0.07
value	$5214	$104,285
Waste Heat, MMBtu	268	5361
Rate, $/MMBtu	$5	$5
value	$1340	$26,805
Fuel Costs, $/ton	$0	$0
Annual Fuel Costs	$0	$0
Total Revenue	**$6554**	**$131,090**
Maintenance Costs		
5 year	$4194	$70,817
20 year	$8030	$102,000
20-year Salvage Value, 10%	$3320	$35,362

Table 7. Investment Performance over a 20-year Time Period

Investment Performance over 20 years (zero-cost fuel)				
	10-kWe Biomass Power System		200-kWe Biomass Power System	
End of Period	Net Cash Flow	Cumulative Present Worth	Net Cash Flow	Cumulative Present Worth
		0%		0%
0	($33,198)	($33,198)	($353,617)	($353,617)
1	$6554	($26,644)	$131,090	($222,526)
2	$6554	($20,090)	$131,090	($91,436)
3	$6554	($13,535)	$131,090	$39,654
4	$6554	($6,981)	$131,090	$170,744
5	$2360	($4,621)	$60,273	$231,017
6	$6554	$1933	$131,090	$362,107
7	$6554	$8488	$131,090	$493,198
8	$6554	$15,042	$131,090	$624,288
9	$6554	$21,596	$131,090	$755,378
10	$2360	$23,956	$60,273	$815,651
11	$6554	$30,511	$131,090	$946,741
12	$6554	$37,065	$131,090	$1,077,831
13	$6554	$43,619	$131,090	$1,208,922
14	$6554	$50,173	$131,090	$1,340,012
15	$2360	$52,533	$60,273	$1,400,285
16	$6554	$59,088	$131,090	$1,531,375
17	$6554	$65,642	$131,090	$1,662,465
18	$6554	$72,196	$131,090	$1,793,556
19	$6554	$78,750	$131,090	$1,924,646
20	($2350)	$76,400	($6365)	$1,918,281
MARR*	15.0%		15.0%	
Present Worth	$3646		$397,105	
Annual Worth	$582		$63,442	
Future Worth	$59,669		$6,499,237	
Internal Rate of Return	17.07%		34.95%	
External Rate of Return	16%		19%	

* Minimum attractive rate of return.

Table 8. Sensitivity Analysis of 20-year Economics

20-year Sensitivity-to-Fuel Costs				
	10-kWe System		200-kWe System	
Fuel Costs, $/ton	Internal Rate of Return	Simple Payback	Internal Rate of Return	Simple Payback
($15)	20%	5.5	39%	2.8
($10)	19%	5.7	38%	2.9
($5)	18%	6.0	36%	3.0
$0	17%	6.2	35%	3.2
$5	16%	6.6	33%	3.3
$10	15%	6.9	32%	3.5
$15	14%	7.3	30%	3.6
20-year Sensitivity-to-Fuel Cell Costs				
	10-kWe System		200-kWe System	
Stack Costs, $/kWe	Internal Rate of Return	Simple Payback	Internal Rate of Return	Simple Payback
$300	17%	6.2	35%	3.2
$500	15%	7.2	30%	3.8
$1000	10%	10.3	20%	5.9
$1500	5%	15.5	13%	9.3
$2000	-2%	26.2	5%	15.8
20-year Sensitivity-to-Heating Rates				
	10-kWe System		200-kWe System	
Heating Credits, $/MMBtu	Internal Rate of Return	Simple Payback	Internal Rate of Return	Simple Payback
$0	12%	8.4	27%	4.2
$3	15%	6.9	32%	3.5
$4	16%	6.6	33%	3.3
$5	17%	6.2	35%	3.2
$6	18%	5.9	37%	3.0
$7	19%	5.7	38%	2.9
$8	20%	5.4	40%	2.8
$9	21%	5.2	41%	2.7
20-year Sensitivity-to-Electricity Rates				
	10-kWe System		200-kWe System	
Electricity Credits, $/kWh	Internal Rate of Return	Simple Payback	Internal Rate of Return	Simple Payback
$0.03	5%	14.2	16%	6.8
$0.05	12%	8.7	26%	4.3
$0.07	17%	6.2	35%	3.2
$0.09	22%	4.9	44%	2.5
$0.11	27%	4.0	52%	2.1
$0.13	32%	3.4	61%	1.8
$0.15	36%	2.9	70%	1.5

period (less than 1-year difference) for the 200-kW_e system and a 9% difference in the rate of return. The smaller system was a little more sensitive to fuel costs, showing a simple payback period difference of approximately 1.5 years. Variances in the credit-for-process heat also have a moderate effect on the long-term economics. When zero credit is given for process heat, the simple payback for the 10-kW_e demonstration system increases to 8 years, with an overall rate of return of 12%. The 200-kW_e system has a payback in 4 years, with a rate of return of 27%. A variance of $5/MMBtu provides a difference of 6% for the smaller system and 9% for the larger system. However, the base case assumes a biomass moisture level of 30%. Biomass with very low moisture levels (less then 10%) will exhaust approximately 50% more heat. In that case, as long as the additional energy is not needed to process or dry the biomass, the system may show slightly greater sensitivity to variances in heating costs.

The fuel cell stack costs and the electricity rates have the greatest impact on the long-term economics. Stack costs as high as $1000/$kW_e$ will provide a 10% return rate for the 10-kW_e system and 20% return rate for the 200-kW_e system. The simple payback period is 10 and 6 years, respectively. Above a stack cost of $1000/$kW_e$, the smaller system is not economically viable without external subsidies or credits. However, even with stack costs as high as $1500/$kW_e$, the 200-$kW_e$ system still provides a rate of return comparable to the long-term performance of the stock market. The electricity rates also have a very strong influence on the internal rate of return and payback period. A slight increase or decrease in the electricity rates over the baseline assumption of 7 cents/kWh affects the payback period by over 2 years for the 10-kW_e system. For the larger system, the internal rate of return increases by more than 5% for every cent increase in the electricity rate. This makes the system an extremely attractive buy for distributive generation in remote or rural areas where the electricity rates can often exceed 10 cents/kWh.

In this system, the SOFC serves as the enabling technology. The high gas-to-electricity conversion efficiency of the SOFC increases the system efficiency on the tail end, while the high-energy effluents from the SOFC increase the biomass-to-gas conversion efficiency on the front end. The net system performance of 38% HHV efficiency is unprecedented for a 10-kW_e biomass power system. The closest comparison can probably be made with medium- to large-size gasifier–IC engine or microturbine systems. Many medium to large (500 to 10,000 kW) biomass gasification power plants boast efficiencies of 20%–22% (3), but are still in the development phase. Even conventional fuel cell gasification designs are expected to achieve only a modest increase of only 25% in conversion efficiency over conventional designs.

Although the conversion efficiency is impressive, a more important characteristic is the hydrophilic nature of the design. Moisture in the biomass is converted into an essential gasification medium. The optimum biomass moisture level is in the range of most waste biomass and green wood, typically 25%–40%. This decreases the operational cost of drying biomass and the associated capital investments in the drying equipment. Likewise, the system does not emit a liquid waste stream, typical for most gasification systems. This decreases the operational costs of (hazardous) waste removal and the capital costs associated with waste storage and mitigation. The overall workflow is streamlined from biomass feed to ash disposal. The unique combination of scalability, biomass moisture range, and high efficiency increases the range of viable biomass fuel sources.

SECTION II: GASIFICATION EXPERIMENTS

The goal for this work was to construct, test, and characterize the performance of the biomass reactor under simulated operating conditions to more accurately predict the gasifier performance in an integrated system. A 10-kW_{th} bench-scale reactor was constructed and tested on a variety of biomass and MSW fuels. The power system is designed to operate at elevated temperatures (>600°C) from the output of the gasification reactor to the heat exchanger for preheating the cathode side air. The choice of actual operating temperature is dictated by material constraints, reaction rates, and the fuel cell operating characteristics. As the reactor operating temperature increases, the gasification reaction rates increase, allowing close-to-equilibrium compositions to be attained at designed gas residence times. Higher operating temperatures also increase the tar-cracking reactions.

The producer compositions presented in Table 3 are equilibrium gas compositions calculated for a reactor operating at a temperature of 950°C. Reactor operating temperatures between 800° and 1100°C provided similar equilibrium gas compositions. The latter temperature is the upper operating range of SS 310, the current material of choice for reactor construction. The former temperature is the minimum temperature necessary for reasonable reaction rates in the gasifier. The ideal operating temperature is high enough to ensure good gasification reaction rates, but low enough to allow the use of more common stainless steel materials to be used for reactor construction to minimize capital costs.

The gasification experimental was designed to determine the full operating range of the gasifier. For different feed conditions, the gasifier was operated under various levels of heat assist. Heat-assisted gasification increases gas energy density and gas quality from the gasifier. In this mode, the gasification reaction zone is maintained within a narrow temperature zone by an external heat source, in this case, a natural gas combustor. In a working system, the natural gas combustor is replaced by the fuel cell exhaust combustor.

Experimental Apparatus

For the gasification experimental, a laboratory-scale gasification system capable of simulating the range of operating conditions from self-sustained gasification to fully heat-assisted gasification was constructed. Figure 10 shows the schematic diagram of the gasifier experimental apparatus. Figure 11 provides a photo of the experimental apparatus after construction. A 10-kW_{th} packed-bed gasifier is auger-fed from a closed hopper at feed rates up to 2.27 kg/h (5 lb/h). The biomass feed (typically wood chips) enters a packed-bed gasifier at the top of the reactor. Ash and char are extracted through an auger at the bottom of the reactor and transported to a smaller extraction hopper. For reactor start-up and to simulate heat assist of the gasification zone, a natural gas combustor is used. The natural gas combustor is an off-the-shelf combustor that was modified to allow the injection of producer gas from the outlet of the gasifier into the hot zone of the combustor. The combustor effluent convectively heats the gasification zone of the reactor and is exhausted to the atmosphere. Primary air is injected through the top of the reactor for the gasification reactions. Nitrogen purge is introduced to the reactor through the top of the gasification reactor and feed hopper.

The output of the gasification reactor passes through two particulate cyclone filters in series. At this point, the bulk of the gas passes through a series of cold-water condensers before being injected into the hot zone of the combustor. The gas flow rate is measured between the condensers and the combustor. A slipstream of producer gas is isokinetically extracted from the bulk producer gas between the cyclone train and the cold-water condenser train. The producer gas sample immediately passes through a hot ceramic filter maintained at 450°C to quantify the particulate levels. The producer gas sample is then cooled by a cold-water condenser and passed through a series of anisol impingers for tar quantification. After the tars are extracted, the producer gas sample is passed through a calcium chloride bed to dry it before passing it through a gas analyzer. The gas analyzer determined the percentage of H_2, CO, CO_2, CH_4, and O_2 in the dry gas sample. Nitrogen levels in the dry gas sample are calculated by difference.

Limitations of Gasification Reactor Experimental Apparatus

A source of experimental uncertainty is the difference in the temperature and mass flow rate characteristics between the natural gas combustor and the fuel cell exhaust combustor in the system design. The natural gas combustor is an off-the-shelf combustor with a maximum designed power output of 115 kWth when using natural gas. For a given power output, the fuel cell combustor exhaust temperature is expected to be significantly higher than the natural gas combustor. The result is that the natural gas combustor requires a higher power output to simulate a given isothermal reaction condition in the gasifier. The minimum combustor output in the experimental apparatus was 5 kWth when using natural gas. The range needed to maintain the desired temperatures was 5–9 kWth. To account for this difference, the gasifier output is analyzed with respect to the reaction temperature of the gasifier bed.

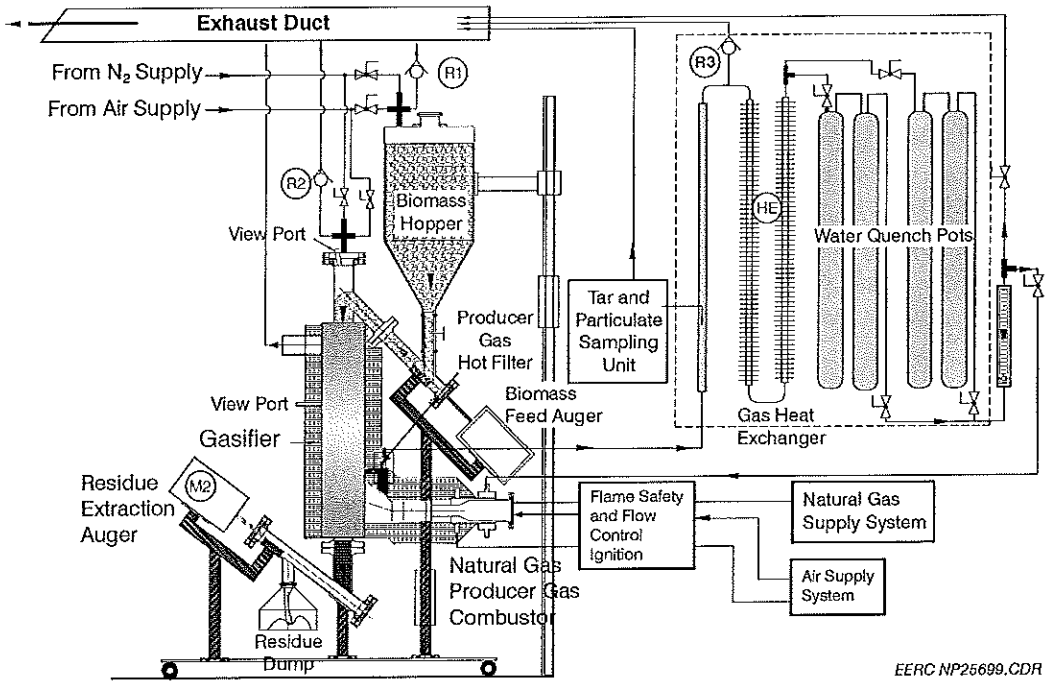

Figure 10. Gasifier experimental apparatus.

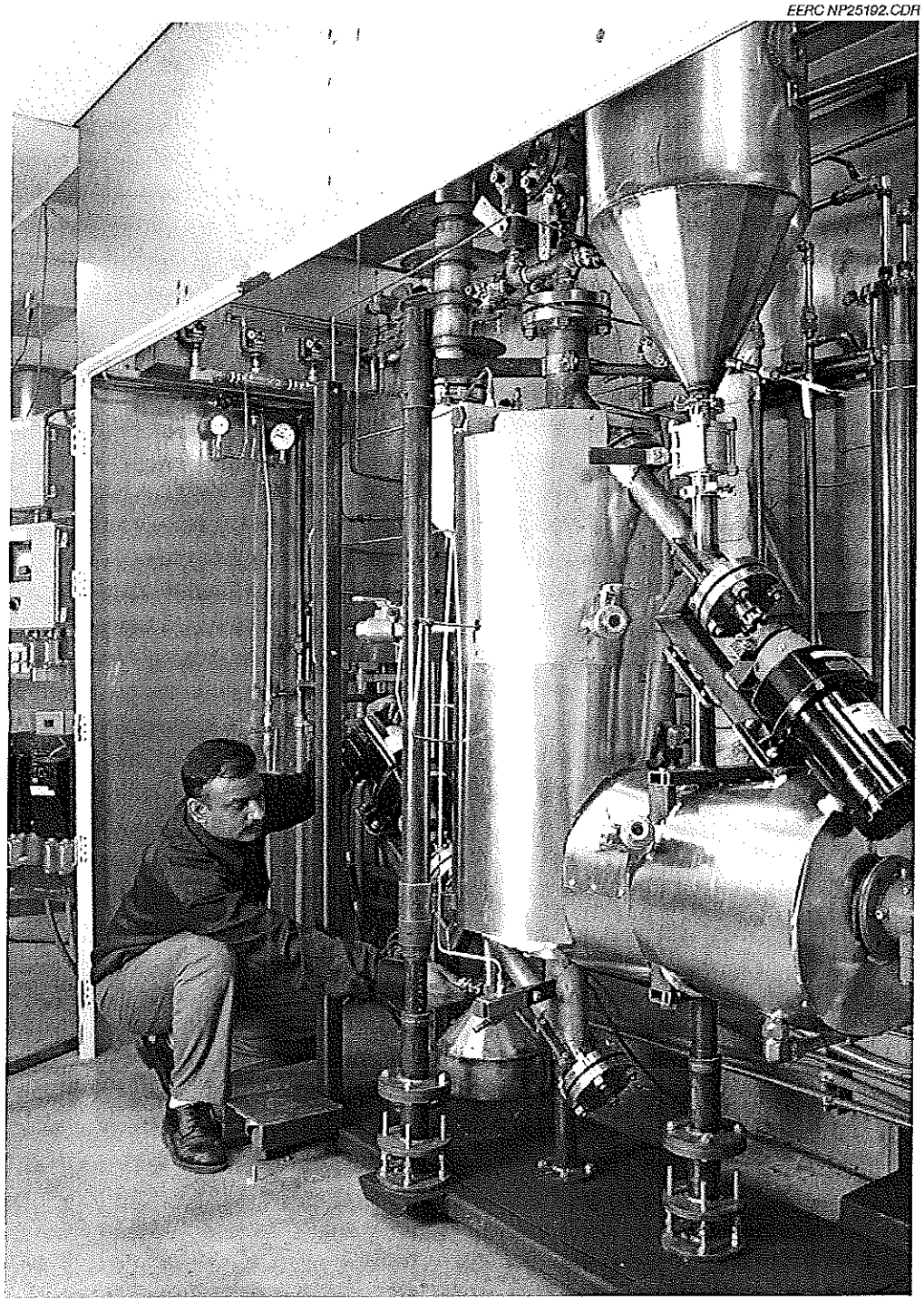

Figure 11. Photo of experimental apparatus after construction.

Gasifier Performance on Biomass

Wood chips and wood char with moisture levels below 10% provide ideal gasifying conditions for conventional gasifiers. Higher-moisture biomasses are often problematic with respect to producer gas tar levels and volumetric energy density. The heat assist characteristic of this gasifier, made possible by integration with the SOFC, reverses these characteristics. High-moisture biomass, typical of green wood, provides the highest potential for recycling the waste heat into the producer gas. The high moisture levels and uniform high temperatures in the gasification zone provide the optimal conditions for effective tar cracking. Because of time limitations, the bulk of the experimental operated in the high-biomass-moisture region to quantify the ability of the gasifier to crack tars and recycle high-quality waste heat, indicative of the SOFC effluent characteristics, back into the producer gas.

Table 9 shows the input conditions of the gasification experiments. With the exception of Test 3, waste pinewood was used for the bulk of the experiments. In Test 3, commercially available oak wood pellets were used. The oak wood pellets were purchased at a local hardware store and were designed for use in wood-burning stoves. The waste pinewood was obtained from a local sawmill as small irregular-shaped pieces. The size of the softwood was reduced using a hammer mill. Photos of the oak wood pellets and reduced-size pinewood are shown in Figure 12. Proximate–ultimate analyses were performed on the pinewood and oak wood pellets, and results are presented in Table 10. The pinewood was received with approximately 5.5% moisture level and 0.15% ash on a weight basis. To simulate higher-moisture-level waste wood, indicative of green wood, the pinewood cubes were soaked in a known amount of water and stored in an

Table 9. Biomass Gasification Test Conditions

Test No.	Moisture, % w/w	HHV, Mj/kg	Biomass Consumed, g	Steady-State Duration, sec	Biomass Feed Rate, g/s	Air Flow Rate, g/s	Equivalence Ratio
1	5.50	18.0	5365	13075	0.4103	0.7788	0.34
2	7.35	17.7	9618	18780	0.5121	0.7788	0.28
3	30	13.4	1223	6329	0.1933	0.0779	0.10
4	30	13.4	4801	15499	0.3098	0.3894	0.30
5	30	13.4	8000	17056	0.4690	0.7788	0.40
6	30	13.4	1449	10339	0.1402	0.0000	0.00
7	30	13.4	361	1040	0.3472	0.2726	0.19
8	30	13.4	275	1166	0.2359	0.1168	0.12
9	30	13.4	438	1570	0.2790	0.1557	0.14
10	30	13.4	563	3572	0.1575	0.0390	0.06
11	30	13.4	1575	7940	0.1984	0.0778	0.10
12	30	13.4	1335	10358	0.1289	0.0000	0.00
13	40	11.5	2807	20168	0.1392	0.0000	0.00
14	40	11.5	682	2508	0.2718	0.0787	0.08

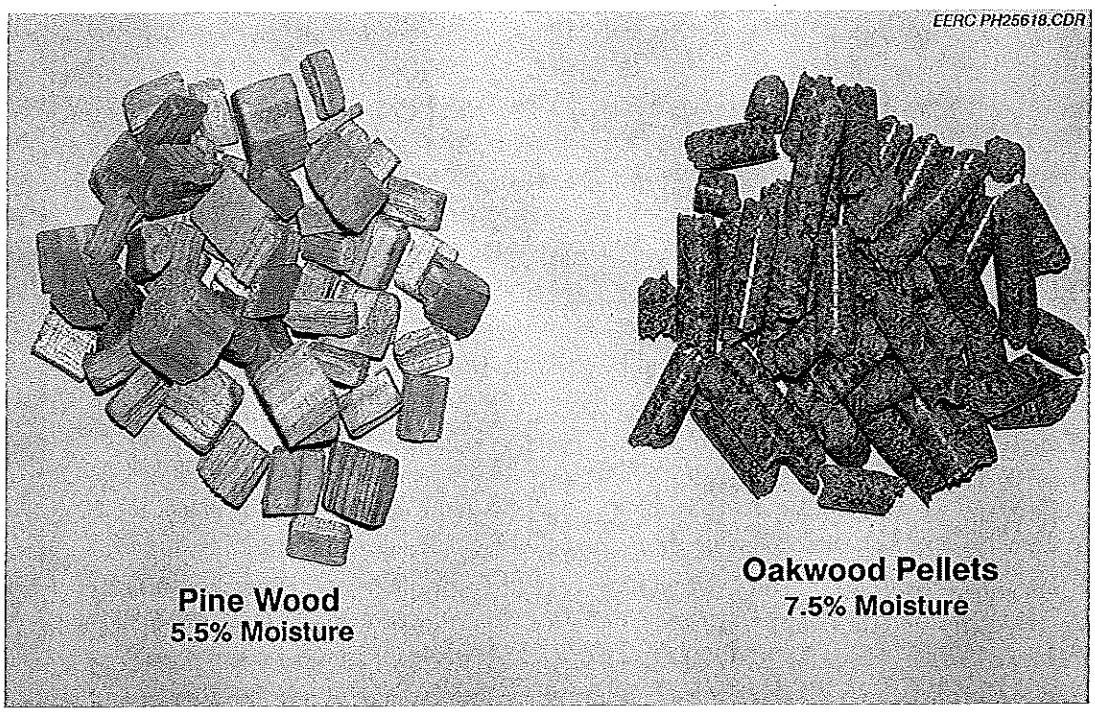

Figure 12. Photos of oak wood pellets and reduced-size pinewood.

Table 10. Proximate–Ultimate Analysis of Pine and Oak Wood Pellets

Proximate Analysis, dry basis, % w/w	Pinewood	Oak Wood (tan oak)
Volatile Matter	84.83	87.1
Fixed Carbon	15.01	12.4
Ash	0.16	0.5
Ultimate Analysis, dry basis, % w/w		
Hydrogen	6.12	6.12
Carbon	49.22	48.34
Nitrogen	0.16	0.03
Sulfur	0.22	0.03
Oxygen	44.12	44.99
Ash	0.16	0.5
Higher Heating Value, MJ/kg	19.1	19.12

airtight plastic container. The saturated moisture in the biomass was observed to have achieved uniformity within 2 days; however, the minimum storage period was 1 week. Prior to each experiment, samples of the pinewood were tested for moisture in order to verify the biomass moisture level.

A total of 14 experiments were performed. Two experiments were performed on low-moisture biomass: one with the oak pellets and one with pinewood. Ten experiments were

performed with 30% moisture pinewood, and two experiments were performed with 40% moisture pinewood.

Gasifier Reaction Rates and Gas Compositions

Tables 11–13 show the producer gas characteristics for each experiment. The gas analyzer for the test apparatus required clean, dry gas for accurate measurements. The CH_4, CO, CO_2, H_2, and O_2 represent direct measurements of the producer gas after tars, particulates, and water were extracted. The N_2 levels in the dry gas compositions were calculated through difference. The hot-gas composition was determined through nitrogen balance. The moisture in the gas was increased until the dry gas equivalent of the hot-gas composition matched the measured values. All experiments were conducted at 100% carbon consumption.

Table 11. Measured Gas Composition Compared to Equilibrium Gas Composition for Five Test Conditions

		CH_4	CO	CO_2	H_2	O_2	H_2O	N_2
Test 14	Equilibrium (wet basis)	0.1	25.3	8.4	39.1	0.0	16.5	10.5
	Equilibrium (dry basis)	0.1	30.4	10.1	46.8	0.0	0.0	12.6
	Measured	2.8	29.2	11.7	43.3	0.0	0.0	13.0
Test 13	Equilibrium (wet basis)	0.0	30.9	6.9	47.6	0.0	14.5	0.1
	Equilibrium (dry basis)	0.0	36.1	8.1	55.7	0.0	0.0	0.1
	Measured	1.5	42.0	3.2	52.2	0.0	0.0	1.1
Test 12	Equilibrium (wet basis)	0.0	39.0	4.1	50.4	0.0	6.3	0.1
	Equilibrium (dry basis)	0.0	41.7	4.4	53.8	0.0	0.0	0.1
	Measured	1.3	42.0	3.3	52.1	0.0	0.0	1.3
Test 6	Equilibrium (wet basis)	0.0	39.0	4.1	50.4	0.0	6.3	0.1
	Equilibrium (dry basis)	0.0	41.7	4.4	53.8	0.0	0.0	0.1
	Measured	2.6	38.0	6.4	53.0	0.0	0.0	0.0
Test 2	Equilibrium (wet basis)	0.0	27.9	6.2	22.9	0.0	5.9	37.0
	Equilibrium (dry basis)	0.0	29.7	6.6	24.3	0.0	0.0	39.3
	Measured	1.8	28.1	7.2	21.8	0.0	0.0	35.2

Table 12. Performance of Gasifier Operated at ER Close to Zero Using Biomass Containing 30% and 40% Moisture

		Test 12	Test 6	Test 10	Test 13	Test 14
Moisture, wt%		30	30	30	40	40
Biomass HHV, MJ/kg		13.37	13.37	13.37	11.46	11.46
Biomass Injection Rate, g/s		0.1289	0.1402	0.1575	0.1392	0.2718
Gasification Air Flow Rate, g/s		0.00	0.00	0.039	0.00	0.08
Equivalence Ratio		0.00	0.00	0.06	0.00	0.08
Bed Temperature, °C		900	900	925	900	900
		Energy Balance				
Biomass Thermal Input, kWth		1.723	1.874	2.106	1.595	3.115
Reactor Output, kWth		2.369	2.597	2.485	2.269	3.846
Difference,* kWth		1.121	1.170	1.111	1.330	1.295
		Gas Composition				
Measured Dry Gas Composition, vol%	CH_4	1.33	2.65	2.27	1.52	2.82
	CO	42.00	37.98	33.08	41.95	29.19
	CO_2	3.25	6.39	8.54	3.18	11.70
	H_2	52.11	52.99	42.21	52.21	43.29
	O_2	0.00	0.00	0.00	0.00	0.00
	N_2	1.31	0.00	13.90	1.14	13.00
Calorific Value HHV, MJ/kg		20.35	20.41	13.95	20.88	13.64
Average Hot-Gas Composition, vol%	CH_4	1.25	2.48	2.10	1.30	2.35
	CO	39.26	35.60	30.57	35.82	24.37
	CO_2	3.03	5.99	7.89	2.72	9.77
	H_2	48.70	49.68	39.01	44.60	36.14
	O_2	0.00	0.00	0.00	0.00	0.00
	H_2O	6.25	6.25	7.60	14.50	16.50
	N_2	1.51	0.00	12.84	1.06	10.86
Calorific Value HHV, MJ/kg		18.41	18.55	12.66	16.33	10.98
Hot Producer Gas Flow Rate, g/s		0.1287	0.1400	0.1963	0.1390	0.3501
Producer Gas Residence Time in bed (@ 850°C), sec		2.59	2.39	2.02	2.61	1.20

* Includes sensible heat.

In all of the experiments, the gas compositions achieved close to equilibrium values. Table 11 shows the difference between the calculated equilibrium gas compositions for five test conditions and the measured gas compositions. In most cases, the gas compositions were within 12 percentage points of the ideal conditions.

Table 13 shows the set of experiments with high-moisture biomass, very low reactor equivalence ratio (little to no air input to the reactor), and a bed temperature of 900°C. The reactor output was higher than the thermal energy of the biomass input. This is an indication that endothermic gasification reactions were effective at transferring heat from the combustor back into the producer gas. The difference in energy includes the sensible heat of the hot producer gas.

Table 13. Performance of Gasifier Operated at ER Close to Zero Using Biomass Containing 30% and 40% Moisture

		Test 3	Test 4	Test 7	Test 8	Test 9	Test 11
Moisture, wt%		30	30	30	30	30	30
Biomass Injection Rate, g/s		0.1933	0.3098	0.3472	0.2359	0.2790	0.1984
Gasification Air Flow Rate, g/s		0.0779	0.3894	0.2726	0.1168	0.1557	0.0778
Equivalence Ratio		0.10	0.30	0.19	0.12	0.14	0.10
Bed Temperature, °C		830	900	930	920	915	890
				Energy Balance			
Biomass Thermal Input, kWth		2.584	4.142	4.642	3.154	3.730	2.653
Reactor Output, kWth		2.410	5.028	4.708	3.618	3.888	2.767
Difference,* kWth		0.693	1.100	1.091	1.153	0.984	0.750
				Gas Composition			
Measured Dry Gas Composition, vol%	CH_4	0.76	1.73	1.90	3.06	2.45	1.90
	CO	31.57	27.74	24.42	26.58	25.55	30.21
	CO_2	5.78	9.28	11.94	12.53	12.02	8.71
	H_2	31.59	27.20	30.47	37.97	34.66	35.46
	O_2	0.00	0.20	0.00	0.00	0.00	0.00
	N_2	30.30	34.34	31.26	19.86	25.32	23.71
Calorific Value HHV, MJ/kg		9.74	5.76	8.57	11.50	10.09	11.07
Average Hot-Gas Composition, vol%	CH_4	0.70	1.51	1.69	2.77	2.19	1.75
	CO	29.04	23.75	21.74	24.03	22.86	27.80
	CO_2	5.32	8.09	10.63	11.33	10.76	8.02
	H_2	29.07	23.72	27.12	34.33	31.02	32.63
	O_2	0.00	0.00	0.00	0.00	0.00	0.00
	H_2O	8.00	13.00	11.00	9.60	10.50	8.00
	N_2	27.88	29.94	27.83	17.95	22.66	21.81
Calorific Value HHV, MJ/kg		8.90	7.20	7.60	10.27	8.95	10.03
Hot Producer Gas Flow Rate, g/s		0.2709	0.6987	0.6193	0.3523	0.4343	0.2759
Producer Gas Residence Time in bed (@ 850°C), sec		1.63	0.68	0.75	1.22	1.03	1.56

* Includes sensible heat.

At close to zero equivalence ratio, the gas flow rates decreased to between 0.1289 and 0.1402 g/s. Complete carbon conversion was achieved; however, the conversion rate was very low. This is an indication of low reaction rates at these operating conditions. At very low equivalence ratios, the throughput of the biomass can be increased by augering char out at a constant rate. This would produce a higher gas flow rate and, consequently, a higher power output. However, it would decrease the overall system efficiency, increase the amount of waste char generated and, possibly, increase tar during operation.

Table 14 shows the experimental results of the pinewood tests conducted with reactor equivalence ratios between 0.10 and 0.34. The bed temperatures for these tests were maintained between 890° and 930°C. In all tests, the measured gas compositions were close to equilibrium values. Figure 13 shows the reactor output as a function of reactor equivalence ratio. Overall, the

reactor output power increased with respect to reactor equivalence ratio. As in Table 12, the reactor output power for all cases was higher than the thermal input of the biomass. This is an indication that heat was successfully recycled back into the producer gas, a key concept for maximizing the energy efficiency of the system.

Table 14 shows the three test conditions in which the reactor output power was greater than the combustor power used to heat the reactor. The first two test conditions used dry wood. Since natural gas was used in the combustor, the combustor power was limited to 5 kWth or higher. The first test condition used dry pinewood chips. The second used dry oak wood pellets tested under gasifying conditions similar to the first. Test 5 used 30% moisture pinewood and recycled the producer gas into the combustor in place of the natural gas. For this test, the air was injected into the combustor at approximately half stoichiometry to more closely simulate the thermal conditions when thermally integrated with a fuel cell. This condition more closely matched the temperature–power characteristics in the system design. The ER for all three tests was above 0.28 to obtain high reactor power outputs.

The oak wood pellets were used to compare reaction rates and gas characteristics with the pinewood chips. The oak wood pellets were found to be more reactive than the pinewood under the same gasifying conditions as a direct effect of the fuel density. The overall conversion rates of the oak wood pellets were approximately 50% higher than the pinewood chips, providing a reactor output power of 9.5 kW as opposed to 6.4 kW from the pinewood chips. This is an indication that biomass feed characteristics have a significant impact on output power. In both cases, natural gas was used in the combustor to simulate the waste heat recirculation.

Test 5 demonstrated the ability of the reactor to maintain high throughput and clean gas characteristics over a sustained operating period using high-moisture biomass as the input and low combustor power to heat the reactor. Producer gas was recycled into the combustor in place of the natural gas at 3.4 kWth. The gas throughput was found adequate to maintain an average reactor bed temperature of 845°C. The combustor power level was controlled by the partial combustion of the producer gas by injecting air at half the stoichiometric requirement. This simulated one of the primary conditions of integrated system operation: that recirculation of the unconverted thermal energy to the reactor can maintain the isothermal condition necessary to produce a clean, near-equilibrium producer gas. In this case, an SOFC electrical conversion efficiency of 40% would allow self-sustained system operation.

Figure 13 provides an overview of the reactor output characteristics throughout the test. The reactor was started on natural gas and brought to steady-state operation on producer gas. As with the other gasification tests, the steady-state test duration for this test was 5 hours. The graph of the producer gas HHV shows a stable output throughout the test period (Figure 14). The three troughs between 7:30 and 19:00 were artificially induced by cutting off the feed rate. This was done to observe the effect that transients in the feed have on the output of the gasifier. In all three cases, the thermal inertia of the system immediately brought the system back up to a stable steady-state condition when feeding commenced. Throughout the test, the combustor gas temperature and bed temperature were stable. This test demonstrated the ability of the system to maintain self-sustained operation without external heat sources.

Table 14. Test Conditions Where Output Power Was Greater than Combustor Power

		Test 1	Test 2	Test 5
Biomass Used		Pine Wood	Oak Wood	Pine Wood
Moisture, wt%		5.5	7.35	30
Biomass HHV, MJ/kg		18.0495	17.696	13.37
Biomass Injection Rate, g/s		0.4103	0.5121	0.4690
Gasification Air Flow Rate, g/s		0.7788	0.7788	0.7788
Equivalence Ratio		0.34	0.28	0.40
Bed Temperature, °C		880	880	845
			Energy Balance	
Biomass Thermal Input, kWth		7.406	9.063	6.271
Reactor Output, kWth		6.412	9.529	6.349
Difference,* kWth		0.000	0.942	0.432
Combustor Fuel		NG[2]	NG	RPG[3]
Thermal Input of Combustor, kWth		5	5.4-8.6	3.4
			Gas Composition	
Measured Dry Gas Composition, vol%	CH_4	2.21	1.87	1.76
	CO	21.81	29.82	17.22
	CO_2	12.16	7.70	15.18
	H_2	18.20	23.15	23.07
	O_2	0.00	0.00	0.00
	N_2	45.62	37.46	42.77
Calorific Value HHV, MJ/kg		5.76	7.84	5.79
Average Hot Gas Composition, vol%	CH_4	2.05	1.76	1.53
	CO	20.29	28.05	14.98
	CO_2	11.31	7.24	13.21
	H_2	16.92	21.78	20.07
	O_2	0.00	0.00	0.00
	H_2O	7.00	5.93	13.00
	N_2	42.43	35.24	37.21
Calorific Value HHV, MJ/kg		5.40	7.38	5.09
Hot Producer Gas Flow Rate, g/s		1.1885	1.2904	1.2471
Producer Gas Residence Time in bed (@ 850°C), sec		0.44	0.37	0.41

[1] Includes sensible heat.

[2] Natural gas.

[3] Recycled producer gas.

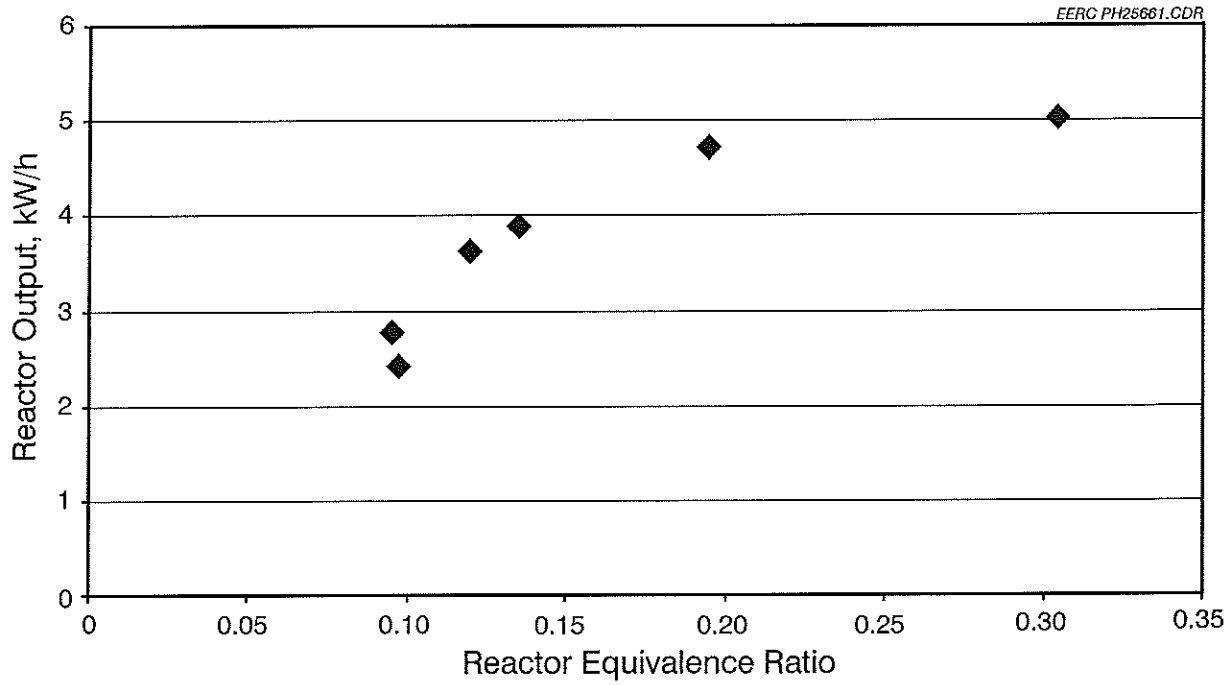

Figure 13. Maximum reactor power output as a function of equivalence ratio for biomass with a moisture level of 30%.

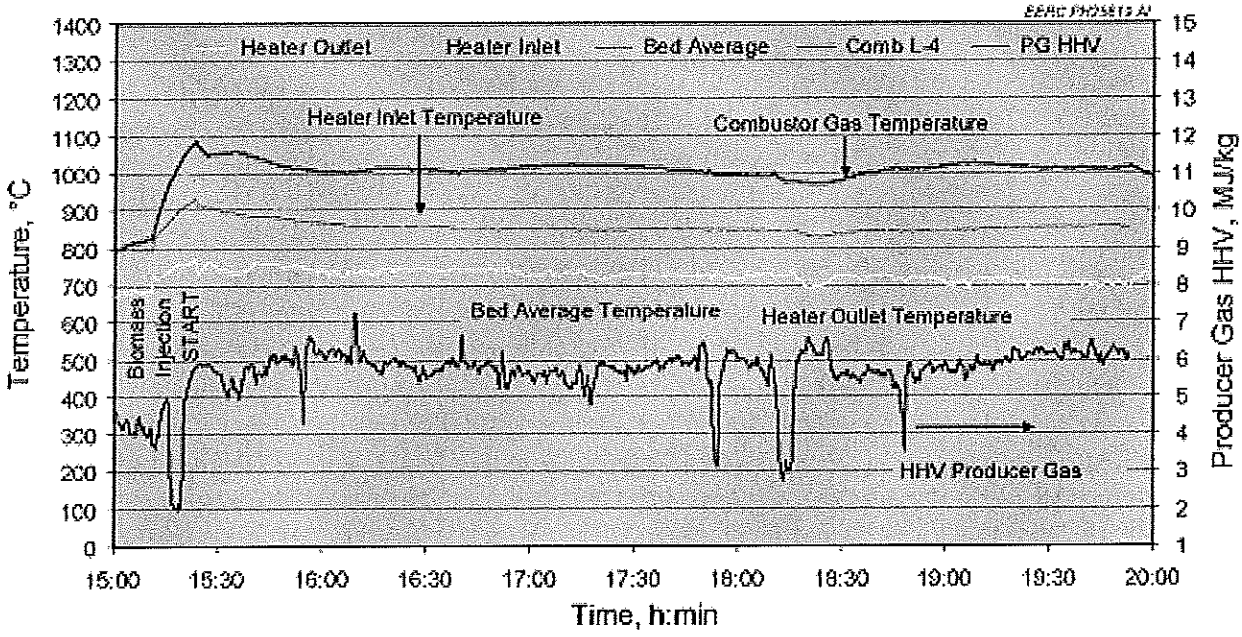

Figure 14. Run chart of Test 5.

Contaminant Analysis Results

The contaminant sampling methodology requires meticulous attention to detail to ensure accurate results. For this reason, Appendix A provides a detailed explanation of the sampling methodology and results. This section provides an overview and analysis of the results presented in Appendix A.

The raw producer gas generated by the gasifier was analyzed for particulate matter, tars, light hydrocarbons (BTX), and inorganic contaminants known to affect SOFC performance (H_2S, NH_3, and HCl). Table 15 shows the level of contaminants measured from the raw producer gas. Gravimetric analysis of tar and particulate matter was conducted on four tests. The general trend observed was that higher moisture content and higher gasification equivalence ratio produced lower tar levels. The highest level of tars detected was for the case of very low moisture pinewood. The lowest level of tars detected was 8.5 ppm. These equate to a range of 8.5 to 235 mg/m^3 of tars in the raw producer gas. To put in perspective the savings in equipment and capital costs, Abatzoglou et al. (7) report tar levels ranging from 4.2 to 30 mg/m^3 after scrubbing with a cooling tower, venturi scrubber, and demister. Using the same tar-sampling protocols at the EERC, tar levels as high as 550 ppm are often detected on conventional gasification systems after scrubbing with a cooling tower, coarse filter, and fine particulate filter.

Gas chromatography (GC) analysis of the tars detected no BTX. There was the possibility that the tar-sampling procedures did not adequately capture the lower-weight hydrocarbons. To ensure accuracy of results, additional BTX measurements were conducted online using calorimetric tubes. These results confirmed the tar analysis. The BTX components in the producer gas were all lower than 2 ppm.

Table 15. Measured Hot Producer Gas Contaminants

Test No.	H_2S, ppm	NH_3, ppm	Benzene, ppm	Toluene, ppm	Xylene, ppm	Total Tar, ppm	Particulate, ppm	HCl, ppm
1	5	<10	–[1]	–	–	234	22	BDL[2]
2	28	–	–	–	–	66.5	< 50	BDL
3	–	–	–	–	–	–	–	BDL
4	8–10	<10	BDL	BDL	BDL	90	33	BDL
5	28–30	75	<2	<1.5	<2	8.5	119	BDL
6	<10	–	–	–	–	–	–	BDL
7	<10	<10	–	<2	<2	–	–	BDL
8	<10	<10	–	<2	<2	–	–	BDL
9	<10	<10	–	<2	<2	–	–	BDL
10	<10	<10	–	<2	<2	–	–	BDL
11	<10	<10	–	<2	<2	–	–	BDL
12	<10	<10	–	<2	<2	–	–	BDL
13	<5	60–85	<0.3	<2	<2	–	–	–
14	<5	60–85	<0.3	<2	<2	–	–	–

[1] No test performed.

[2] Below detection limits.

For the majority of tests, the H_2S measurements were below 10 ppm. Peak H_2S measurements of approximately 30 ppm were detected in two tests. Ammonia measurements behaved similarly. For the majority of tests, NH_3 measurements were below 10 ppm. However, three tests gave NH_3 levels of approximately 60–80 ppm. Hydrogen chloride (HCl) measurements were taken in 12 of the 14 tests. In every case, no HCl was detectable in the parts per million range.

As part of the tar-sampling procedure, particulate matter (PM) was separated out and measured. Typical PM levels were between 22 and 119 ppm. The trend for PM was opposite that of tars. Higher moisture levels tended to increase PM levels. Scanning electron microscopy analysis of the PM indicated that approximately two-thirds of the PM was inorganic matter in the form of oxides or carbonates. These were identified primarily as calcium, magnesium, potassium, chloride, and oxygen. Analysis of the cyclone dumps also revealed small amounts of aluminum, silica, and negligible iron. The iron may be an indication of its presence in the virgin biomass, contamination of the biomass during size reduction, or it could be due to internal erosion of the reactor during operation. The effects of the inorganic constituents in the PM on SOFC performance are unknown. It is possible that these may cause long-term fouling of the anode surface; however, without additional experiments, this is uncertain. If these do cause detrimental performance to the SOFC, then an additional high-temperature fine filter will be needed to capture these before the SOFC.

These low levels of contaminants and near-theoretical gas compositions make gas conditioning for the fuel cell much simpler and less capital-intensive. The near-equilibrium gas compositions minimize the risk of carbon formation on the SOFC anode due to the producer gas. The low tar levels significantly reduce the risk of carbon formation due to tars. Ammonia and HCl levels are below the known tolerance limits of SOFC technology. And H_2S levels are low enough to either use H_2S scrubbing filters or to use directly in higher-sulfur-tolerance SOFC technology. If scrubbing filters are used, then the lower H_2S levels increase the filter replacement intervals. Initial tar-screening experiments demonstrated short-term tar tolerance of 2–3 orders of magnitude higher than the tar levels in the raw producer gas. This finding demonstrates that direct use of the raw producer gas in an SOFC is technically feasible. However, the long-term effects of low-level tars are unknown.

The biomass conversion rates produced variable results. Very low equivalence ratios produced near-equilibrium gas compositions. However, the conversion rates were very low. This decreased the overall power output due to low gas throughput. Test 5 demonstrated that a heat-recycling rate of 3.4 kW_{th} was sufficient to maintain the necessary isothermal condition in the reactor bed to produce a clean, near-equilibrium gas composition for 30% moisture pinewood. This would indicate that a minimum equivalence ratio of 0.2 is necessary to maintain a self-sustained system for this feed. This produces a reactor output power of approximately 5 kW, allowing 20%–30% conversion efficiency to electricity and 70% thermal recirculation to the reactor. For higher electricity conversion rates, the ER would have to be increased. An ER of 0.35 produced a reactor output of 6.4 kW, allowing 30%–40% of the available energy to be converted to electricity and/or lost because of thermal inefficiencies.

Other biomass types would have slightly different operating characteristics, as witnessed by the higher conversion rates for the oak wood pellets. However, the dependency of the reactor output to the ER, moisture content, and recirculated heat would likely be similar to the pinewood.

The predicted operating characteristics of the system as shown in Table 16 were modified to take into account the performance constraints observed during the experiments. This is shown in Table 16. The ER was increased to 0.30 to allow reasonable conversion rates. The gas compositions were modified slightly from the equilibrium composition to contain 2%, on average, CH_4 content as observed in the experimental. This also produced a more uniform gas composition and specific energy of the producer gas. The net result of these modifications on system efficiency is to reduce it to 27%. At an ER of 0.3, the gasifier is exothermic. The combustor gases are used to maintain the isothermal temperature condition by minimizing heat losses.

Figures 15a and 15b show the ternary plots of the carbon deposition boundary lines in a fuel cell and the relative positions of the producer gas compositions from Tables 3 and 16. The plots shown in Figure 15b include 250 ppm tars in the producer gas. The higher ER increases the moisture contents of the producer gases in Table 16. This moves the relative positions of the producer gases well below the carbon deposition lines, significantly decreasing the propensity of carbon deposition in the fuel cell.

Gasifier Performance on MSW

Additional gasification tests were performed on simulated municipal solid waste (MSW). The solid waste was received courtesy of the U.S. Army Natick Soldier Center, located at the U.S. Army Soldier Systems Center in Natick, Massachusetts. The solid waste was received in the form of cardboard trays, plastic bags, plastic utensils, and paper cups, as shown in Figure 16. To facilitate feeding, the solid waste was shredded and compacted. Initially a Komarek briquetter was used to produce oval 2" x 1" bricks, as shown in Figure 17. Initial gasification trials with these bricks were unsuccessful because of excessive bridging in the hopper and the feed screw. A second attempt was made to pelletize the shredded MSW by mixing the MSW in a water slurry. The slurry was then allowed to air-dry under weight. The dried mixture had a rough cardboard consistency and was cut into ½-inch cubes. These did bridge in the hopper slightly; however, flow was consistent enough to allow gasification tests to be performed.

The approximate composition of the solid waste cubes was 47% cardboard, 10% plastic utensils, 30% plastic bags, and 13% miscellaneous content. The miscellaneous content included aluminum foil, plastic, and other unidentified material. Gasification tests were performed on the solid waste and a 50% mixture of wood and solid waste. In both gasification run measurements of the dry gas composition, H_2S levels, HCl levels, tar levels, particulate levels, and NH_3 levels were taken of the raw producer gas.

Proximate and ultimate analysis of the wood and solid waste are shown in Table 17. The total feed varied in moisture level from 2.6% to 13.6%. Both sulfur and ash in the raw wood and

Table 16. Nonideal System Performance for a 10-kWe Biomass Power System

Biomass Feed					
Type	Woody Biomass				
Chem. Composition	$CH_{1.4}O_{0.59}N_{0.017}$				
Ash, wt% basis	0.1–1.0				
Sulfur, wt% basis	0.00–0.2				
Moisture Content, wt% basis	0	10	20	30	40
HHV, MJ/kg	22.2	20.0	17.8	15.5	13.3
Gasifier Conditions					
Optimum ER	0.30	0.30	0.30	0.30	0.30
Feed Rate, g/s	1.370	1.520	1.706	1.944	2.260
Airflow In, g/s	2.627	2.622	2.617	2.609	2.600
Power Input, kW_{th}	30.4	30.4	30.4	30.2	30.1
Power Output, kW_{th}	26.4	26.4	26.4	26.4	26.4
Rx Efficiency	87	87	87	87	88
SOFC Input (Equilibrium Composition)					
CO, mol% basis	29	26	23	19	16
H_2, mol% basis	19	19	20	20	20
CH_4, mol% basis	2	2	2	2	2
CO_2, mol% basis	5	6	8	9	10
H_2O, mol% basis	4	7	10	14	20
N_2, mol% basis	41	39	37	35	32
HHV, MJ/kg	6.6	6.4	6.1	5.8	5.4
Gas Temp., °C	900	900	900	900	900
Flow Rate, g/s	3.997	4.142	4.323	4.554	4.859
Cathode Flow Rate, g/s	27.0	27.0	27.0	27.0	27.0
Cathode Air Temp, °C	700	700	700	700	700
Combustor Output					
Gas Temp., °C	1127	1128	1127	1127	1120
Flow Rate, g/s	30.997	31.142	31.323	31.554	31.859
Heat Exchanger					
Hot-side Gas Temp. Input, °C	1131	1137	1141	1145	1146
Hot-side Gas Temp Output, °C	607	618	629	641	652
System Output					
Gas Temp., °C	548	546	542	536	523
Flow Rate, g/s	30.997	31.142	31.323	31.554	31.859
Efficiency Calculations					
Energy Input, kW_{th}	30.4	30.4	30.4	30.2	30.1
SOFC Input, kW_{th}	26.4	26.4	26.4	26.4	26.4
SOFC Output, kW_e	10	10	10	10	10
SOFC Efficiency	38	38	38	38	38
Gross System Efficiency*	33	33	33	33	33
Parasitic Losses					
8% Conv. Losses, kW_e	0.80	0.80	0.80	0.80	0.80
Air Pump, 0.57 kW max	0.18	0.18	0.18	0.18	0.18
Blower, 0.8 kW max	0.56	0.56	0.56	0.56	0.56
Feed Screw, 0.15 kW max	0.11	0.13	0.14	0.16	0.19
Discharge Screw, 0.15 kW max	0.01	0.01	0.01	0.00	0.00
Total Losses, kW_e	1.66	1.67	1.69	1.70	1.73
Net Power Output, kW_e	8.34	8.33	8.31	8.30	8.27
Net System Efficiency	**27%**	**27%**	**27%**	**27%**	**27%**

*Gross efficiency neglects parasitic losses.

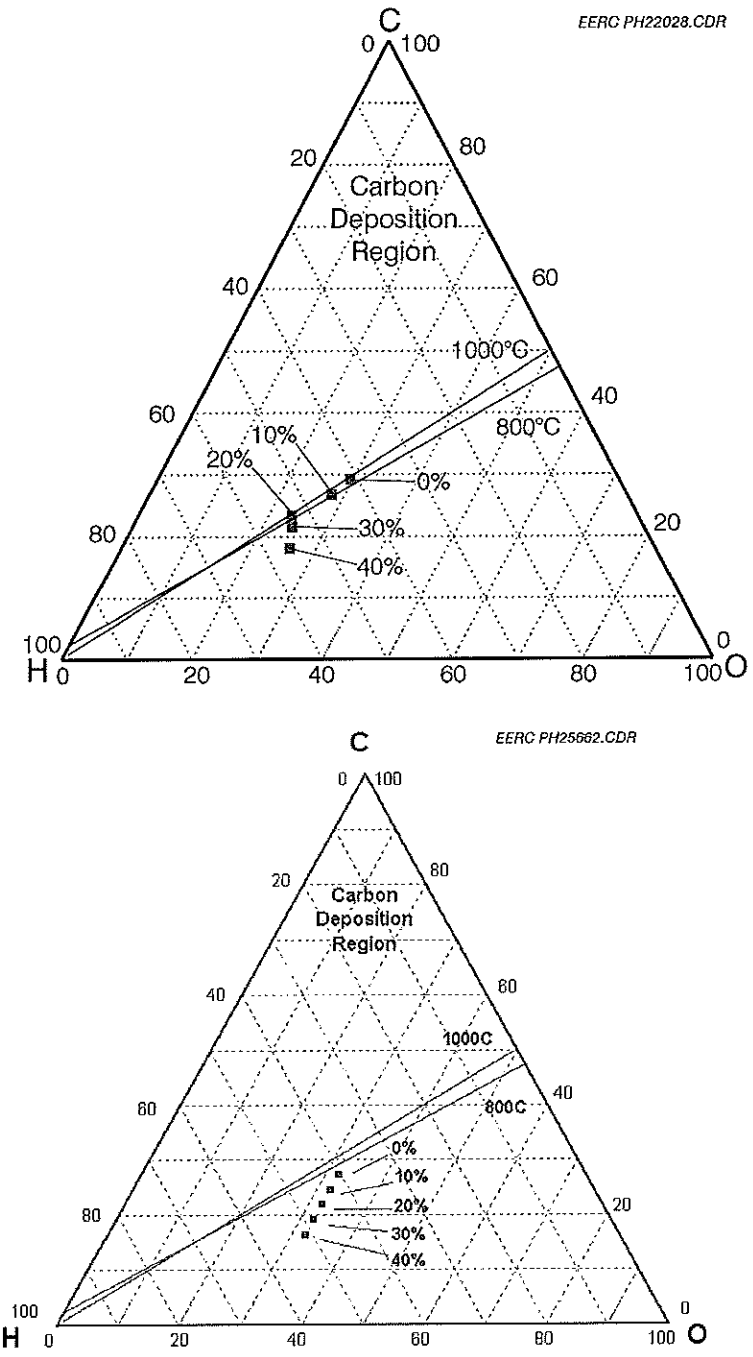

Figure 15. Ternary plot of ideal wet gas compositions (top) and ternary plot of wet gas compositions produced in experimental (bottom).

Figure 16. Solid waste before shredding.

Figure 17. Komarek briquetter.

Table 17. Proximate/Ultimate Analysis

Proximate Analysis, % w/w	Solid Waste	Mixed Wood & Waste
Moisture	2.6	13.6
Volatile Matter	88.62	76.92
Fixed Carbon	5.82	7.69
Ash	2.96	1.82
Hydrogen	6.61	7.02
Carbon	48.37	42.80
Nitrogen	0.29	0.22
Sulfur	0.13	0.14
Oxygen	41.63	47.99
Ash	2.96	1.82
HHV, MJ/kg (BTU/Lb)	18.71 (8062)	17.00 (7142)

solid waste were low. The sulfur was measured at 0.22% and 0.13%, respectively. The ash was measured at 0.16% and 3%, respectively. The higher plastic content in the solid waste is reflected in the proximate analysis in the form of higher volatile matter and lower fixed carbon than the wood samples.

Table 18 shows the average steady-state gas compositions measured in the gasification runs. Gas compositions for wet wood and dry wood are included for comparison. The gas composition was consistent with the moisture content in the feed. The runs with higher moisture content tended to have significantly higher hydrogen levels and lower nitrogen dilution in the producer gas. This is an indication that moisture in the raw feed was being converted to hydrogen through the endothermic water–carbon reaction.

Table 18. Steady-State Dry Gas Composition

	Dry Wood	Wet Wood	Solid Waste	Mixed Wood & Waste
CH_4, %v/v	2	2	3	6
CO, %v/v	22	28	23	23
CO_2, %v/v	12	9	9	9
H_2, %v/v	18	27	18	27
O_2, %v/v	0	0	0	1
N_2, %v/v	46	34	48	34
Btu Value, Btu/scf	110	141	115	160

Figure 18 shows a C–H–O ternary diagram of the gas compositions shown in Table 18. The dry gas compositions for both tests were below the carbon deposition boundary lines, indicating that these gas compositions should not lead to carbon deposition in the fuel cell.

Table 19 shows the measured contaminants in the raw producer gas. Typical contaminant levels for wet wood and dry wood are provided for comparison. The measured tar content for the solid and mixed waste is in the 4000- to 9000-mg/m^3 range, due primarily to the plastic content in the solid waste. While higher than the wood, this level of tars is still below 1% of the total producer gas by volume and, thus, should be relatively simple to condense out prior to the fuel cell.

The HCl levels are shown to be less than 20 ppm in Table 19. In reality, there was no measurable amount of HCl in the producer gases. However, our lower measurable limit was 20 ppm. The particulate measurements were typically 40 mg/m^3, with one measurement showing 120 mg/m^3. All of the H_2S measurements were very consistent and lower than 50 ppm. This may pose a problem with some fuel cells, and an additional H_2S adsorbent reactor may be necessary. In-house testing on a passive sponge iron adsorbent reactor demonstrated that the H_2S content could be reduced below 1 ppm with a commercially available sponge iron catalyst. Simple calculations show that a reasonably sized H_2S adsorbent reactor could operate in the order of 6 months to a year between replacements, primarily because of the low levels of H_2S in the raw producer gas.

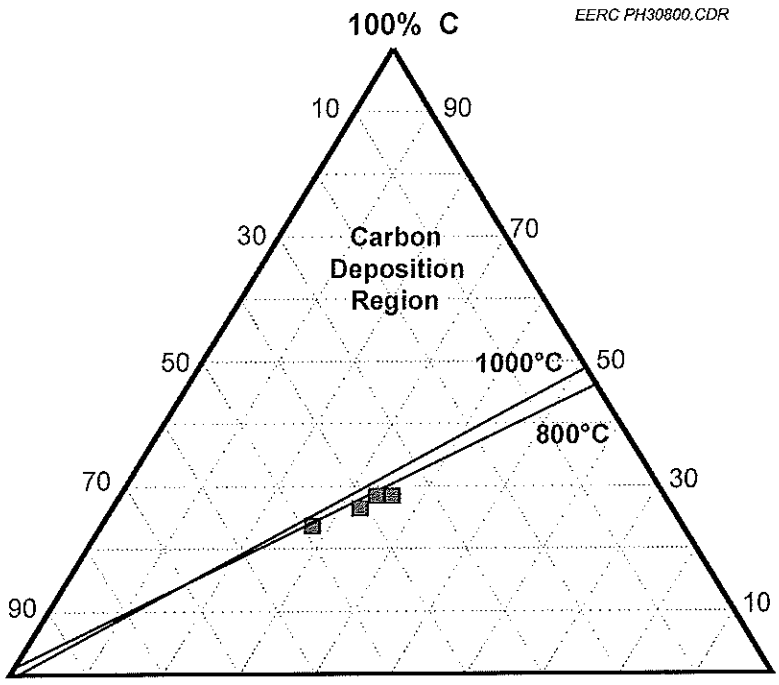

Figure 18. Ternary plot of dry gas compositions shown in Table 18.

Table 19. Contaminant Levels in Raw Gas

	Dry Wood	Wet Wood	Solid Waste	Mixed Wood and Waste
H_2S, ppm	5	30	50	25
NH_3, ppm	< 10	< 10	–	12
Total Tar, mg/m^3	234	8.5–91	8165	4458
PM, mg/m^3	22	33–120	34	–
HCl, ppm	<20	<20	<20	<20

SECTION III: FUEL CELL EXPERIMENTS

The fuel cell is the electrical conversion component of the power system. The unique operating characteristics of high-temperature fuel cells convert the chemical energy of the producer gas to electrical energy at high conversion efficiencies, while producing a high-temperature waste effluent ideal for cogeneration or use in a secondary converter. In this system, the high-temperature waste effluent from the fuel cell is combusted and used to heat the gasification zone of the biomass reactor. The advantages of this approach are that the gasification reactions are stabilized and the tar-cracking reactions within the gasifier are increased. In addition, biomass with high moisture levels recycles a portion of the waste heat back into the producer gas through endothermic gasification reactions, primarily the steam–carbon reaction and Bouduoard reaction.

Controlled heating of the biomass reactor is the key to producing a high-energy, low-tar-content producer gas clean enough to be fed directly to the fuel cell. The cleaner gas from the gasifier reduces intermediate gas-conditioning equipment between the fuel cell and gasifier. This decreases overall capital and operating costs, significantly improving the overall economics of the system.

Button cells were tested on simulated syngas and tars to determine the raw tar levels that would produce catastrophic failure of the cells. Button cells were then tested from syngas from the bench scale gasifier. Final testing was performed on a 122-watt stack on syngas from the gasifier. Originally, the final objective was to operate a 2–3-kW$_e$ SOFC stack from the bench-scale gasifier in a thermally self-sustained system. This final objective was not completed because of the inability of the fuel cell to undergo multiple thermal cycles and the high cost of SOFC technology at the time of testing. The minimum cost of a 2-kW$_e$ SOFC stack at the time of testing was approximately a quarter million dollars. The final decision to forego the final objective was based on the reliability and expected lifetime of SOFC stack technology at the time of testing. Vendors capable of supplying stacks could ensure no more than one thermal cycle. Experience dictated that the system would likely undergo several start-ups and shutdowns before the bugs were worked out of the system and a thermally self-sustained test could be achieved. A single thermal cycle for the stack was simply inadequate, given the stack cost and uncertainty level in the test procedure.

The producer gas composition is expected to vary depending on the biomass feed and the operating conditions of the gasifier. To maximize the economics of the system, the fuel cell must be capable of operating on variable composition producer gas with low-level contaminants. In this case, the primary contaminants of concern are tars, HCl, NH_3, and H_2S. Data on HCl, NH_3, and H_2S tolerance of SOFCs are publicly available and vary widely based on fuel cell manufacturers and technology. Published reports (22) cite SOFC tolerance levels for NH_3 at 5000 ppm. These are well above the levels measured from the gasifier. SOFC tolerance toward HCl and H_2S are a little less definitive. Experiments (22) show no SOFC degradation when exposed to HCl of 1 ppm and report that irreversible degradation of the SOFC occurs above 200 ppm. For H_2S, published reports (22–24) cite tolerance levels from 5 ppb to 3000 ppm. Most reports cite an immediate decrease in power levels of approximately 10% when exposed to H_2S, but then a leveling off of performance.

During the gasification experiments, the HCl levels in the producer gas could not be detected in the parts per million range. The H_2S levels during the biomass tests varied from lower than 5 ppm to as high as 30 ppm. Additional scrubbing of sulfur is possible with dry sponge iron sorbent beds; however, this required reducing gas temperatures to near ambient. If H_2S scrubbing is necessary, the low contamination levels in the raw producer gas increase the intervals between sorbent replacements. Another option is to use SOFC technologies with higher sulfur tolerance.

Bench-Scale Button Cell Testing

Data on tar tolerance of SOFC technology are not available in current literature. For the gasification experiments, the levels of tars varied from 8.5 ppm to as high as 234 ppm. The fuel cell experimental performed initial screening studies to determine the magnitude of tars that typical anode-supported (AS) SOFCs could tolerate. These data were then checked against thermodynamic calculations on carbon deposition in the fuel cell to determine if the tar levels measured in the producer gas were significant enough to warrant further study. In addition, simple experiments were performed on different producer gas compositions to more accurately predict fuel cell performance within the system.

Fuel Cell Experimental Apparatus

Figure 19 is a diagram of the SOFC test apparatus. Both combustible and noncombustible gas tanks are connected to a gas box through dual-stage regulator valves. The combustible gases are H_2, CO, and CH_4. The noncombustible gases are CO_2 and N_2. House air and house nitrogen are also connected to the gas box to provide air for the cathode of the fuel cell and nitrogen purge for the fuel lines. Inside the gas box, all gas lines are connected to a back-pressure check valve and a flow controller. The outputs of the flow controllers for the N_2, CO_2, CO, H_2, and CH_4 lines are manifolded and sent to the SOFC anode. The air line is connected to the SOFC cathode. Both the anode gas line and the cathode air line are coiled inside the furnace to preheat the gases prior to entering the SOFC test fixture. Two swagelok connections are installed on the anode gas line for water and tar injection. A micropump was used to deliver water to the fuel cell. The micropump injects liquid water into the anode gas line upstream of the coil. The water is converted to steam in the coil and brought to temperature along with the rest of the anode gas.

The tar injection system also uses a micropump. The micropump injects low-level tars into the anode gas line downstream of the coil, just prior to entering the SOFC test fixture. The tar injection lines utilize a silicon-coated ⅛-inch tube to minimize carbon deposition in the tube when in the furnace. Approximately 6 inches of tubing from the tar injection system are exposed to the hot zone of the furnace before being injected into the SOFC test fixture. The injected tar levels are approximately 3% or less by volume of the total anode gas. The SOFC test fixtures are designed to exhaust the anode gas and cathode air into the furnace, where the anode gas is subsequently combusted. The furnace is vented to atmosphere through movable ventilation ducts.

The electrical output of the SOFC is directed to a MOSFET variable-load center. The load center provides automated load control of voltage, current, and power in both constant control functions and sweep functions. For all tests, a two-probe measuring system was used, so the voltage at the load center includes ohmic losses through the current collection lines. The SOFC test fixtures were not optimized for maximum power, so the test data were analyzed relative to varying test conditions within the same test fixture.

The overall system is computer-controlled and designed to operate unattended. After testing, the furnace is shut down, cooled, and the fuel cell removed for postexperimental analysis.

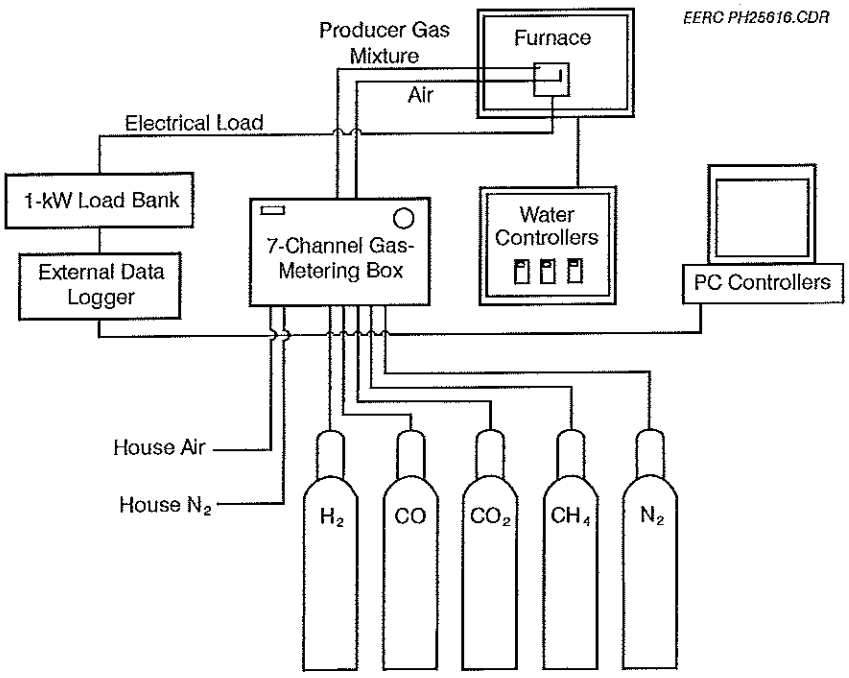

Figure 19. Fuel cell test apparatus.

SOFC Tar Tolerance Testing

All gasification systems emit small amounts of aromatic and polynuclear aromatic hydrocarbons (PAHs) along with their producer gas. These range from benzene up to the heavier PAHs, such as pyrene. The definitions of which compounds constitute tars are variable and often dependent upon the end use of the producer gas. In most practical situations, tars are simply defined as those hydrocarbons that have the potential to foul systems downstream of the gasifier. In most cases, fouling occurs either through condensation of the hydrocarbons in the cooler areas of the system or through soot formation from combustion of the producer gas.

The SOFC–gasification system design mitigates system fouling through condensation by maintaining the system temperature above the tar condensation temperatures from the gasifier to the combustor, where any residue tars left in the producer gas are subsequently combusted. This leaves the SOFC as the primary constraint to determining acceptable tar levels from the gasifier. No public literature is currently available providing information on the tolerance levels of SOFC technology to tars.

Since the SOFC operates at temperatures above the tar condensation temperature, the primary mechanism for tar fouling of the SOFC is expected to be carbon sooting of the anode because of decomposition of the tars during operation. The screening experiments were performed to determine the magnitude of tars in the producer gas that causes catastrophic failure of the fuel cell during operation. Hydrogen gas was flowed into an AS button cell with an active surface area of 9 cm^2 at a constant flow rate. The button cells were ASC1 anode-supported fuel cells from InDec. Prior to each test, an I–V curve was performed to baseline the performance of the cell. The load center was then set to provide a constant current output from the fuel cell. Once a constant current operating condition was attained, a simulated tar mixture, as described by Singh et al. (23), was injected into the fuel cell. The simulated tar mixture was composed of 65% toluene, 20% naphthalene, 10% phenol, and 5% pyrene. The average molecular weight of the simulated tars was 100.6 g/mol. The fuel cell voltage was observed for changes over a specified time period. If no drop in performance was observed, then the tar injection rate was stepped up. This procedure was repeated until the fuel cell voltage started to decline. Once this point was attained, the test was shut down and the cell removed for postexperimental analysis.

For the first experiment, the fuel cell was operated at a constant current of 0.4 amps. The initial voltage at 0.4 amps was 0.45 V. The hydrogen and air flow rates were 0.34 slpm and 1.0 slpm, respectively. The furnace temperature was held constant at 750°C. The tar injection rate was maintained constant for a minimum of 1 hour to ensure that a steady state was reached prior to stepping up the tar injection rate. Figure 20 is a graph of the fuel cell output and the tar injection rates. Three tar levels were injected, corresponding to tar mole percentages of 0.5%, 1.1%, and 1.8%, respectively. The fuel cell provided a stable output up to tar levels of 1.1%. As soon as the tar injection rate was stepped above 1.1%, the fuel cell output degraded linearly with respect to time. It can be concluded from this test that catastrophic carbon deposition occurred at tar mole percentages between 1.1% and 1.8%. Figure 21 provides an image of the cell during postexperimental breakdown.

For the second screening experiment, the fuel cell test fixture was redesigned to improve overall power densities of the fuel cell. The redesigned test fixture significantly decreased the contact resistance of the current collectors. The maximum power densities increased to 216 mW/cm^2. This allowed higher flow rates for both the hydrogen and tars, increasing the resolution of the test. For the second test, the hydrogen and air flow rates were set to 0.44 and 1 slpm, respectively. The higher hydrogen flow rate allowed more step increases in the tar injection rate. The steady-state duration was decreased to a minimum of 15 minutes. The furnace temperature was regulated at 750°C. The fuel cell was operated at a constant current output of 4 amps. The initial voltage at this current was 0.625 V.

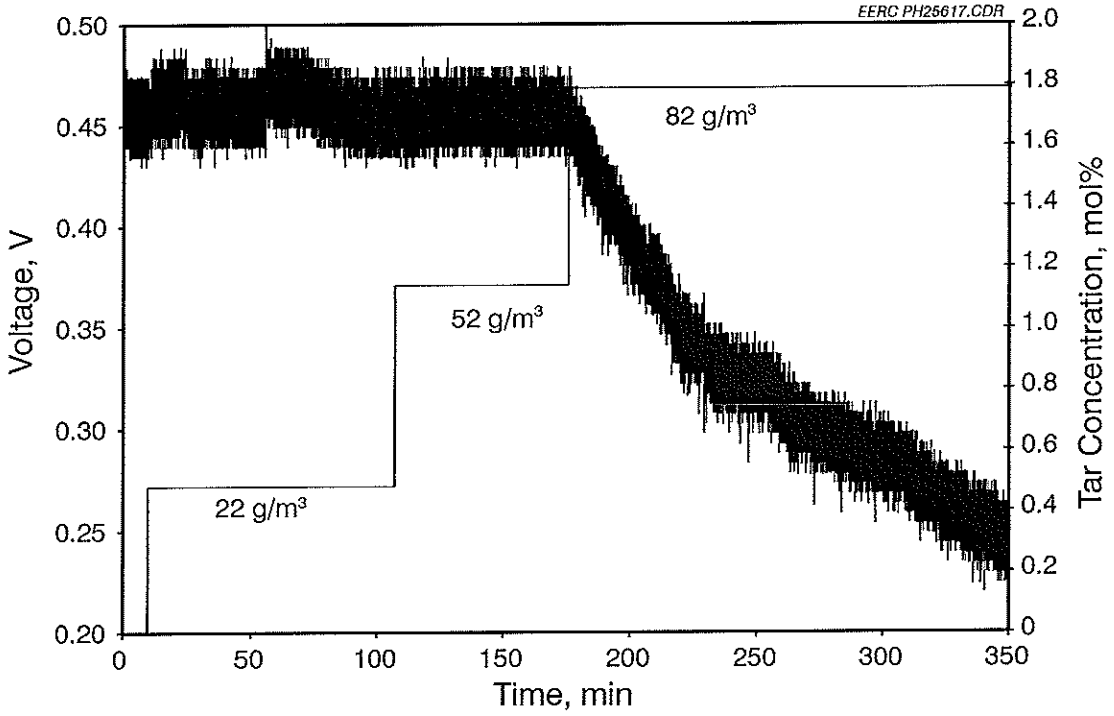

Figure 20. Tar testing using 0.34 slpm hydrogen and 1.0 slpm air at 750°C.

Figure 21. Image of cell with carbon deposition.

Figure 22 shows the fuel cell output of the second test. The cell voltage remains constant at tar concentrations of 17 and 20 g m^{-3}. There is a slight increase and then leveling off in performance at a tar concentration of 63 g m^{-3}. This increase may be an indication of a slight steady-state sooting of the anode. Prior research (26) indicates that slight sooting may increase the overall performance of the fuel cell by decreasing the contact resistance at the anode. In essence, there may be just enough carbon buildup to increase the current collection paths in the porous anode structure, but not enough to significantly obstruct flow through the anode pores.

The performance remains constant at this increased level up to a tar concentration of 86 g m^{-3}. The fuel cell output started decreasing as soon as the tar injection level increased to 110 g m^{-3}. This corresponds to a tar mole percentage of 1.9%. It can be concluded from these results that catastrophic carbon deposition occurred in this test at a tar mole percent between 1.9% and 2.4%. This is in relatively close agreement with the first test, considering the differences in test fixtures and power densities.

The third experiment was performed with a new button cell to verify the repeatability of the data. Figure 23 shows the performance of the third experiment. The cell gave a lower power performance than the second experiment; however, thermodynamic decomposition of the fuel depends only on current and not on voltage. Since the same current draw as the second experiment was used, the results should be similar. As in the second experiment, 4 amps were

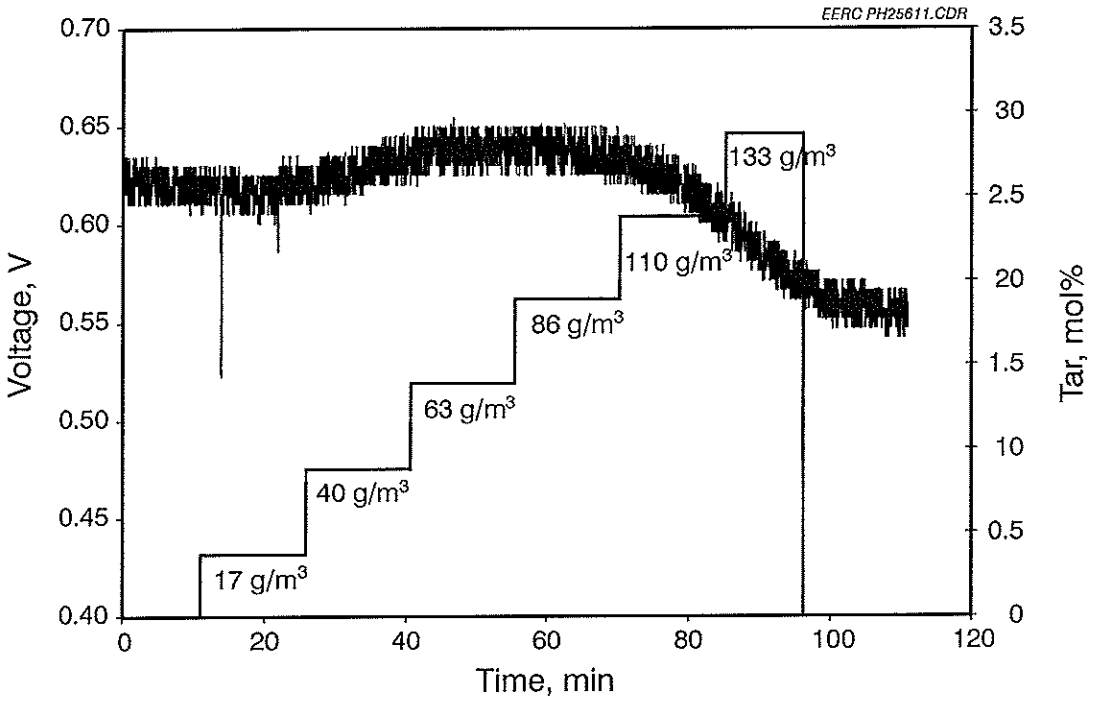

Figure 22. Tar testing using 0.44 slpm hydrogen and 1.0 slpm air at 750°C, Test 1.

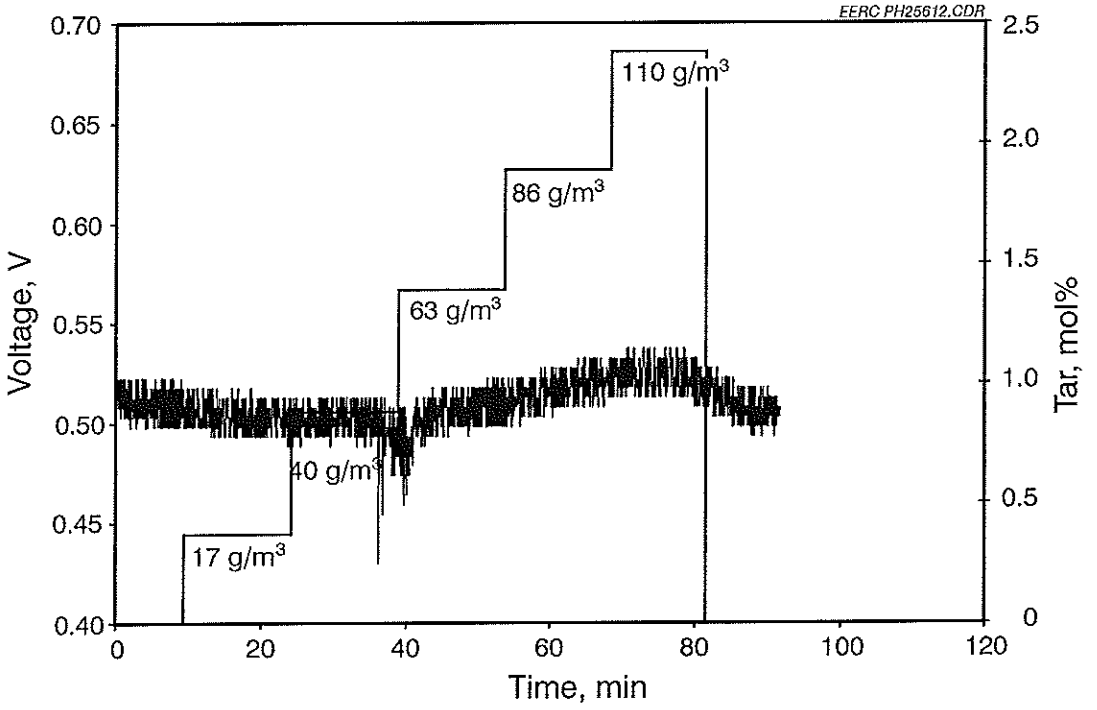

Figure 23. Tar testing using 0.44 slpm hydrogen and 1.0 slpm air at 750°C, Test 2.

drawn from the fuel cell. The initial voltage for this cell was 0.51 V. The hydrogen and air flow rates were set to 0.44 and 1 slpm, respectively. The steady-state duration was set to a minimum of 15 minutes. The furnace temperature was regulated at 750°C.

The results of the third experiment were cut short because of carbon blockage of the injection tubes. However, before the experiment was shut down, the trends were very similar to the second experiment. A slight increase in performance is observed at a tar concentration of 63 g m^{-3} and continued to a tar concentration of 86 g m^{-3}. The voltage then slowly began to decline as soon as the tar concentration was increased to 110 g m^{-3}.

The tar tolerance tests show the magnitude of tar levels in the fuel gas that cause immediate and irreversible damage to the fuel cell. These levels were 2 to 3 orders of magnitude higher than the tar levels in the raw producer gas. Long-term damage due to corrosion or other factors were not studied.

Fuel Cell Reaction Rates and Gas Compositions

To predict fuel cell performance on variable composition producer gas, large-surface-area fuel cells with active surface areas of approximately 100 cm^2 were tested on several gas compositions. The gas compositions corresponded to equilibrium gas compositions of different reactor operating conditions from the gasifier. Table 20 summarizes the gas compositions and input flow rates for the fuel cell tests. The flow controllers required a minimum of 0.2 lpm, which limited the minimum total flow rates. Two commercially available fuel cells, one AS and one electrolyte supported (ES) fuel cell, were tested on all eight gas compositions. The furnace temperature for the AS fuel cell was 800°C. The furnace temperature for the ES fuel cell was 820°C. Both fuel cells were initially run on pure hydrogen, Test Condition A, to baseline their performance. They were then run at the other seven conditions in a randomly determined order. The test fixtures were not optimized, so the test results were analyzed relative to the different gas compositions in the same test fixture and furnace temperature.

Figures 24a and 24b show the power output characteristics of the AS and ES fuel cells. With the exception of Test Condition J, the power output curves for the ES cell were grouped in a very narrow operating zone. The performance curves for the AS cell were much more dispersed and showed a much greater power dependence on gas composition. Figure 25 shows this dependence better. The maximum power output for each gas composition was compared to its volumetric energy density. Both cells show a very nearly linear dependence of power density to volumetric energy density. However, the AS cell curve has a much steeper slope than the ES cell. This effect may be due to mass transfer limitations in the porous anode structure. The AS cell produced a 25% drop in maximum power density throughout the range of producer gas compositions. The ES cell produced a 15% drop in power density throughout the range of gas compositions.

Fuel Cell Operation on Biogas

Two button cells and a stack were operated directly on syngas from the bench-scale gasifier. For these tests Ceramatec, Inc., was contacted and agreed to provide button cells and a

small stack for testing. Ceramatec cells and stacks have been reported to operate for up to 4000 hours on hydrogen with sulfur content as high as 1000 ppm (25). In all tests, wood chips were gasified, and a slipstream of the syngas was fed to the fuel cell after being scrubbed of H_2S through a passive H_2S scrubber. The first test was an initial screening run, in which the operating range of the fuel cell on producer gas was determined and the testing procedure refined for the second test. Both scrubbed and unscrubbed syngas was run on the fuel cell during this test. The second test was a 12-hour run in which the output of the button cell was observed for changes over time to determine if a relatively stable steady-state condition could be achieved within that time period. For the third test, a 100-watt stack was operated on a combination of hydrogen and syngas through a period of 118 hours. Initially, two tests were planned, similar to the button cells, with the first being a screening test. Only one test was completed, however. In that test, the stack operated through the full 100-hour break-in period and approximately 3 hours on syngas. A malfunctioning flow controller stopped flow to the stack during operation on syngas. During this time, the voltage dropped and could not be recovered, prematurely ending the first test. We were unable to restore power from the stack, preventing a second test run on the stack.

Table 20. Gas Compositions and Flow Rates for Fuel Cell Tests

	Test Condition	A	F	I	H	G	E	K	J
	Thermal Energy								
	HHV at 300 K, kJ/L	9.469	11.432	4.93	6.36	8.23	8.122	5.79	7.38
Actual Flow Input Rates	Flow Rate, lpm	3.11	4.35	4.28	4.29	4.30	3.74	4.28	4.29
	H_2, lpm	3.11	2.02	0.99	1.29	1.69	1.86	1.28	1.65
	CO, lpm	0.00	1.09	0.86	1.10	1.41	1.25	0.90	1.13
	CH_4, lpm	0.00	0.00	0.00	0.00	0.00	0.00	0.00	0.00
	CO_2, lpm	0.00	0.38	0.39	0.32	0.22	0.22	0.39	0.33
	Water, g/min	0.00	0.64	0.41	0.34	0.25	0.30	0.51	0.44
	N_2, lpm	0.00	0.00	1.48	1.12	0.64	0.00	1.02	0.58
Producer Gas Composition	H_2, mol%	100	46	23	30	39	50	30	38
	CO, mol%	0	25	20	26	33	33	21	26
	CH_4, mol%	0	0	0	0	0	0	0	0
	CO_2, mol%	0	9	9	7	5	6	9	8
	H_2O, mol%	0	20	13	11	8	11	17	14
	N_2, mol%	0	0	34	26	15	0	24	13

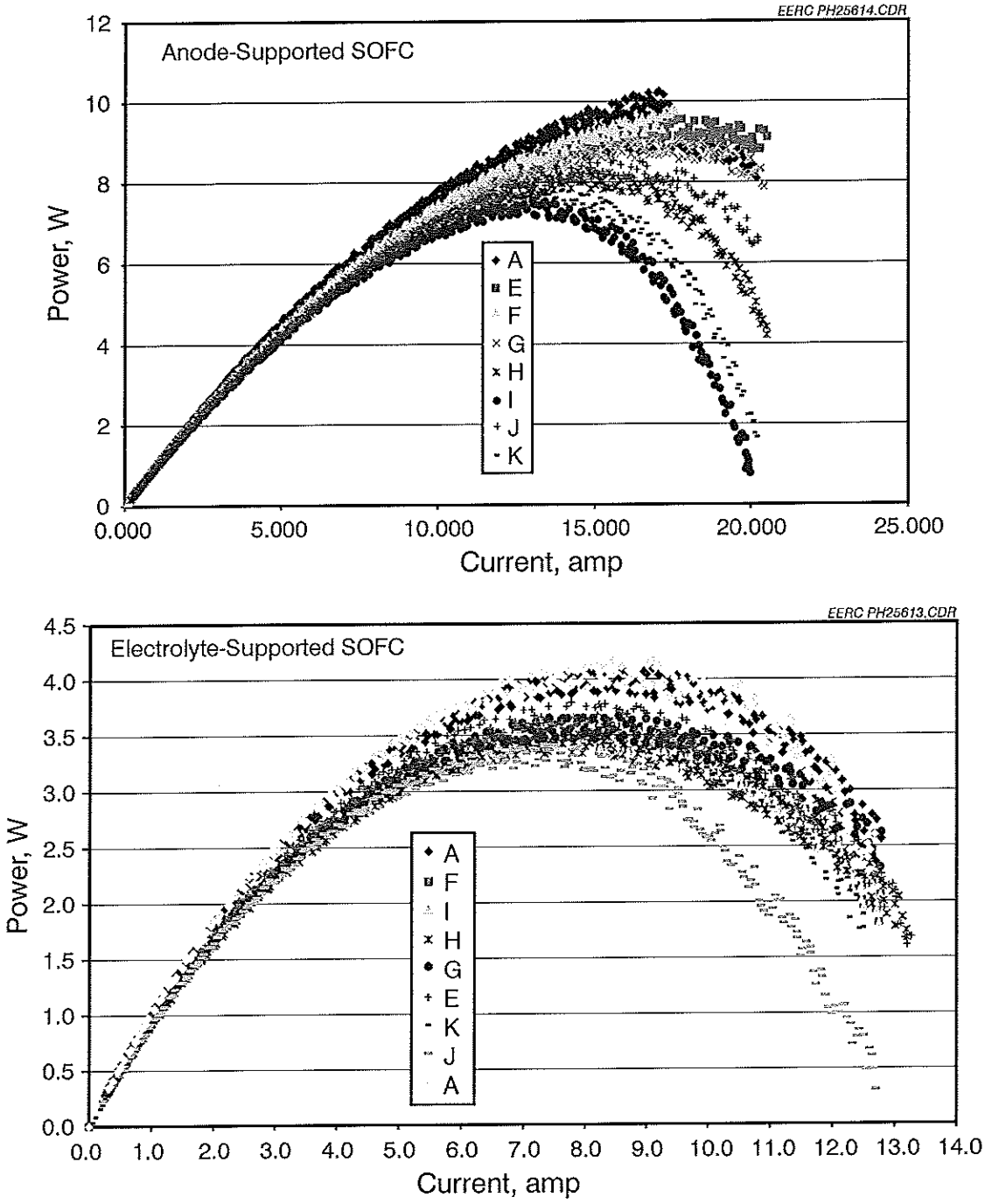

Figure 24. Power curves for anode-supported fuel cell on various gas compositions (top); power curves for electrolyte-supported fuel cell on various gas compositions (bottom).

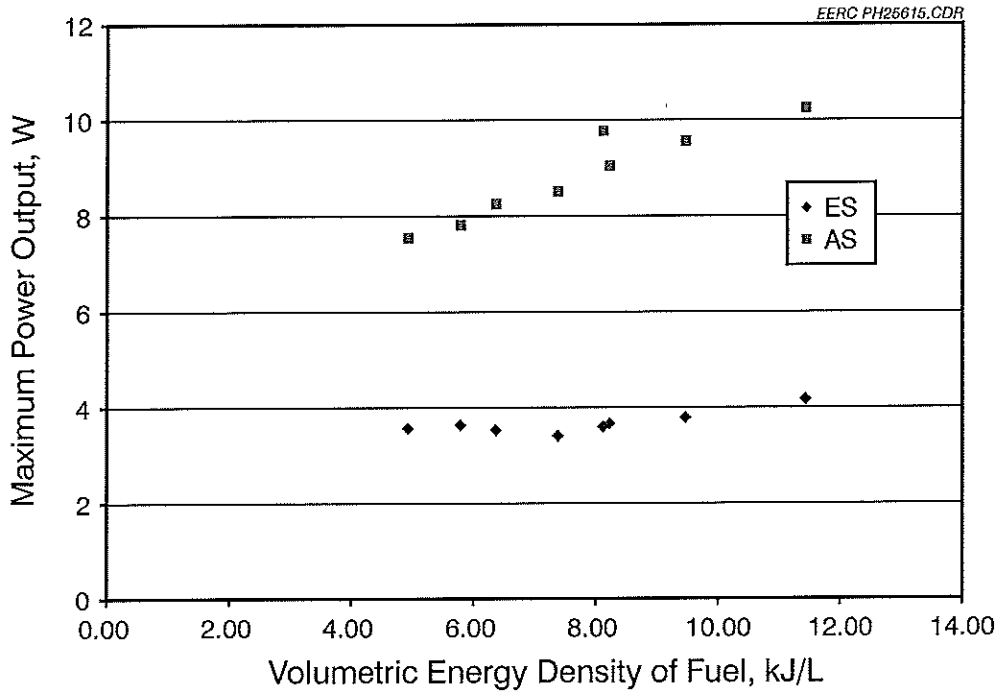

Figure 25. Dependence on power density to gas energy density for different gas compositions.

Figure 26 shows the button cell test fixture in the furnace just prior to testing. Ceramatec provided two button cell test fixtures. Each test fixture consisted of a 1-inch-diameter zirconia tube with the button cell attached to one end and a rubber stopper at the other end. The button cell was attached to the tube with the anode side in the tube and the cathode exposed to atmosphere. Two sets of platinum wires were used to provide four-point electrical measurements. Hydrogen and simulated producer gas were delivered to the cell through a ¼-inch-diameter tube centered within the larger 1-inch tube and passing through the rubber stopper. Fuel gas flows through the ¼-inch tube, impinges upon the button cell anode, flows radially outward along the anode, and then down through the annular space between the two tubes. It is exhausted through an opening at the bottom of the test fixture.

The two button cell tests were operated on syngas from dry oak wood pellets and high-moisture pine wood cubes. The stack was tested on syngas from high-moisture pine wood cubes. Figure 27 provides an image of the Ceramatec stack in the furnace prior to testing. Hydrogen/syngas is introduced through a manifold at one end of the stack and extracted through a manifold at the other end. Air is introduced to a manifold at the back of the stack and exhausted into the furnace through flow passages in the interconnects. The fuel gas and air are preheated to furnace temperature prior to entering the stack. Thermocouples are positioned at fuel and air input. Power is drawn from the stack through end plate power leads.

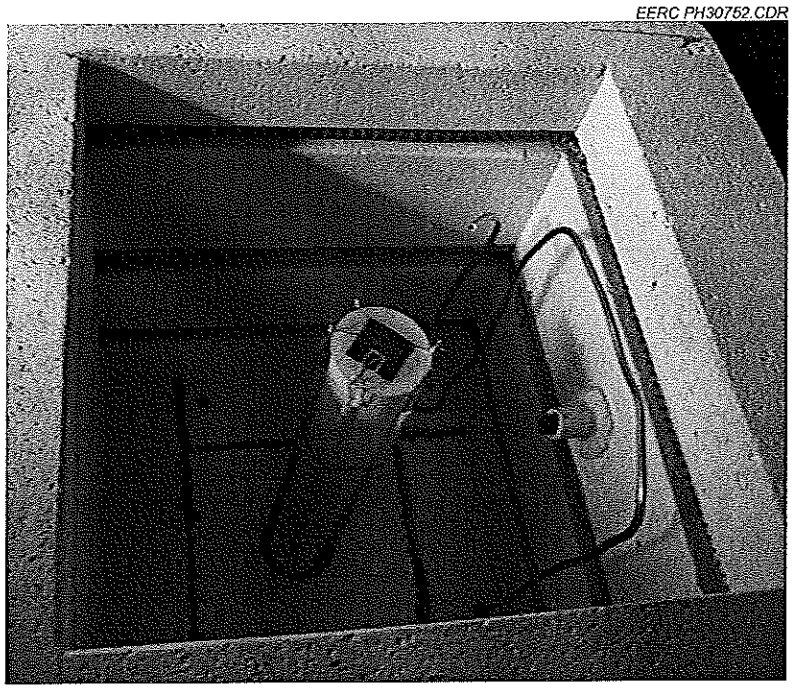

Figure 26. Button cell test fixture in furnace prior to test.

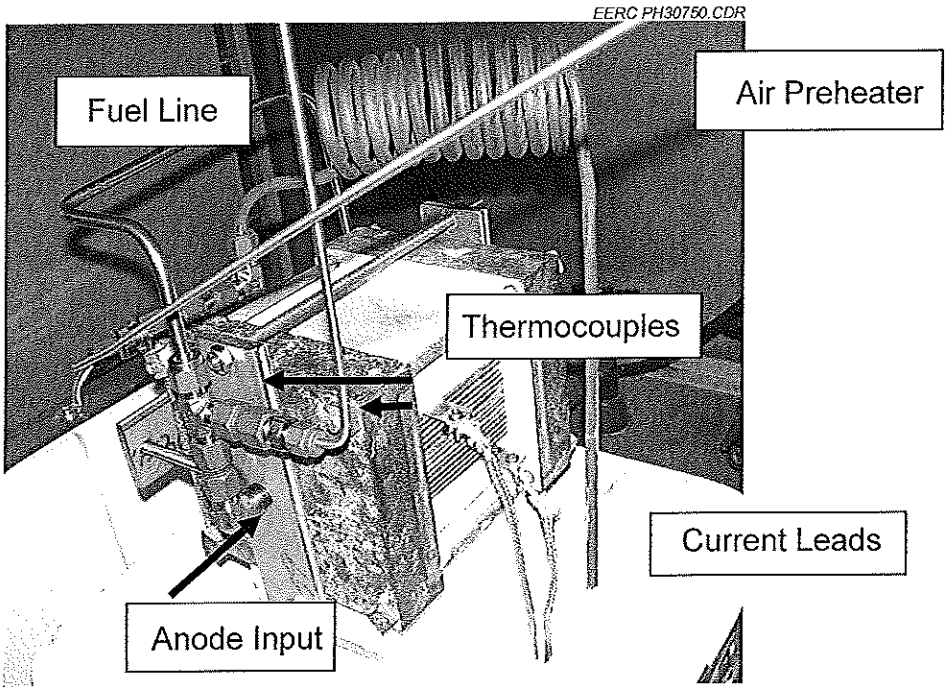

Figure 27. 100-watt SOFC stack in furnace prior to testing.

The test apparatus for both the button cell tests and the small stack test are very similar and shown in Figure 28. Figures 29–31 provide images of the test setups. The bench-scale gasifier is located in a walk-in hood as shown in Figure 30. Because of space constraints and safety considerations, the fuel cell was located in an adjacent hood. The test apparatus was designed to feed either bottled hydrogen or a slipstream of syngas from the gasifier to the fuel cell. A stainless steel bubbler was used to select gases, either hydrogen or syngas, through two valved inputs for Tests 2 and 3. For the first test, a bubbler was not used. In its place was a two-way valve. A rotameter located downstream of the bubbler acted as the fuel gas flow controller for the button cell tests. For the stack test, an Omega FMA-2608A digital flow controller was used to control flow to the rotameter. For the button cell tests, the anode exhaust of the fuel cell was also passed through a small glass bubbler as an air seal. For the stack test, the exhaust bubbler was eliminated because the back pressure reduced stack voltage significantly. This may have been caused by leaks either at the input to the stack or within the stack. The air exhaust was vented into the hood. A Lynntech load center and input box were used for current control and data acquisition.

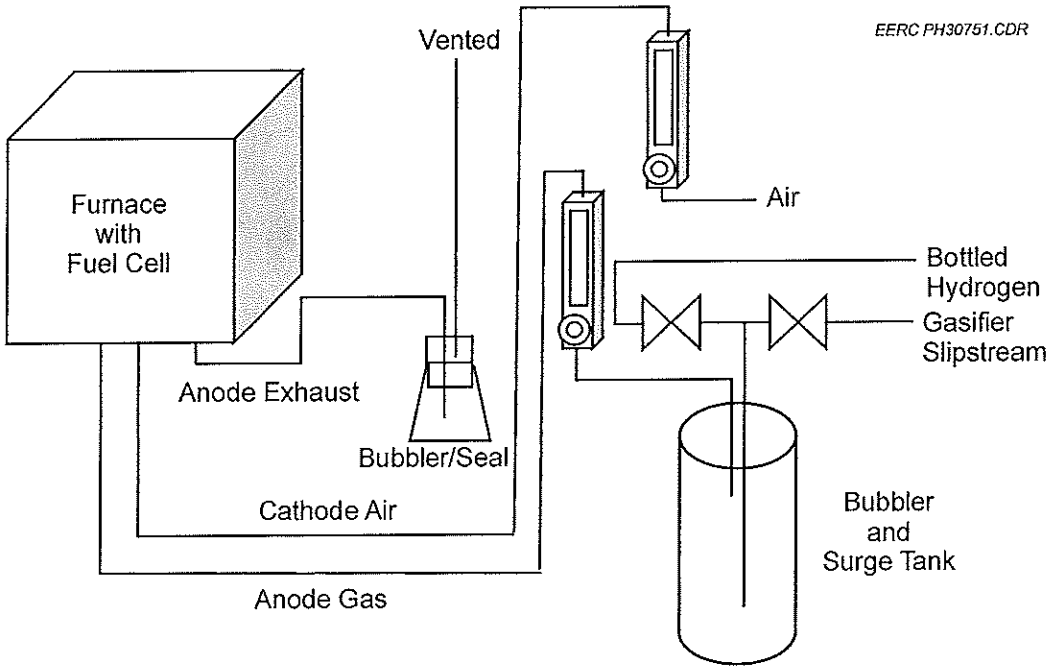

Figure 28. General fuel cell test apparatus.

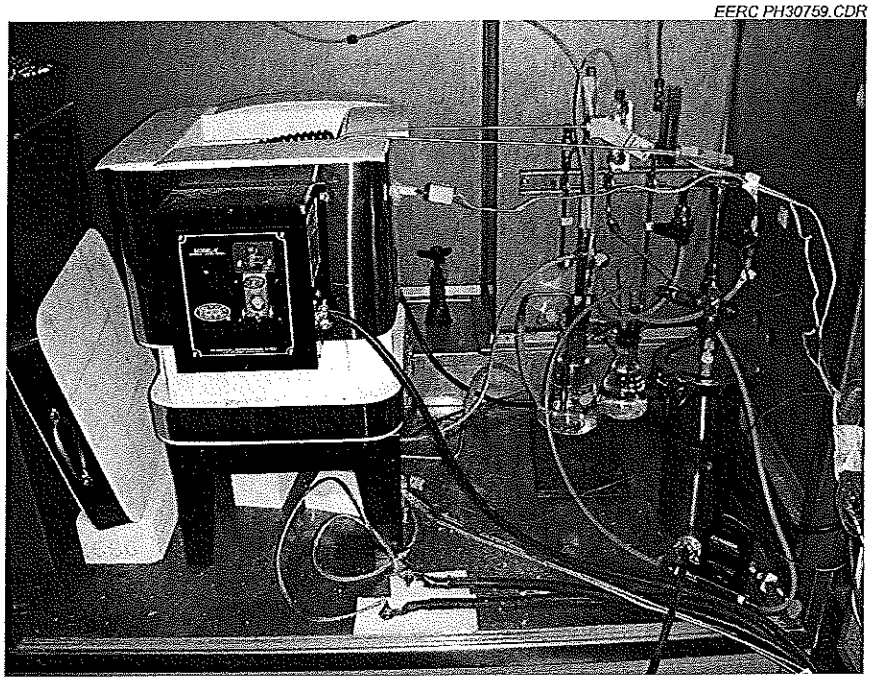

Figure 29. Fuel cell test apparatus in air hood.

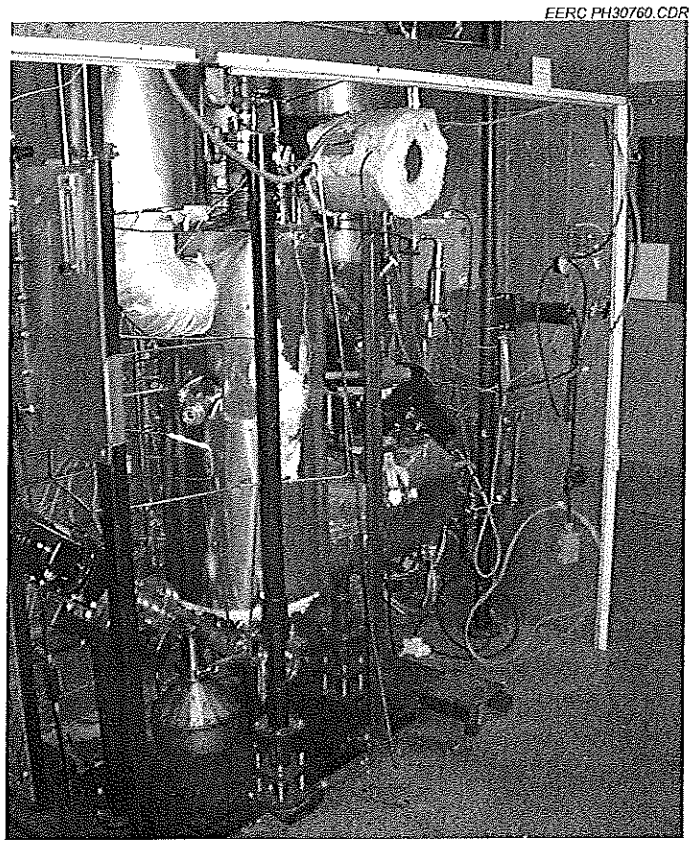

Figure 30. Bench-scale gasifier in walk-in hood.

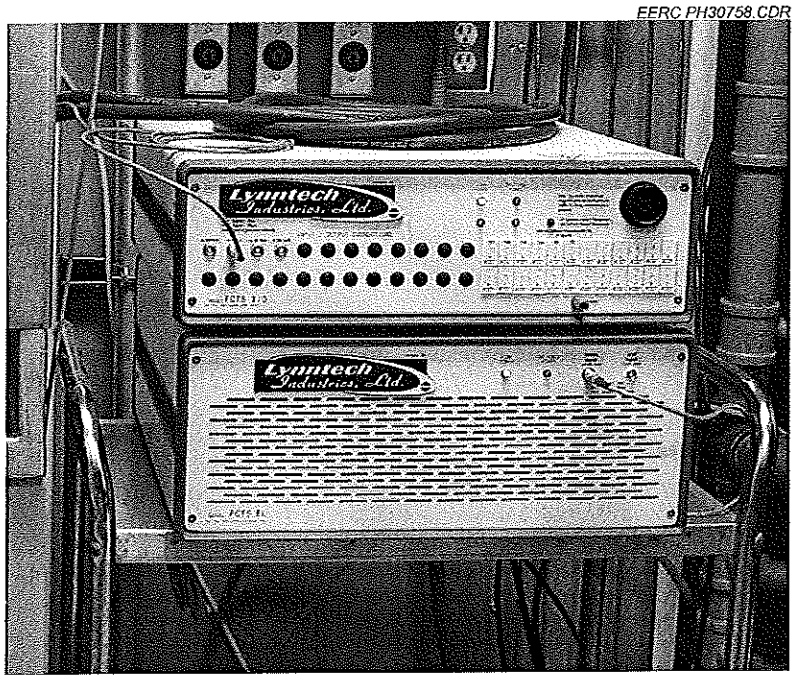

Figure 31. Load center and input box.

The general test procedures for all tests were similar. Exceptions are described below. The fuel cell was brought up to a temperature of 750°C over a 15-hour period under bottled hydrogen. Once at temperature, a baseline sweep was performed. Based on the sweep data, the steady state current was set to provide a voltage of 0.7–0.8 V per cell. The bench-scale gasifier was then brought online. Once the gasifier was at temperature and producing gas, the input to the fuel cell was switched to syngas. The syngas was passed through a H_2S scrubber. At shutdown, the fuel gas was switched back to hydrogen. The gasifier was shut down and the fuel cell allowed to cool to room temperature under a hydrogen atmosphere.

The first test was a screening test to refine test procedure and qualify performance expectations. This test ran for approximately 6 hours. For this test, a bubbler was not used. The gases were selected directly from two valved inputs connected to a tee. The second cell test ran for over 12 hours to determine if a relatively stable steady-state condition could be achieved on syngas. Neither cell underwent the manufacturer recommended break-in period of 100 hours. For the stack test, the general procedure was followed for the first day of operation. The fuel cell was then switched to hydrogen and operated at open circuit voltage for an additional 100 hours to break in the stack. The gasifier was then brought back online and the fuel cell switched back to syngas.

For the first test, both steady-state and sweep data were obtained. Figure 32 shows the steady state voltage of the cell over time. Hydrogen was input to the cell at 114 cm^3. The scrubbed syngas input fluctuated between 134 and 201 cm^3. Overall, the cell experienced a drop of 23% in average voltage from 0.71 to 0.55 volts when going from hydrogen to syngas. Both energy density and input power to the cell from the syngas were lower than the hydrogen input.

The energy density of the syngas was 201 Btu/scf compared to 343 Btu/scf for hydrogen. The input power for syngas was 16.7 watts compared to 32.3 watts for hydrogen. Throughout all three tests, water would periodically condense in the tubing from the H_2S scrubber to the valved inputs. This occurred in the first test and caused a temporary shutdown of the test while the line was purged. When the system was brought back, up the cell voltage dropped to approximately 0.4 volts. The input was switched back to hydrogen in an attempt to recover the cell. However, cell output remained steady at 0.4 volts. The test was shut down. The high fluctuation and condensed water in the syngas line was addressed in subsequent tests by installing a bubbler, providing a surge capacity to absorb pressure fluctuations and deposit water.

Figure 33 provides a comparison of the I–V sweeps for hydrogen and syngas. Instrument resolution limited the precision of measurements to ±0.025 volts. The data points in Figure 33 are the average of 3–5 sweeps each. Throughout the full operating range of the cell, power dropped by approximately 24% when operating on syngas as compared with hydrogen.

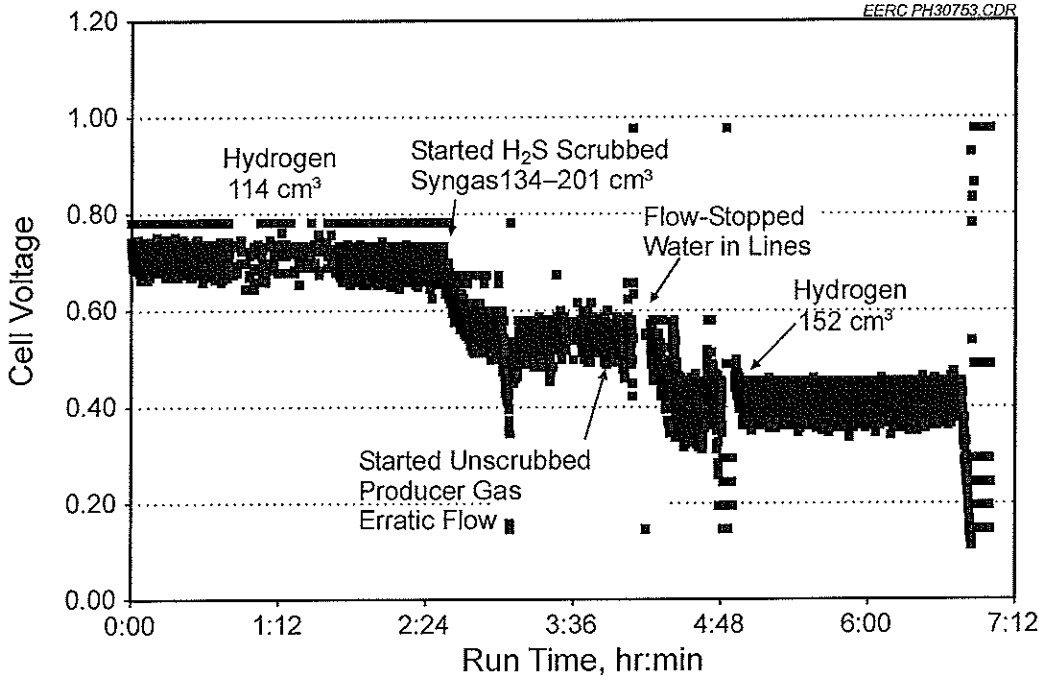

Figure 32. Cell voltage for current draw of 0.8 amps and average syngas composition of 23% CO, 13% CO_2, 3% CH_4, 25% H_2, and 36% N_2.

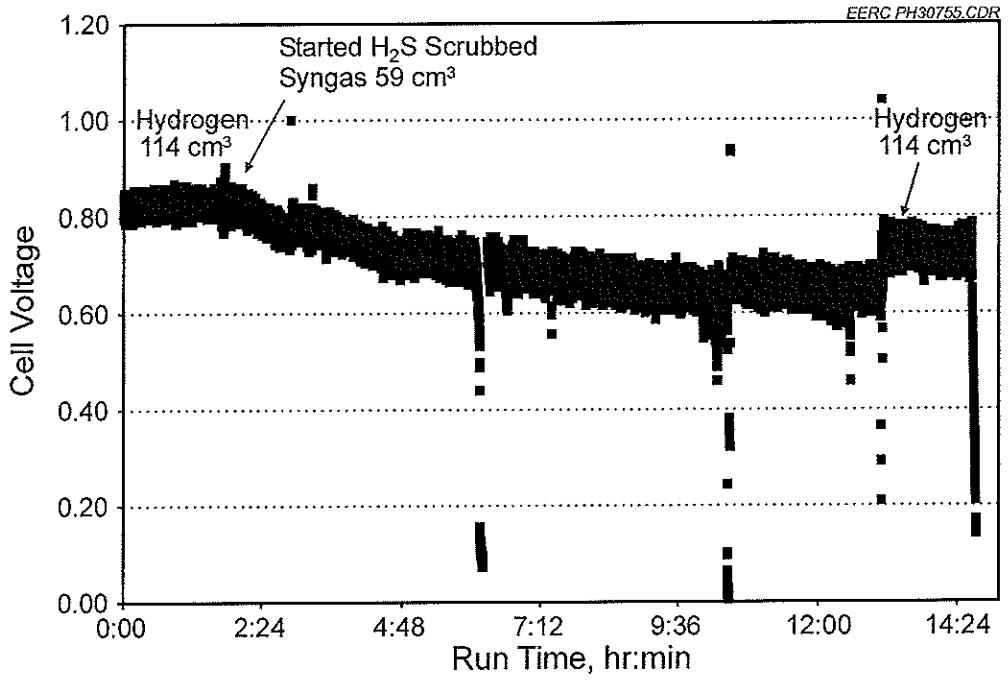

Figure 33. I–V curves of hydrogen and syngas with an average composition of 23% CO, 13% CO_2, 3% CH_4, 25% H_2, and 36% N_2.

A bubbler was installed for the second test to mitigate pressure and water surges in the syngas line. The objective of the test was to determine if a relatively stable steady state condition could be achieved over an extended period of time. Figure 34 shows the cell voltage over time. This test was carried out over a 14-hour period, with the cell operating on syngas for approximately 11 of those hours. The results are similar to the first test but demonstrate more stability because of the bubbler/surge vessel was in place. The average syngas energy density was 230 Btu/scf, slightly higher than the first test. Both the hydrogen and syngas flow rates were reduced to 114 and 59 cm^3, respectively, providing power inputs of 24.2 and 8.4 watts, respectively. Overall, the cell output dropped by 21% on syngas as compared to hydrogen. Average cell voltage for syngas once steady state was achieved was 0.65 volts, compared to 0.83 volts for hydrogen. After operating on syngas for 11 hours, the average cell voltage for hydrogen lowered to 0.73 volts. It is unclear whether the drop in performance was due to break-in of the cell or a side effect of operating on syngas. For the next test, a 100-hour break-in period, as recommended by Ceramatec, was performed in an attempt to determine if syngas operation irreversibly reduced fuel cell performance.

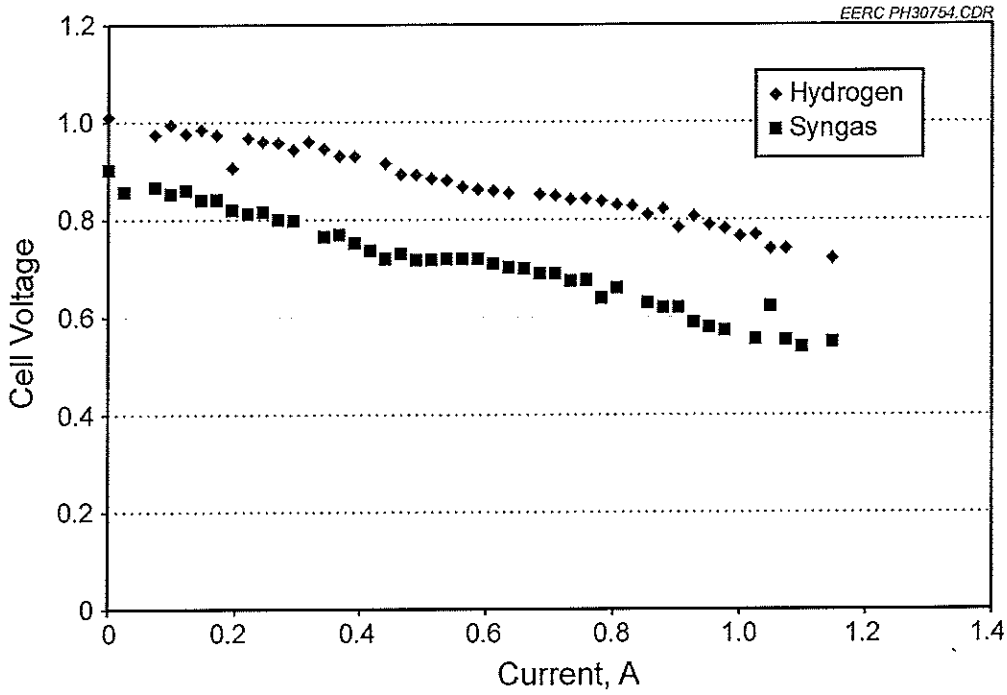

Figure 34. Cell voltage for current draw of 0.8 amps and average syngas composition of 26% CO, 11% CO_2, 2% CH_4, 24% H_2, and 27% N_2.

A 100-watt SOFC stack was used for the third test. The original plan was similar to the button cell tests. The first stack test was approached as a screening test to refine test procedure and qualify expectations. If the stack survived the first test, a second stack test would be conducted to obtain refined performance data. In this case, the stack did not survive the first test because of a flow controller malfunction, and a second stack test was not conducted.

Figure 35 shows the steady state stack performance before the break-in period. After the initial heatup, the stack current was set to 8.6 amps, producing a stable stack voltage on hydrogen. The gasifier was fired up on pine cubes and the stack input switched to syngas. Upon switching to syngas, flow was briefly lost. The gasifier output was increased and the exhaust valve choked slightly to increase back pressure to the slipstream line. At this point, stack input fluctuated from 2.8 to 4.4 lpm. After about 1 hour of operation on syngas, the stack was switched back to hydrogen and the gasifier shut down. The stack was then set to open circuit voltage for the next 100 hours to break it in. Open circuit voltage was 16.6 volts. During this time, a small pump was installed in the slipstream line to increase syngas flow to the stack. At the end of the break-in period, the gasifier was fired up and stack set back to 8.6 amps. Figure 36 shows the steady-state stack output after the break-in period. The stack was operated on hydrogen for approximately 1.5 hours. It was then switched to syngas and operated for an additional 1.5 hours. Steady-state operation on hydrogen was cut short because of a malfunctioning flow controller.

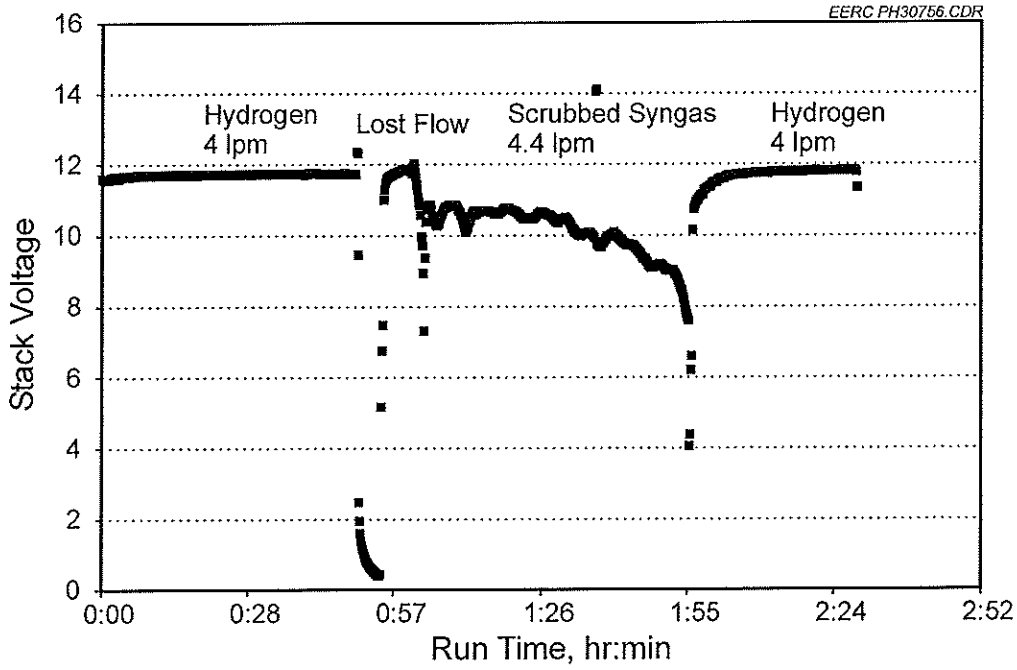

Figure 35. Steady-state stack voltage before break-in period for a current output of 8.6 amps and average syngas composition of 20% CO, 13% CO_2, 2% CH_4, 28% H_2, and 37% N_2.

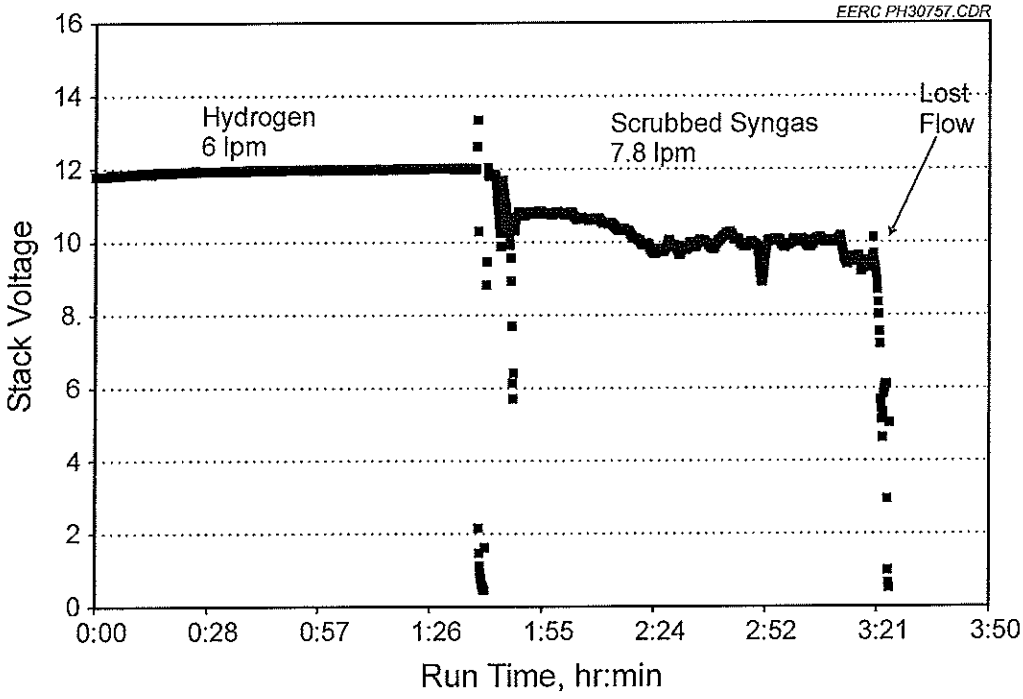

Figure 36. Steady-state stack voltage after break-in period for a current output of 8.6 amps and average syngas composition of 22% CO, 11% CO_2, 1% CH_4, 24% H_2, and 41% N_2.

Figure 36 shows a more stable output on syngas than Figure 35 because of the increased flow rate from the slipstream pump. The average voltage on syngas, however, for both tests was very similar. The average syngas voltage in Figure 35 was 10.2, as compared with 10.3 in Figure 36. Likewise, operation on hydrogen was also stable. Output voltage during operation on hydrogen was 11.7 and 12 volts for Figures 35 and 36, respectively. In Figure 35, the energy inputs were 851 and 511 watts for hydrogen and syngas, respectively. The average energy density of the syngas was 189 btu/scf. In Figure 36, the energy inputs were 1277 and 855 watts for hydrogen and syngas, respectively. The average energy density of the syngas was 176 btu/scf.

Figure 36 demonstrates that while operation on syngas was brief, it did stabilize to 10.3 volts for approximately 1 hour prior to the malfunctioning flow controller. Stable operation was also demonstrated at the button cell level in Figure 34. Overall, these tests demonstrate the feasibility of operating an SOFC stack on syngas with minimal cleaning. Of course, additional testing should be performed; however, testing to date revealed no showstoppers in developing the technology.

REFERENCES

1. Energy Information Administration. *Renewable Energy Annual 1998 with Data for 1997*; DOE/EIA-0603 (98)/1, Distribution Category UC-950; U.S. Department of Energy Office of Coal, Nuclear, Electric, and Alternate Fuels: Washington, DC, Dec 1998.

2. Schmidt, D.; Gunderson, J. Opportunities for Hydrogen: An Analysis of the Application of Biomass Gasification to Farming Operations using Microturbines and Fuel Cells. In *Proceedings of the 2000 Hydrogen Program Review*, 2000.

3. Schmidt, D.D.; Pinapati, V. *Opportunities for Small Biomass Power Systems*; Final Technical Report for U.S. Department of Energy Contract No. DE-FG02-99EE35128. EERC Publication 2000-EERC-11-01; Energy & Environmental Research Center: Grand Forks, ND, Nov 2000.

4. Devi, L.; Ptasinski, K.J.; Janssen, F.J. A review of the primary measures for tar elimination in biomass gasification processes, *Biomass and Bioenergy*, **2003**, *24*, 125–140.

5. Reed, T.B.; Das, A. *Handbook of Biomass Downdraft Gasifier Engine Systems*; The Biomass Energy Foundation Press, 1988; p. 24.

6. Milne, T.A.; Evans, R.J.; Abatzoglou, N. *Biomass Gasifier "Tars": Their Nature, Formation, and Conversion*; National Renewable Energy Laboratory Report for Contract No. DE-AC36-83CH10093, 1998.

7. Abatzoglou, N.; Fernandez, J.C.; Laramee, L.; Gasso, S.; Chornet, E. The BIOSYN Waste Biomass Gasification: Environmental Performances. In *Biomass Gasification and Pyrolysis*;

Kaltschmitt, M.; Bridgwater, A.V., Eds; CPL Scientific Ltd.: Newbury, UK, 1997; pp 259–268.

8. Sasaki, K.; Hori, Y.; Kikuchi, R.; Eguchi, K.; Ueno, A.; Takeuchi, H.; Aizawa, M.; Tsujimoto, K.; Tajiri, H.; Nishikawa, H.; Uchida, Y. Current–Voltage Characteristics and Impedance Analysis of Solid Oxide Fuel Cells for Mixed H_2 and CO Gases. *Journal of the Electrochemical Society* **2002**, *149* (3), A227–A233.

9. Sasaki, K.; Teraoka, Y. Equilibria in Fuel Gases Part II: The C–H–O Ternary Diagrams, *Journal of the Electrochemical Society*, **2003**, *150* (7), A885–A888.

10. Sasaki, K.; Hori, Y.; Kikuchi, R.; Eguchi, K. *Electrochemistry*, **2002**, *70* (18), as referenced by Sasaki and Teraoka (9).

11. Koh, J.H.; Kang, B.S.; Lim, H.C.; Yoo, Y.S. Thermodynamic Analysis of Carbon Deposition and Electrochemical Oxidation of Methane for SOFC Anodes. *Electrochemical and Solid-State Letter* **2001**, *4* (2), A12–A15.

12. Horita, T.; Sakai, N.; Kawada, T.; Yokokawa, H.; Dokiya, M. *J. Electrochem. Soc.* **1996**, *143*, 1161, as referenced by Koh et al. (11).

13. Abudula, A.; Ihara, M.; Komiyama, H.; Yamada, K. *Solid State Ionics* **1996**, *86–88*, 1203, as referenced by Koh et al. (11).

14. Elongovan, S.; Hartvigsen, J.; Khandkar, A.; Privette, R.; Kneidel, K.; Perna, M.A.; Tharp, M. *Planar SOFC Integrated System Technology Development*; Technical Report for the U.S. Army Research Office Contract No. DAA H04-94-C-0012, 1997.

15. EG&G Technical Services, Inc. Science Applications International Corporation. *Fuel Cell Handbook 6th Edition*; Technical Report for U.S. Department of Energy under Contract No. DE-AM26-99FT40575, Nov 2002.

16. Weadman, S., Global Solar Energy Institute. Personal communication with P. Hutton, July 18, 2003.

17. Sales Engineer, TEMCo, Tower Electric Motor Company. Personal communication with P. Hutton, July 18, 2003.

18. Cunningham R. *Fuel Cell Gas Turbine Hybrids – A Key Part of a Clean Future.* The Rolls-Royce Development Programme for Pressurised Hybrid Fuel Cell Systems, Fuel Cells Group, 2001.

19. Fuhs, S. *Solid Oxide Fuel Cell Hybrids: Challenges & Benefits*, GE Hybrid Power Generation Systems, May 2003.

20. EG&G Technical Services, Inc.; Science Applications International Corporation. *Fuel Cell Handbook 7th Edition*; Technical Report for U.S. Department of Energy Under Contract No. DE-AM26-99FT40575, Nov 2004.

21. Hartvigsen, J.; Elangovan, S.; Larsen, D.; Timper, M.; Czernichowski, P.; Czernichowski, A., SOFC Operation on JP-8 Reformate from a Cold Plasma Reformer. Connecticut Global Fuel Cell Center, First International Conference on Fuel Cell Development and Deployment, Session 5B.4, March 2004.

22. Franklin Fuel Cells Technology Overview. www.franklinfuelcells.com/Tech_ overview.htm (accessed June 2005).

23. Singh, D.; Hernandez-Pacheco, E.; Hutton, P.N.; Patel, N.; Mann, M.D. Carbon Deposition in an SOFC Fueled by Tar-Laden Biomass Gas: A Thermodynamic Analysis. *J. Power Source* **2005**, *142*, 194–199.

24. Kim, H.; Lu, C.; Worrell, W.L.; Vohs, J.M.; Gorte, R.J. Cu-Ni Cermet Anodes for Direct Oxidation of Methane in Solid-Oxide Fuel Cells. *J. Electrochemical Society* **2002**, *149*, A247–A250.

25. Stoots, C.M.; O'Brien, J.E.; Hawles, G.L.; Herring, J.S.; Hartvigsen, J.J. High-Temperature Co-Electrolysis of H_2O and CO_2 for Syngas Production. Fuel Cell Seminar, Nov 2006.

Supplemental References

1. Mukunda, H.S.; Paul, P.J.; Dasappa, S.; Srinaivasa, U. Results on an Indo-Swiss Programme for Qualification and Testing of a 300-kW IISc/Gasag Gasifier. *Energy for Sustainable Development* **1994**, *1* (4).

2. Reed, T.B.; Graboski, M.S.; Levie, B. Fundamentals, *Development and Scale-Up of the Air–Oxygen Stratified Downdraft Gasifier*; 1994; pp 3–15.

3. Hasler, P. *Producer Gas Quality from Fixed-Bed Gasifiers Before and After Gas Cleaning – IC Engines for LCV Gas from Biomass Gasifiers*; IEA Bioenergy and Swiss Federal Office of Energy, 1998; p. 21.

APPENDIX A

CONTAMINANT SAMPLING METHODOLOGY AND QUANTIFICATION

CONTAMINANT SAMPLING METHODOLOGY AND QUANTIFICATION

GENERAL INTRODUCTION

The basic contaminants in raw (or hot) producer gas are tar, particulate matter, and trace gases (HCl, H_2S, NH_3) produced during gasification reactions. The quantification of these contaminants is imperative in order to understand their effects on the performance of solid oxide fuel cells (SOFC). Moreover, it is a direct measure of the performance of biomass gasifiers in general and, more specifically, to the specially designed thermally integrated gasification system for the project.

The fixed-bed gasifier is designed such that it maintained an average bed temperature in the range of 875°–950°C. Another design criterion chosen was the gas-phase residence time in the uniform high-temperature zone of the reactor. The residence time of the producer gas is in the range of 0.37–2.6 s, depending primarily on the equivalence ratio.

Since the integrated SOFC–gasifier system is aimed to operate directly on raw gas (without wet scrubbing), these design criteria were aimed at reducing the tar throughput in the producer gas. Both residence times and bed temperature are critical to tar levels. The bed temperature in the current system is about 400°–450°C higher than the typical downdraft biomass gasifier. Therefore, the tar composition and amount including species distribution, based on molecular weight, are expected to be significantly different compared to a typical downdraft gasifier.

Milne et al. (1) have recorded a trend of tar distribution based on their classification of tar (four tar component classes) with respect to temperature at a fixed 0.3-s gas-phase residence time on a plot. According to this plot, the current gasifier is expected to generate more tertiary alkyl products (including methyl derivatives of aromatics such as methyl acenaphthylene, methylnaphthalene, toluene, and indene) and tertiary polynuclear aromatic hydrocarbons (PAHs, including benzene, naphthalene, acenaphthylene, anthracene/phenanthrene, and pyrene.

The detailed species characterization has not been conducted since the performance deterioration of the SOFC has not been observed at low tar loading. These tests will be conducted if there is any unexpected performance deterioration observed during prototype testing and species characterization is necessary to design cell operating conditions. The primary aim was to first determine tar concentration in the producer gas through gravimetric analysis.

Trace gases such as hydrogen sulfide (H_2S) and hydrogen chloride (HCl) are known to have caused serious performance deterioration of the SOFC. These trace gas quantifications using colorimetric gas detection tubes (CGDTs) are found to be a simple and effective technique for producer gas. A few expected tar species such as benzene, toluene, and xylene (BTX) were determined using similar techniques, and findings were substantiated using gas chromatography (GC) analysis of sampled tar. Identification of ammonia (NH_3) was also carried out using the same CGDT technique.

An important constituent of the producer gas besides tar is particulate matter; yet, no reports are found in the open literature on the effect of particulate matter on the performance of SOFCs. However, it is expected to deteriorate the performance of the SOFC beyond a critical loading level in the producer gas. Therefore, it is important to determine the level of particulate loading, its size, fraction of carbon, and inorganic residue morphology for relating the drop in SOFC performance, if any. This information is also useful in arriving at an effective particulate filter design and its predicted operation.

Two approaches were adopted to determine particulate loading: 1) simultaneous sampling along with tar from a slipstream of gas matter where particulate matter is collected on heated quartz thimble and 2) particulate matter collected in the heat exchanger and gas-quenching pots of the system, as shown in Figure A-1.

The carbon in the particulate matter was analyzed using differential thermal analysis (DTA)–thermogravimetric analysis (DTA–TGA). The inorganic content in the particulate matter was analyzed using scanning electron microscope (SEM) morphology.

A separate test was conducted to determine the presence of tar on the particulate matter collected in the cyclone dump. The carbon fraction on the particulate matter is expected to have adequate surface area for promoting chemisorption and physisorption of tar at favorable temperature conditions upstream of the cyclone. This hypothesis was verified through this test. Results are analyzed in the concluding section.

TAR AND PARTICULATE SYSTEM AND PROCESS OVERVIEW

An elaborate tar and particulate sampling and analysis procedure has been developed and implemented. A general outline of the procedures is in the European Tar Protocol (2). Further developmental efforts in order to generate reliable information on the tar species are in progress. The schematic view of the setup is shown in the Figure A-1. A brief description of the system follows.

A modular configuration for sampling tar and particulate matter is used in the procedure. It consists of five modules connected in series, as depicted in Figure A-1.

Module 1 consists of a sampling probe comprising a gas inlet nozzle with geometry that can maintain isokinetic sampling conditions at gasifier operating flow rates and gas temperature. A slipstream of producer gas was sampled from an insulated vertical tube located downstream of the cyclone. Isokinetic conditions were manually adjusted by varying sample gas flow rate using a needle valve for any change in the main producer gas flow conditions and gas temperature. For this, the gas temperature and main gas flow were constantly monitored.

Module 2 is a particulate filter module consisting of a gastight metal container configured to hold up to four thimble filters and a gas heat exchanger. This module is placed in a cylindrical heater such that the thimble filter temperature can be maintained at 350°–400°C, the

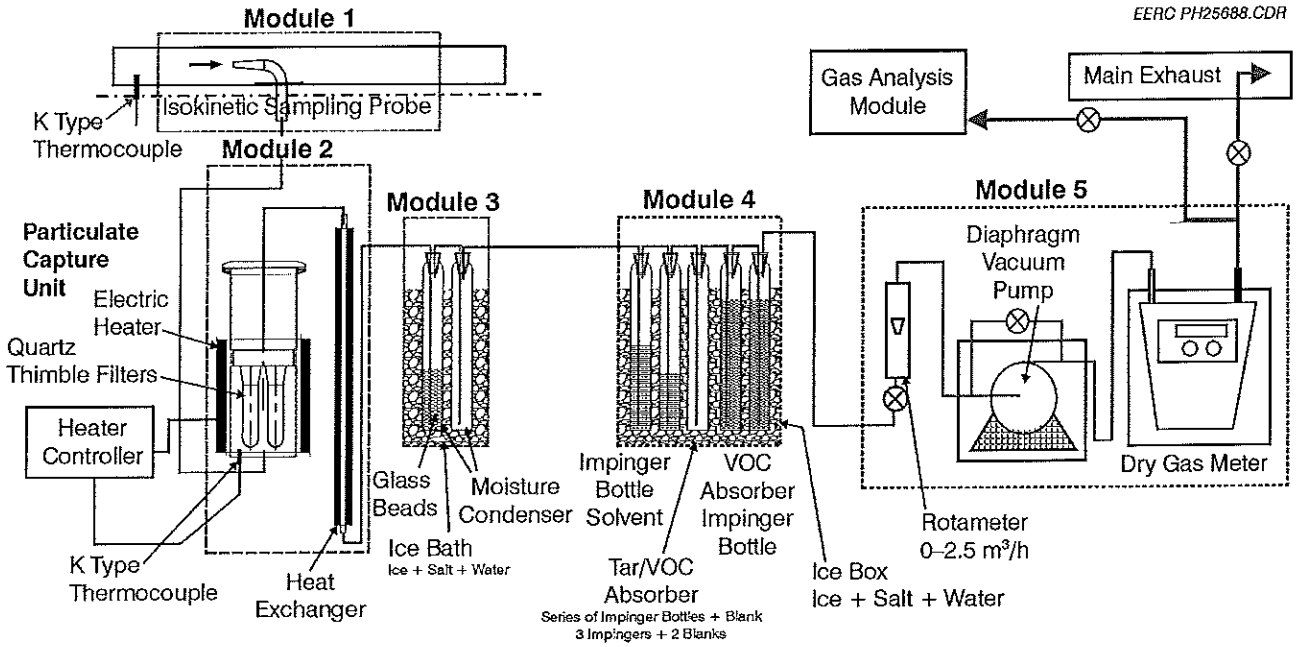

Figure A-1. Tar and particulate sampling arrangement.

recommended temperature range (1). The temperature of the sampled raw gas ranged from 450° to 750°C, depending on the gasifier operating conditions. The purpose of maintaining a thimble filter temperature above 350°C is to avoid tar and moisture condensing on the thimble filters. High-temperature quartz filters are used in this module. Since the particulate loading in the gas was found to be less than 200 ppm, two thimble filters (25.4 mm diameter, 100 mm length) were found to provide adequate surface area for capturing particulate matter without clogging, which may cause a large pressure drop, resulting in flow reduction during sampling. The hot gas leaving the thimble filters is cooled down to room temperature using a water-cooled tubular heat exchanger.

Modules 3 and 4 consist of 500-mL impinger bottles placed in an ice box. A mixture of salt, ice fines, and water was used to improve effective cooling of the impinger bottles below −10°C. Polyethylene spheres were used as insulation to cover the ice–salt–water mixture (Figure A-2).

The cooled gas from the condenser section (of Module 2) is passed through Module 3 consisting of two impinger bottles connected in series. The moisture in the gas is condensed in these bottles. The first bottle is filled with glass beads (3-mm diameter), and the second one is left empty and used as a blank. It was found that a large fraction of the tar condensed along with moisture in this module.

Module 4 consists of five (or four) impinger bottles. The first three are filled with organic solvent in varying quantities (250 to 75 mL). Tar in the producer gas is captured in the solvent by dissolution. The last two blank bottles are the backup solvent vapor condenser.

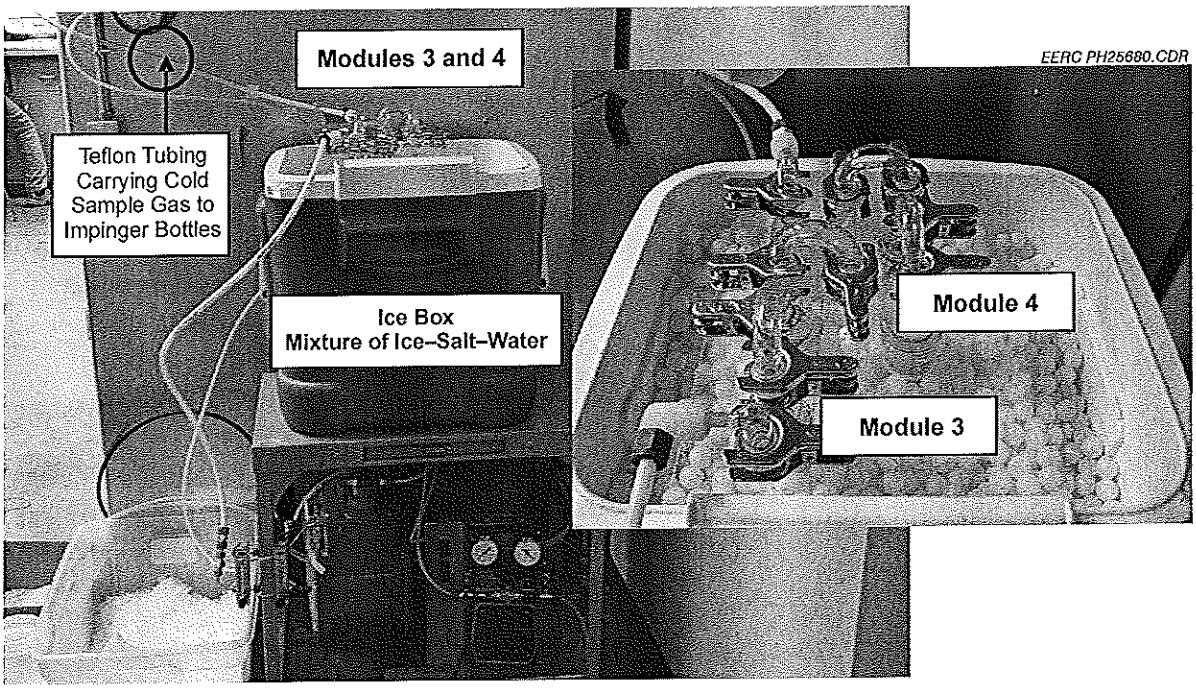

Figure A-2. Tar and particulate sampling system and its location with respect to the gasifier.

Module 5 is a gas flow control and record module, consisting of a pump, a rotameter, a gas flowmeter, stainless needle and ball valves, and pressure and temperature indicators. The gas leaving Module 5 is either exhausted or injected into the combustor.

TAR AND PARTICULATE ANALYSIS

Gravimetric analysis of tar and particulate matter was conducted. This procedure is based on conventional and well-proven methods for the gravimetric determination of both solid particles and organic species. Detailed information is available in the Tar Protocol (2).

The thimble filters were maintained at temperatures of 400°–450°C throughout the entire sampling duration. The weight of particulate on the thimble filters is obtained by determining the difference between the final and the initial weight of the thimble filters. After filters were removed from the holder, they were dried and cooled in a desiccator prior to determining weights in accordance with the procedure (1).

The tar was separated from the solvent by simple evaporation procedures as in the Tar Protocol (2). It was observed that during both the tests no particulate matter escaped the filters. A fraction of heavier tars condensed in the water-cooled heat exchanger inner wall, Teflon tube connecting the heat exchanger and Bottle 1, and in Bottles 1 and 2. A careful cleaning procedure was followed to remove tar from these surfaces. Through a phase separation technique, tar and water were separated. Methylene chloride was used as the solvent for this process. Anisole tar was separate by evaporation in accordance with the procedure (1).

A total of four long-duration (up to 5 h) tests were conducted, and the results are summarized in Table A-1. Since the amount of tar loading in the gas was low compared to typical gasification systems, semiquantitative GC analysis was used to substantiate the gravimetric results. Solvent recovery was below 100%; therefore, the distilled tar concentrate was subjected to GC analysis in order to subtract the residual solvent present in the tar. This procedure helped increase the degree of accuracy and confidence in the results obtained. The recovered solvent appeared clean of tar, and this was substantiated by GC analysis. In fact, a test was repeated using the recovered solvent.

GAS CHROMATOGRAPHY ANALYSIS OF TAR CHARACTERISTICS

The results obtained through this analysis helped estimate the components not present in the tar system leaving the thermally heated gasifier. Based on the literature review on tars and earlier in-house experience with tar analysis in the case of a downdraft gasifier, the internal calibrations for phenols and BTX were carried out to determine the concentrations of major expected components. The primary finding was that no BTX was present in any of the tests. The possibility of BTX leaving with the anisole during the evaporation process was also ruled out by conducting a separate GC analysis on the condensed anisole. Online colorimetric tube detection for BTX also revealed similar observations, indicating extremely little (below 2 ppm) or no BTX. Analysis of the results is presented in later sections.

The components determined were higher than BTX and phenol. Plausible explanations for the presence of higher tar are the operating temperature of the gasifier and gas-phase residence time, which ranged from 850°–1000°C and 0.37–2.6 s, respectively (see the performance table). A more detailed analysis will call for an elaborate analytical test procedure involving GC–mass spectrometry (GC–MS) and sampling procedure. Future efforts will be directed toward obtaining quantitative species identification, and the above tests have laid a strong foundation for achieving the desired goals.

Table A-1. Summary of the Tar and Particulate Analysis

Test No.	Weight					Total Flow, Nm^3	Concentrations	
	Particulate Filters, g	Tar					Particulate, mg/Nm^3	Tars, mg/Nm^3
		Water, g	Solvent, g	Filters, g	Total, g			
1	0.03707	0.3731	0.0252	0.0	1.3941	1.6960	22	235
2	0.0503	0.1338		0.0	0.1338	2.0126	25	66.5
4	0.0428	0.117		0.0	0.117	1.2999	33	90
6	0.2150	0.0154		0.0	0.0154	1.8075	119	8.5

QUANTITATIVE ESTIMATION OF PHENOLIC COMPOUNDS IN WATER IN GAS QUENCH POTS

In order to capture contaminants leaving the gasifier, the gas is bubbled through water in a long cylindrical container (48 in. × 3.9 in.) filled with 4.5 L of tap/deionized water. It was observed contaminant capture efficiency of these pots was very good. A photo of the gasification system (Figure A-3) depicts the location of pots with respect to the gasifier.

The water sample recovered from Pots 1 and 2 after Tests 7 and 14 was analyzed for phenols using the U.S. Environmental Protection Agency (EPA) 4AAP colorimetric method. Besides phenol, this method determines all ortho- and meta-substituted phenols, the results being reported as equivalents of phenol. Although this method has some limitations, i.e., upper limit to concentration and inability to accurately measure para-substituted phenols, it offers a rapid, inexpensive estimation of the quantity of phenolic compounds in the sample. If it is necessary to speciate the phenols, GC–MS is the method of choice. Results of both tests are shown in Table A-2.

ONLINE TRACE GAS MEASUREMENT

Hydrogen sulfide and hydrogen chloride were analyzed online using CGDTs. Since tar species usually expected in biomass gasification tar BTX were not determined, an alternative technique was found suitable for online, single-point detection. Results are shown in Table A-3.

Table A-4 lists the components measured and standard and extended range of measurement conducted using CGDT.

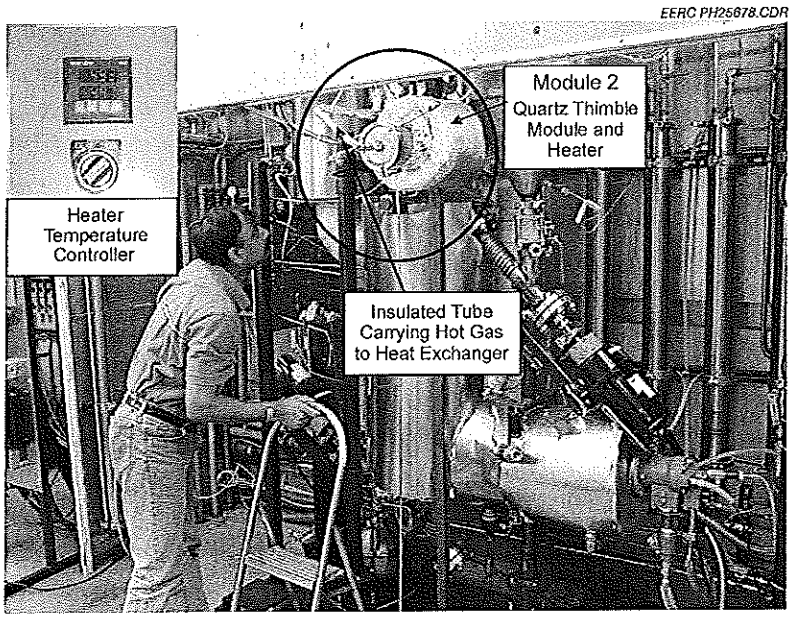

Figure A-3. Gasification system and Module 2 (particulate filter holder).

Table A-2. Tests 7 and 14 Results

	Pot 1, µg/L	Pot 2, µg/L	Total Volume of Water, L		Total Phenol, µg		Total Vol. of Gas, m^3	Phenol, $\mu g/m^3$ (ppm)	
			Pot 1	Pot 2	Pot 1	Pot 2		Pot 1	Pot 2
Test 7	152	–	4.531	4.631	689	–	2.34	0.294	
Test 14	120	30	4.853	4.953	582	149	4.56	0.127	0.032

Table A-3. Test Results

Test No.	H_2S, ppm	NH_3, ppm	Benzene, ppm	Toluene, ppm	Xylene, ppm	HCl
1	5	<10	NA[1]	NA	NA	BD[2]
2	28	NA	NA	NA	NA	BD
3	NA	NA	NA	NA	NA	BD
4	8–10	<10	Trace	Trace	Trace	BD
6	28–30	75	<2	<1.5	<2	BD
7	<10	NA	NA	NA	NA	BD
8	<10	<10	BD	<2	<2	BD
9	<10	<10	BD	<2	<2	BD
10	<10	<10	BD	<2	<2	BD
11	<10	<10	BD	<2	<2	BD
12	<10	<10	BD	<2	<2	BD
13	<10	<10	BD	<2	<2	BD
14	<5	60–85	<0.3	<2	<2	NA
15	<5	60–85	<0.3	<2	<2	NA

[1] Not analyzed.
[2] Below detection limits.

Table A-4. Trace Gas Analysis Using CGDT

	Standard Range, ppm	Extended Range, ppm
Hydrogen Sulfide	10–120	5–60
Ammonia	5–100	2.5–50
Hydrogen Chloride	20–500	10–250
Benzene	0.5–10	0.25–5
Toluene	10–300	5–150
Xylene	10–200	5–100

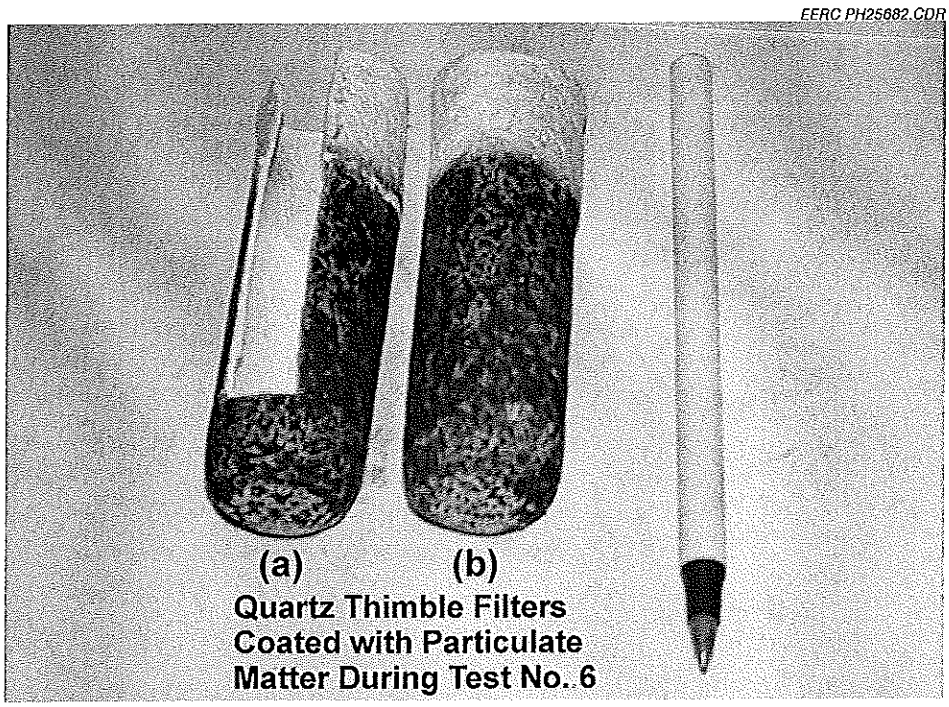

Figure A-4. Pair of thimble filters laden with particulate matter. Filter a depicts the internal surface (cut section was used for SEM study).

The detail on the operation procedure, measurement accuracy, and correction factor for this tube quantification technique has been documented in the literature (3).

If the concentration of components is below detection limits (BTX and HCl), the volume of gas passed through the tube was increased (to up to 5 times in case of BTX) in order to detect it. The test with benzene was not successful in Tests 8–13. The discussion with the manufacturer was inconclusive, and a new set of benzene tubes was procured for future tests.

Interference of moisture in the case of ammonia measurement was found significant, especially when the condensed moisture entered the tube during suction. The measurement was conducted with desiccant upstream of the tube in one case and a moisture condenser (basically, a metal surface in a cylinder where gas enters tangentially with respect to the vertical axis). Both techniques produced identical results.

PARTICULATE MATTER MEASUREMENT AND ANALYSIS

Particulates were simultaneously sampled with tar using the system shown in the schematic (Figure A-1) and photographs shown in Figure A-2.

The size and inorganic constituents of the particulate matter are collected on the heated quartz thimble filter, which is analyzed using SEM. The circle in the view graph shown in the

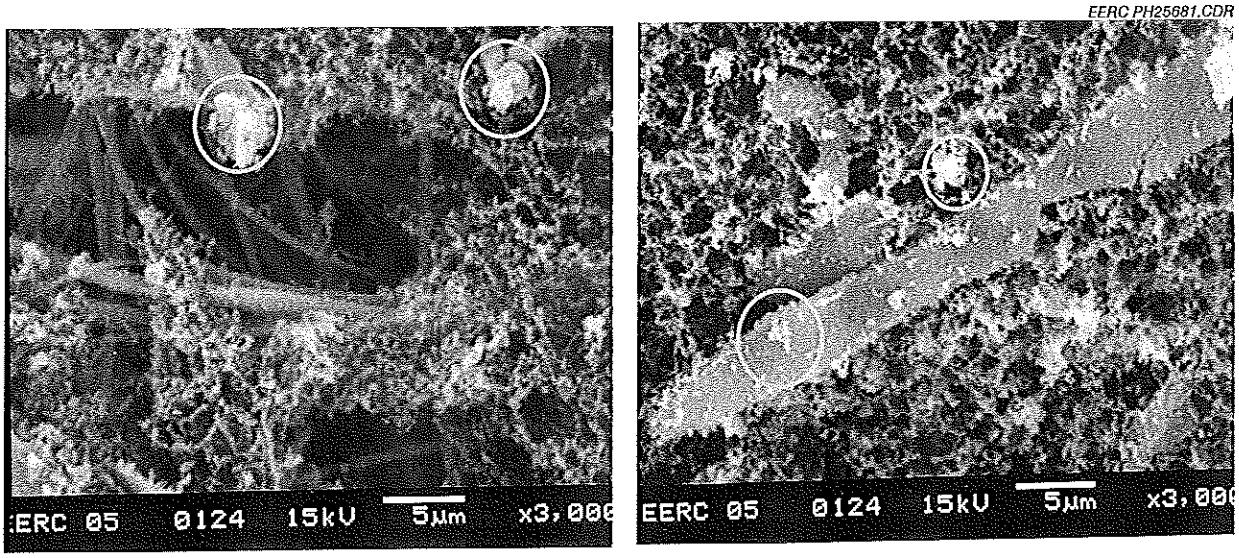

Figure A-5. SEM of particulate matter collected on quartz thimble filter during Test 4.

Figure A-5 on the right is the agglomeration of single particles collected on quartz fibers. These are the particles that are not removed in the second cyclone. The typical size of a single particle is smaller than 1 µm (as can be compared using the scale shown at the bottom of the SEM) as seen in the SEM viewgraph.

Typical inorganic constituents of the particulate matter identified are calcium, magnesium, potassium, chloride, and oxygen. Accurate quantification of the elements could not be achieved owing to the presence of quartz fiber causing a large interference through a large silica number. Figure A-4 depicts a different section of the same thimble filter. To avoid quartz interference, particles were scraped from a few locations on the same thimble filter for analysis. Inorganic morphology analysis at 16 different locations on the scraped particles is depicted in Table A-5. The analysis showed additional information on sulfur and iron species (highlighted cells), indicating the fate of sulfur.

Figure A-6 depicts an SEM of the residue collected in the first cyclone. Table A-6 depicts the elemental weight determined at three locations as shown on the viewgraphs. The alkali (basically potassium and sodium) and chloride that are collected on the quartz filter are missing in the cyclone residue. One possible explanation could be its presence as a chloride of alkali and being leached out or washed out during the wet collection process. There is also a possibility of the release of these inorganics as fine aerosols, and they escaped the cyclone because of the aerodynamics of the flow in the cyclone.

It was observed that the gas-phase hydrogen chloride either could not be detected downstream of the thimble filter or was much below the detection limit of the CGDTs, indicating the possibility of alkali chloride formation. These are a few initial findings and will lead to a detailed study on the fate of alkali as well as chloride during the heterogeneous conversion of the biomass in the thermally integrated reactor.

Table A-5. Inorganic Morphology Analysis at 16 Different Locations on the Scraped Particles, wt% of element

Point	O	Na	Mg	Al	Si	P	S	Cl	K	Ca	Cr	Fe
1	32.8	0.0	0.0	0.0	1.3	0.0	0.0	20.3	45.6	0.0	0.0	0.0
2	21.2	0.9	0.0	0.0	2.0	0.0	0.0	24.0	46.5	5.3	0.0	0.0
3	23.7	0.0	1.0	0.0	0.0	0.0	0.0	24.1	51.2	0.0	0.0	0.0
4	19.0	0.0	0.0	0.0	0.0	0.0	0.0	27.1	54.0	0.0	0.0	0.0
5	21.8	0.0	1.1	0.9	0.9	0.0	0.0	23.3	38.9	13.3	0.0	0.0
6	25.3	0.0	1.1	0.0	0.0	0.0	0.0	23.1	42.1	8.4	0.0	0.0
7	21.1	0.0	0.0	0.0	0.0	0.0	2.1	21.4	51.0	4.5	0.0	0.0
8	9.4	0.0	0.0	0.0	0.3	0.0	0.4	3.2	0.7	0.5	0.0	85.5
9	22.6	0.0	0.0	0.0	1.5	0.0	1.4	22.5	52.0	0.0	0.0	0.0
10	13.1	0.0	0.9	0.0	0.0	0.0	0.0	22.4	48.9	14.7	0.0	0.0
11	15.3	0.0	0.0	0.0	0.0	0.0	0.0	25.3	45.4	14.0	0.0	0.0
12	15.9	0.0	1.6	0.0	2.8	0.0	0.0	19.9	36.9	22.9	0.0	0.0
13	23.6	0.0	1.4	0.0	0.0	0.0	0.0	21.6	39.6	13.9	0.0	0.0
14	24.1	1.1	0.0	0.0	4.3	0.0	0.0	22.1	48.4	0.0	0.0	0.0
15	38.9	0.0	0.0	0.0	2.5	0.0	0.0	18.7	39.9	0.0	0.0	0.0
16	16.8	0.0	1.1	0.0	1.6	0.0	0.0	25.9	54.7	0.0	0.0	0.0

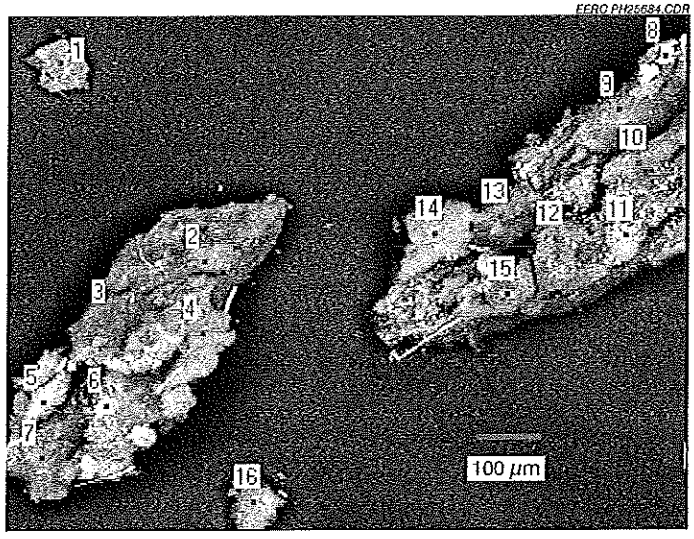

Figure A-6. Scanning electron micrograph of the residue collected in the first cyclone (magnification: 200X).

Table A-6. Elemental Weight Determined at Three Locations as Shown on the Viewgraphs

	Element, wt%		
Element	1	2	3
Mg	14.6	3.8	6.4
Al	1.6	0.0	2.0
Si	0.0	4.5	2.1
Ca	76.5	82.8	89.5
Fe	7.3	8.9	0.0

The fraction of carbon present in the residue collected in the cyclone dump is 34.1%, and the rest of it is inorganics in the form of oxides and carbonates. The DTA–TGA of the sample of the same residue was carried out in an inert atmosphere. The initial weight loss, as shown (25%) in Figure A-7, is in an inert atmosphere is owing to the decomposition of inorganic carbonate in the residue. The weight loss profile achieved a plateau after this initial loss. The weight fraction of carbon was determined by combusting it in air and losing the weight. This weight loss profile is shown in the Figure A-8.

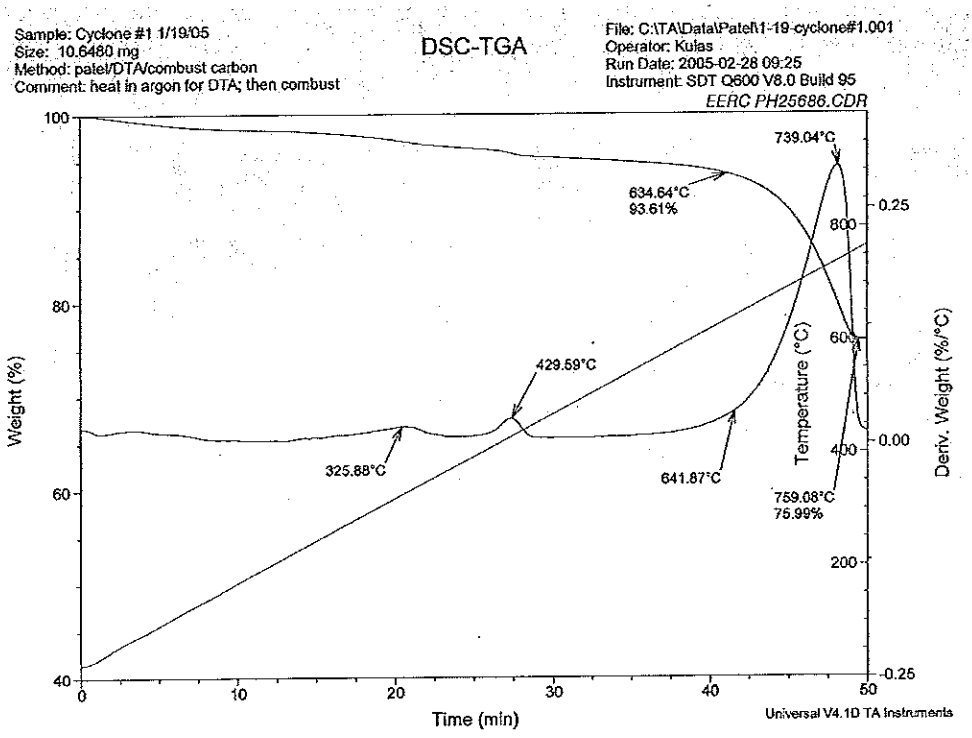

Figure A-7. TGA of residue collected in Cyclone 1. The weight loss is observed in inert atmosphere.

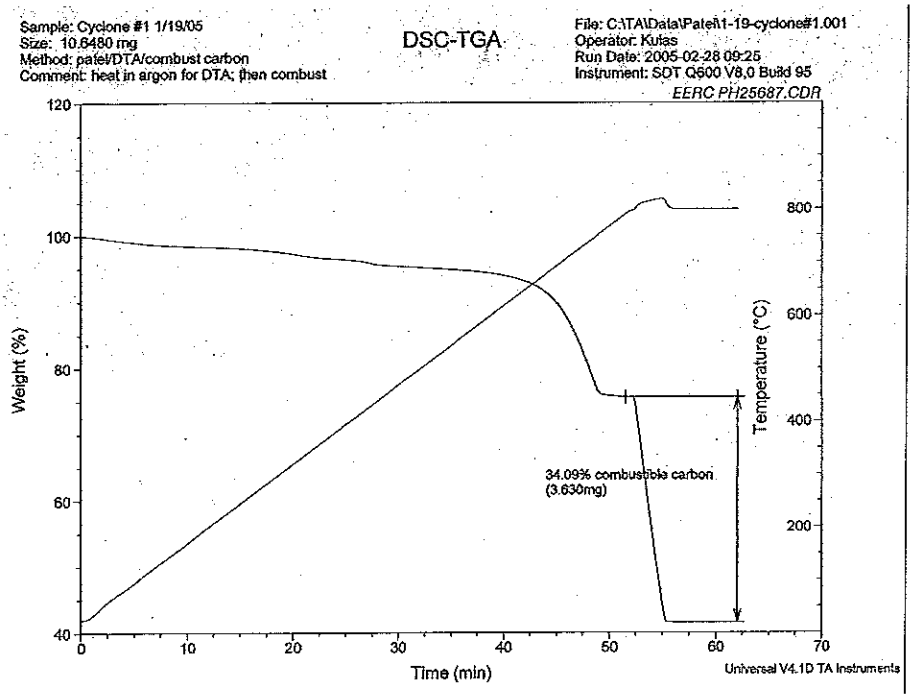

Figure A-8. TGA of residue from Cyclone 1 indicating total weight loss after carbon combustion.

Figures A-9 and A-10 depict residue collected in Cyclone 1, Cyclone 2, heat exchanger, and Pots 1 and 2 of the gasifier.

The above analysis indicates the necessity of high-temperature fine particulate filters for directly utilizing raw gas in the SOFC.

The initial effort of designing a compact particulate filter system for hot, raw gas has already been initiated. The Energy & Environmental Research Center (EERC) has extensive experience in the development of ceramic filters for flue and producer gas with particulate loadings in the range of 10,000 to 100,000 mg/m^3 (4). The typical pressure drop across filters developed at the EERC has been 1 to 1.9 m (40–75 in.) water column. Typical particulate matter measured in the integrated gasifier is less than 300 mg/m^3.

TAR ON THE PARTICULATE MATTER

In order to understand the possibility of chemisorption and physisorption of tar on the active carbon surface at favorable temperature conditions upstream of the cyclone, the following test was conducted and analyzed.

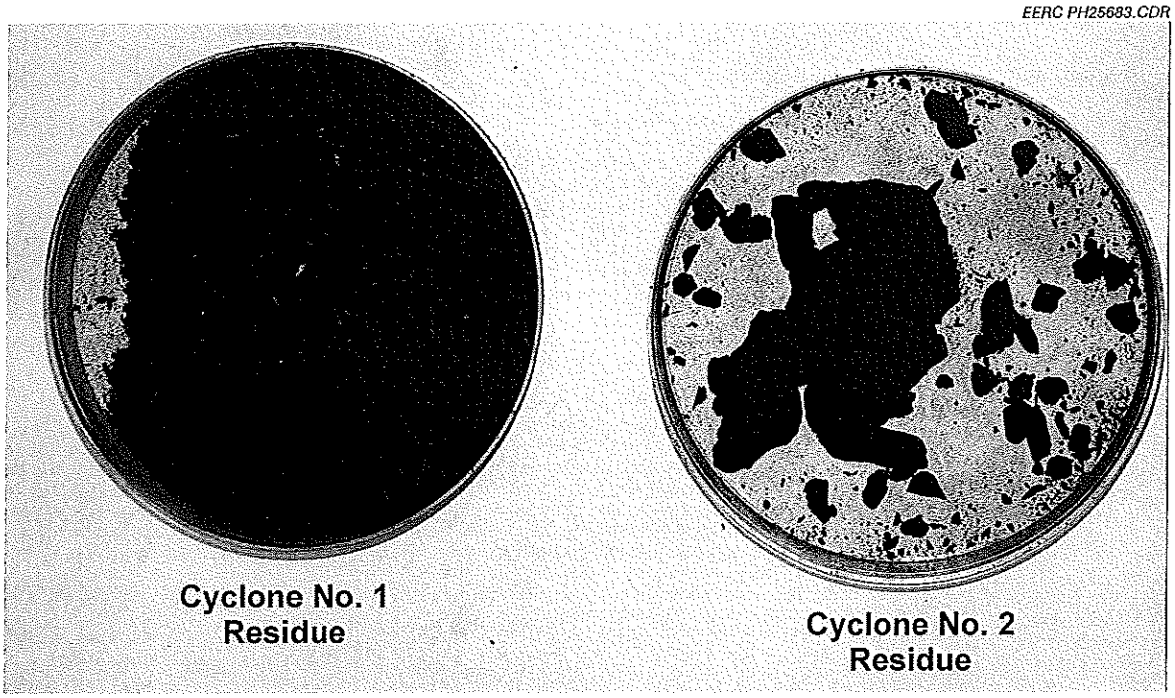

Figure A-9. Total residue collected from Cyclones 1 and 2 after Test 7. Total weights are 1.6616 g and 0.2453 g, respectively. Cyclone 1 collects about 87% of the total residue collected in both of the cyclones.

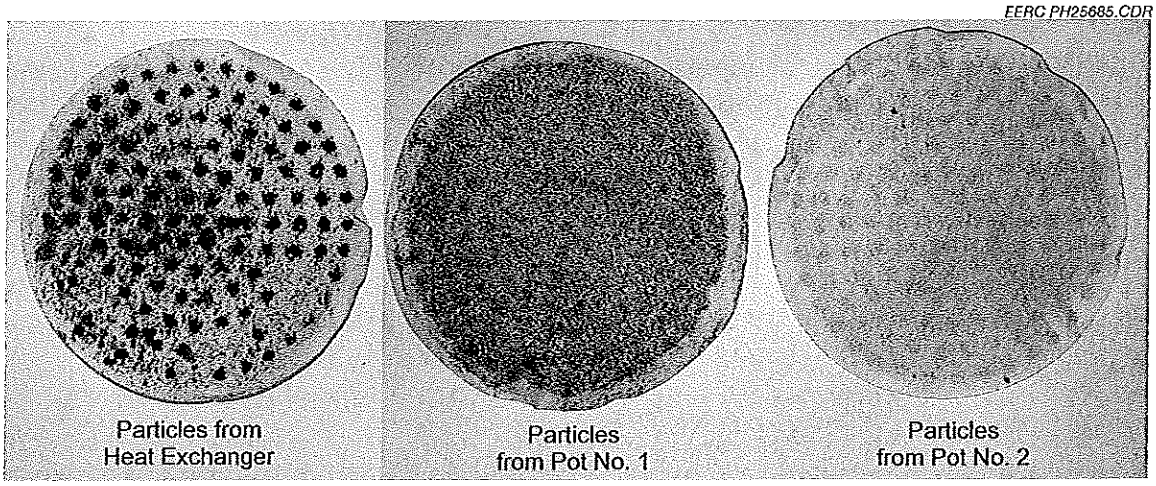

Figure A-10. Total particulate matter collected on cellulose filter after removal from the component's heat exchanger (HE) and Pots 1 and 2 connected in series at the downstream of Cyclone 2. Total particulate weights are 0.0035 g from the HE and 0.0034 g from Pots 1 and 2. Particulate matter could not be determined with the present technique of weight difference.

Adsorbed tar residue was removed for analysis from carbon collected by Cyclone 1 during biomass (40% pine) gasification Test 14. The tar was removed from the carbon by Soxhlet extraction using refluxing methylene chloride (CH_2Cl_2). To perform the extraction, 1.6685 g of carbon from the cyclone was placed in a 33 × 80-mm cellulose thimble in a Soxhlet apparatus and extracted with CH_2Cl_2 approximately 30 times an hour for 6 hours. The volume of the extract and solvent was reduced to less than 50 mL by evaporation and was then diluted to precisely 50 mL at room temperature with CH_2Cl_2 in a volumetric flask. The mass of the tar was determined (by difference in residue mass) to be 0.0058 g. The tar solution (0.116 g/L) was analyzed by GC.

The results of GC analysis showed that no BTX or phenol were present in the extract. The components found by GC were not identified individually, but previous experiences with tars suggest that they were larger components, probably substituted phenols and/or alkylated benzenes. In addition, other heavier components not detected by the GC operating at these conditions were likely. Because of the gasification conditions (temperature and long gas-phase residence time), it is unlikely that long-chain alkyl compounds were present in the extract.

REFERENCES

1. Milne T.A.; Abatzoglou, N.; Evans, R.J. *Biomass Gasifier Tars*; Biomass Energy Foundation Press: Golden, CO, 1999; p. 7.

2. Neeft, J.P.A.; Knoef, H.A.M.; Zielke, U. et al. *Guideline for Sampling and Analysis for Tar and Particles in Biomass Producer Gases Version 2.2*; Energy Project EEN5-1999-00507 (Tar protocol) for European Commission (DGXII), Netherlands Agency for Energy and the Environment (NOVEM), Swiss Federal Office of Education and Science, U.S. Department of Energy (DOE), and National Resources Canada; Nov 2001.

3. Rae Systems. www.raesystems.com/products/tubes (accessed June 2005).

4. Swanson, M.L.; Mann, M.D. Hot-Gas Filter Testing in a Transport Reactor Demonstration Unit. Presented at the Symposium on High-Temperature Particulate Cleanup for Advanced Coal-Based Power Systems, April 20–23, 1998.